# When quantum resources backfire: Non-gaussianity and symplectic coherence in noisy bosonic circuits

Varun Upreti,<sup>1,\*</sup> Ulysse Chabaud,<sup>1</sup> Zoë Holmes,<sup>2,3</sup> and Armando Angrisani<sup>2,3,†</sup>

<sup>1</sup>DIENS, École Normale Supérieure, PSL University,

CNRS, INRIA, 45 rue d'Ulm, Paris, 75005, France

<sup>2</sup>Institute of Physics, École Polytechnique Fédérale de Lausanne (EPFL), Lausanne, Switzerland

<sup>3</sup>Centre for Quantum Science and Engineering, École Polytechnique Fédérale de Lausanne (EPFL), Lausanne, Switzerland

Analyzing the impact of noise is of fundamental importance to understand the advantages provided by quantum systems. While the classical simulability of noisy discrete-variable systems is increasingly well understood, noisy bosonic circuits are more challenging to simulate and analyze. Here, we address this gap by introducing the *displacement propagation* algorithm, a continuous-variable analogue of Pauli propagation for simulating noisy bosonic circuits. By exploring the interplay of noise and quantum resources, we identify several computational phase transitions, revealing regimes where even modest noise levels render bosonic circuits efficiently classically simulable. In particular, our analysis reveals a surprising phenomenon: computational resources usually associated with bosonic quantum advantage, namely non-Gaussianity and symplectic coherence, can make the system easier to classically simulate in presence of noise.

## I. INTRODUCTION

In recent years, a large class of quantum systems known as bosonic systems have emerged as promising candidates for building quantum computers [1–5], driven by experimental breakthroughs such as the generation of complex quantum states [6, 7] and remarkable error-correction capabilities [8–13]. These ubiquitous systems include photonics, superconducting resonators, or motional modes of trapped ions and neutral atoms, and are often referred to as continuous-variable (CV) systems, governed by harmonic oscillator-like, infinite-dimensional degrees of freedom.

In practice, however, noise and imperfections inevitably affect the capability of quantum computers to both perform non-trivial computations and to outperform their classical counterparts. In the presence of such sources of noise, quantum computations that are classically intractable in an ideal, noiseless setting may become trivial (collapsing toward an input-independent fixed point) or otherwise easy to simulate on a classical computer. The standard sources of noise for bosonic systems are (photon) loss and thermal noise. These differ in mathematical structure from standard noise sources, such as depolarizing noise and dephasing noise, in discrete-variable (DV) systems.

The classical simulability of noisy DV systems is increasingly well understood with a series of results establishing efficient classical algorithms for simulating systems in the average case for arbitrary noise levels and models [14–17]

and in the worst case for sufficiently high levels of depolarizing noise [18, 19]. These results rely on the *Pauli propagation* framework [14–17, 19–26] whereby a quantum observable is propagated through a sequence of circuit layers. At each step, the observable is updated according to the action of the corresponding gate or noise channel, with tailored approximation schemes ensuring the process remains tractable on a classical computer.

The simulability of bosonic circuits, both with and without noise, is more challenging than their DV counterparts. For example, the naive approach of propagating observables as polynomials of quadratures scales doubly exponentially with the number of non-Gaussian gates [27], whereas analogous brute-force methods for qubit circuits scale only exponentially with the number of non-Clifford gates. As a result, even relatively shallow bosonic circuits can quickly become intractable for brute-force simulation. More advanced classical simulation algorithms for noisy bosonic computations have instead mostly relied on phase-space simulation methods [28–33]. These methods reduce quantum dynamics to stochastic classical-like trajectories in phase space. Other classical simulation algorithms have focused specifically on noisy linear-optical circuits [34–42]. However, existing classical simulation algorithms do not identify the noise regimes in which universal bosonic computations are classically simulable for typical noise models.

In this paper, we introduce the displacement propagation algorithm for simulating noisy bosonic circuits. This approach uses classical samples from characteristic functions to estimate observable expectation values for noisy bosonic computations. In particular, the displacement propagation formalism can be thought of as (i) a CV analogue of the

<sup>\*</sup> varun.upreti@inria.fr

 $<sup>^{\</sup>dagger}$  armando.angrisani@epfl.ch

Pauli propagation formalism [14–17] for DV systems and (ii) a Fourier space version of phase-space simulation algorithms [28–30]. We show that for the task of estimating local observables in bosonic quantum circuits based on Gaussian and noisy cubic-phase gates, our algorithm scales only exponentially with the number of noisy cubic-phase gates, significantly improving upon the naive doubly exponential scaling.

Moreover, we use displacement propagation to explore how the computational cost of simulating noisy bosonic circuits depends on the noise rate and on the quantum resources supplied by the unitary gates, revealing several regimes where classical simulation remains efficient, with a runtime linear in the number of noisy cubic-phase gates.

As one might expect, in noiseless bosonic circuits. large values of non-Gaussianity [43] and symplectic coherence [27] increase the hardness of classical simulations. In the noisy case, we also identify regimes where sufficiently small non-Gaussianity leads to efficient classical simulation, in line with these previous results. However, intriguingly, we find that also large values of non-Gaussianity and symplectic coherence can render noisy simulations classically easier. In fact, for sufficiently high values of these resources, even a small amount of noise drives bosonic computations into a regime where the expectation values of a large class of both local and global observables are efficiently simulable. Our work thus provides a limit on the allowed noise levels, for different circuit classes and noise models, beyond which bosonic computations become trivial.

The rest of the paper is structured as follows: In section II, we detail the preliminary material and notations. Section III shows how a uniform layer of noise renders universal bosonic computations trivial. In section IV, we consider a weaker noise model with noisy single-mode gates and identify phases of the bosonic system where the output expectation values can either be guessed or efficiently classically simulated. We identify how the interplay of noise and the multiple computational resources characterizing a bosonic system leads to classicality in the bosonic system. Section V explains the intuition behind the new simulation algorithm introduced in this work, which we term "displacement propagation". Finally, section VI summarizes the work and gives an outlook for future directions.

## II. PRELIMINARIES

This section summarizes the notation and preliminary concepts used throughout the main text. Detailed mathematical background relevant to the simulation algorithm is provided in Sections B and C of the Supplementary Ma-

terial.

In CV quantum information, a mode refers to a degree of freedom associated with a specific quantum field of a CV quantum system, such as a single spatial or frequency mode of light, and is the equivalent of qubit in the CV regime. In this paper, m denotes the number of modes in the system. The m-mode vacuum state (the state with zero bosons) is denoted by  $|0\rangle^{\otimes m}$ . The position and momentum quadratures of mode i are denoted by  $\hat{q}_i$  and  $\hat{p}_i$ ,  $\forall i \in \{1, \dots, m\}$ , with the position and momentum quadratures of the same mode satisfying the commutation rule  $[\hat{q}_i, \hat{p}_i] = 2i\mathbb{I}$  with the convention  $\hbar = 2$ . The energy operator is denoted by

$$\hat{N} = \sum_{j=1}^{m} \hat{N}_j = \sum_{j=1}^{m} \frac{\hat{q}_j^2 + \hat{p}_j^2}{2}.$$
 (1)

We provide detailed preliminaries on Gaussian unitaries in Section C of the Supplementary Material. Here, we note that the action of an m-mode Gaussian unitary operation  $\hat{G}$  on the vector of quadratures  $\mathbf{\Gamma} = [\hat{q}_1, \dots, \hat{q}_m, \hat{p}_1, \dots, \hat{p}_m]$  is given by

$$\hat{G}^{\dagger} \mathbf{\Gamma} \hat{G} = S \mathbf{\Gamma} + \mathbf{d}, \tag{2}$$

where S is a  $2m \times 2m$  symplectic matrix and  $\mathbf{d} \in \mathbb{R}^{2m}$  is a displacement vector associated to the Gaussian unitary gate  $\hat{G}$ . Single-mode displacement operators are defined as  $\hat{D}(\alpha) = e^{\alpha \hat{a}^{\dagger} - \alpha^* \hat{a}}$ , where  $\alpha, \xi \in \mathbb{C}$ . Coherent states  $|\alpha\rangle$  are generated by the action of displacement operator on the vacuum state  $|\alpha\rangle = \hat{D}(\alpha)|0\rangle$ .

Non-Gaussian operations are necessary for enabling quantum advantage since Gaussian gates acting on Gaussian states and followed by Gaussian measurements can be classically simulated efficiently [44]. One prominent example of a non-Gaussian gate is the cubic phase gate  $e^{i\gamma\hat{q}^3}$  [1], and a standard model of universal CV quantum computation (CVQC) is defined by a vacuum state input into a circuit with Gaussian unitaries and cubic phase gates [45–47]. While describing the circuit model in this work, we represent the Gaussian and cubic phase gates by the quantum channels  $\mathcal{G}$  and  $\mathcal{C}$ , such that

$$\begin{split} \mathcal{G}(\cdot) &= G(\cdot)G^{\dagger}, \\ \mathcal{C}(\cdot) &= e^{-i\gamma\hat{q}^3}(\cdot)e^{i\gamma\hat{q}^3}. \end{split} \tag{3}$$

Recent work showed that the ability of Gaussian gates to mix position and momentum quadratures, termed symplectic coherence, is necessary for quantum advantage, alongside non-Gaussianity and entanglement [27]. Informally, symplectic coherence in a Gaussian gate is marked by the presence of non-zero off-block diagonal matrix in the symplectic matrix S characterizing the Gaussian gate, when S

is written in the basis  $[\hat{q}_1, \dots, \hat{q}_m, \hat{p}_1, \dots, \hat{p}_m]$ . In this work, we also mention "symplectic coherence with respect to the first mode" to refer to the ability of a Gaussian unitary gate to mix the position and momentum quadrature of the first mode.

Thermal loss arises from the interaction of a system with the thermal state of a finite-temperature environment. We model its effect using a quantum channel  $\Lambda_{\bar{n},\eta}(\cdot)$ . The exact action of this channel on a quantum state  $\rho$  is detailed in Section C of the Supplementary Material.

Finally, the displacement operator basis forms an operator basis, and therefore for any operator  $\hat{O}$  living in the m-mode Hilbert space  $\mathcal{H}^{\otimes m}$ , we can write

$$\hat{O} = \frac{1}{\pi^m} \int_{\boldsymbol{\alpha} \in \mathbb{C}^m} d^{2m} \boldsymbol{\alpha} \chi_{\hat{O}}(\boldsymbol{\alpha}) \hat{D}^{\dagger}(\boldsymbol{\alpha}), \tag{4}$$

where  $\hat{D}(\boldsymbol{\alpha}) = \hat{D}(\boldsymbol{\alpha}_1) \otimes ... \otimes \hat{D}(\boldsymbol{\alpha}_m)$  is the multi-mode displacement operator, and  $\chi_{\hat{O}}(\boldsymbol{\alpha})$  is the characteristic function of the operator  $\hat{O}$ , and is given by

$$\chi_{\hat{O}}(\boldsymbol{\alpha}) = \text{Tr} \left[ \rho \hat{D}(\boldsymbol{\alpha}) \right].$$
(5)

Further, we can write  ${\rm Tr} \left[ \rho \hat{O} \right]$  in terms of the characteristic function as

$$\operatorname{Tr}\left[\rho\hat{O}\right] = \frac{1}{\pi^m} \int_{\boldsymbol{\alpha} \in \mathbb{C}^m} d^{2m} \boldsymbol{\alpha} \chi_{\rho}^*(\boldsymbol{\alpha}) \chi_{\hat{O}}(\boldsymbol{\alpha}). \tag{6}$$

This relation is an optical equivalence theorem for characteristic functions and forms the basis for our simulation algorithms, as explained in section V. We also define the Fourier 1-norm of an operator as

$$\|\hat{O}\|_{\mathbb{F},1} = \frac{1}{\pi^m} \int_{\mathbb{R}^{2m}} d^{2m} \boldsymbol{r} |\chi_{\hat{O}}(\boldsymbol{r})|. \tag{7}$$

Having detailed the necessary prerequisites, we now move to our first warm-up example to elaborate the effect of noise in universal bosonic computations.

# III. WARM UP: OVERLAP ESTIMATION UNDER UNIFORM THERMAL LOSS

In this section we start with a warm-up example showing that thermal loss exponentially suppresses the expectation values of projective measurements on bosonic systems. This can be viewed as an analogous result to the well-known exponential suppression induced by local depolarizing noise in DV systems [48–52]. However, these DV analyses are based on entropy-accumulation arguments and exploit the fact that the depolarizing noise drives any

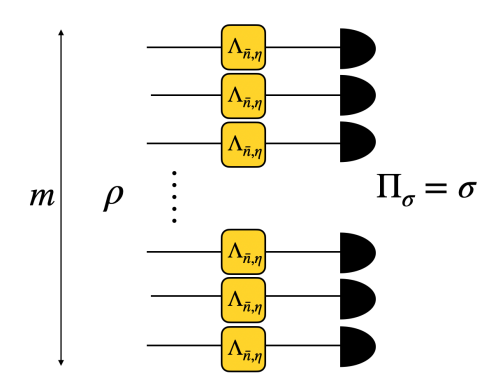


Figure 1. The setting for Proposition 1. Computing the overlap between an arbitrary bosonic quantum state  $\rho$  going through a uniform layer of noise  $\Lambda^{\otimes m}_{\bar{n},\eta}$  and any other arbitrary quantum state  $\sigma$  becomes trivial as the overlap rapidly decays to zero.

quantum state towards the infinite-temperature thermal state, commonly referred as the maximally mixed state. As a result, these analyses are not directly applicable to the continuous-variable setting, where dissipation is modeled by finite-temperature noise channels. Nevertheless, we illustrate an analogous phenomenon for a specific class of observables, namely projective measurements.

To illustrate the effect of thermal loss, we consider a uniform noise model where the output state of a circuit is acted on by a layer of thermal loss on all of its m modes, after which we want to calculate its overlap with another state (Figure 1). A prominent example of this overlap estimation problem is heterodyne detection, where the problem of estimating probabilities of getting different possible outputs in the heterodyne detection maps to problem of estimating overlap with coherent states.

Under this noise model, we find that overlaps are exponentially suppressed:

**Proposition 1** (Overlap decay under thermal channel). Given two quantum states  $\rho$  and  $\sigma$  and the m-mode thermal loss channel  $\Lambda_{\bar{n},\eta}^{\otimes m}$  satisfying  $\bar{n}(1-\eta) \in \Omega(1)$ ,

$$\left| \operatorname{Tr} \left[ \Lambda_{\bar{n},\eta}^{\otimes m}(\rho) \sigma \right] \right| \in \exp(-\Omega(\bar{n}(1-\eta)m)).$$
 (8)

The proof of Proposition 1 is given in section E of the Supplementary Material and follows from combining Hölder's inequality with a technical result on the decay of the purity of a quantum state under a thermal loss channel.

Proposition 1 can be viewed as delineating the boundary for meaningful quantum computations in the presence of thermal loss. Namely, when thermal loss affects all modes of a bosonic system, the expectation value of projective measurements become trivial in the sense of vanishing

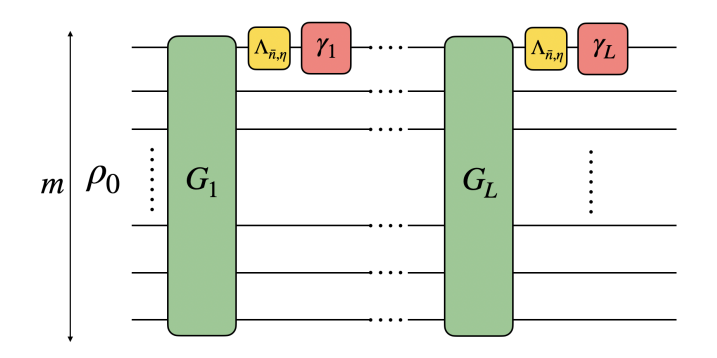


Figure 2. A circuit for bosonic computations with noisy cubic phase gate.  $\forall i \in \{1, ..., L\}$ ,  $G_i$  are Gaussian unitary gates,  $\gamma_i$  represents the cubic phase gate with cubicity  $\gamma_i$  (acting on the first mode), and  $\Lambda_{\bar{n},\eta}$  is the thermal loss channel.

exponentially (in the number of modes m) towards zero. Or, turning it around, a necessary condition for non-trivial quantum computations in this model, is that the noise rate  $\bar{n}(1-\eta)$  shrinks inverse proportionally with the number of modes m.

Note that, while insightful, the noise model behind Proposition 1 suffers from certain limitations. Firstly, the uniform noise model is rather strong and it would be interesting to see if a weaker noise model, where only certain gates are noisy also allows for classical simulation. Further, the result only holds nontrivially for  $\bar{n} \neq 0$ , and as such, does not apply to pure loss channels.

Hereafter, we utilize new simulation techniques (detailed in Section V) for weaker gate-based noise models. These simulation techniques can be seen as a combination of phase-space techniques commonly used in CV quantum information and Pauli propagation techniques used in DV quantum information.

# IV. COMPUTATIONAL REGIMES UNDER GATE-BASED NOISE

In this section, we consider a quantum state  $\rho_0$  evolving under the quantum circuit described by the channel:

$$\mathcal{U} \coloneqq \mathcal{U}_L \circ \mathcal{U}_{L-1} \circ \dots \circ \mathcal{U}_1, \tag{9}$$

where

$$\mathcal{U}_i := \mathcal{C}_i \circ \Lambda_{\bar{n},n} \circ \mathcal{G}_i, \tag{10}$$

 $\forall j \in \{1, ..., m\}$ , where  $C_j$  is a cubic phase gate with cubicity  $\gamma_j$ ,  $\Lambda_{\bar{n},\eta}$  is a single-mode thermal loss channel characterized by  $\bar{n}$  and  $\eta$ , and  $C_j$  is a Gaussian unitary gate

characterized by a  $2m \times 2m$  symplectic matrix  $S_j$  and a 2m-dimensional displacement vector  $\mathbf{d}_j$ . We assume that both  $\mathcal{C}_j$  and  $\Lambda_{\bar{n},\eta}$  act on the same mode, which without loss of generality [53] we take to be the first (see Figure 2). Furthermore, we assume that the characteristic function of the input state  $\rho_0$  is efficiently computable—this is the case for instance for tensor product states with efficiently computable single-mode characteristic functions.

Here, we initiate a systematic study of the interplay between noise and fundamental quantum resources for such noisy bosonic circuits. Specifically, the following sections demonstrate that noise, non-Gaussianity, symplectic coherence, and energy act in concert to delineate regimes of trivial computations and efficient classical simulability.

## A. Theoretical guarantees

Here, we state a series of guarantees that establish the regimes in which the outputs of bosonic circuits become trivial in the sense of concentrating to zero (Theorem 1) or become classically simulable (Theorems 2 and 3). As will be seen, our results are all stated in terms of contraction coefficients that depend on the noise parameters and the quantum resources generated by the circuit (Definition 1). Here we focus on formally stating our theorems and postpone discussing them in Section IVB, where we formally define and analyze these contraction coefficients.

Exponential concentration. We start by deriving an analogous concentration result to Proposition 1, but this time for the gate-based noise defined in Eq. (9) and a vacuum state  $|0\rangle^{\otimes m}$  input.

**Theorem 1** (Noise-induced concentration in bosonic circuits). Consider an input m-mode vacuum state  $\rho_0 = |0\rangle\langle 0|^{\otimes m}$ , a bosonic circuit described by Eq. (9) and an observable  $\hat{O}$  such that the trace norm of  $\hat{O}$  is at most exponential in m. Then for a contraction coefficient (defined below in Definition 1)  $c_1 < 1$  and sufficiently large  $L = \Omega(m)$ , the associated expectation value satisfies

$$\left| \operatorname{Tr} \left[ \mathcal{U}(\rho_0) \hat{O} \right] \right| \in \exp \left( -\Omega(m) \right).$$
 (11)

The proof of Theorem 1 is given in Theorem G.1 in the Supplementary Material and follows by expressing  $\text{Tr}\left[\mathcal{U}(\rho)\hat{O}\right]$  using the optical equivalence theorem and proving that the magnitude of the expectation value goes to zero for  $\mathfrak{c}_1 < 1$  and sufficiently large  $L = \Omega(m)$ . In particular, as quantum states have unit trace norm, Theorem 1 encompasses (global) projective measurements.

Theorem 1 identifies another regime where noisy universal bosonic computations become trivial. This regime is determined by the contraction coefficient  $\mathfrak{c}_1$ , with  $\mathfrak{c}_1 = 1$  marking the computational phase transition between trivial and non-trivial behavior. The value of  $\mathfrak{c}_1$  is set by the interplay of noise and the resources characterizing the universal bosonic circuit, as discussed in the Section IV B.

Classical simulability. Next, we turn our attention to the classical simulability of bosonic circuits and consider the problem of estimating the overlap with coherent state projectors  $\left(\bigotimes_{i=1}^k |\alpha_i\rangle \langle \alpha_i|\right) \otimes \mathbb{I}^{\otimes m-k}$ . Combining Lemmas G.6 and G.9 from the Supplementary Material, we give the following result:

**Theorem 2** (Classically estimating overlaps under gate-based noise). Given an initial m-mode quantum state  $\rho_0$  evolving under the bosonic circuit described by Eq. (9) such that the first two moments of the energies are bounded throughout, the overlap of the output state with the coherent state projectors  $\left(\bigotimes_{i=1}^k |\alpha_i\rangle\langle\alpha_i|\right)\otimes\mathbb{I}^{\otimes m-k}$ , given by

$$\operatorname{Tr}\left[\mathcal{U}(\rho_0)\left(\bigotimes_{i=1}^k |\alpha_i\rangle\langle\alpha_i|\right)\otimes\mathbb{I}^{\otimes m-k}\right]$$
 (12)

for  $k = \mathcal{O}(\log m)$  can be efficiently estimated classically with precision  $\epsilon$  and success probability  $1 - \delta$  in time  $\mathcal{O}(\text{poly}(m, \epsilon) \log(1/\delta))$  in the following three regimes:

- (i)  $\mathfrak{c}_2 < 1$  and  $L \in \mathcal{O}(\operatorname{poly}(m))$ .
- (iii)  $L \in \mathcal{O}(\log(m))$  for arbitrary  $\mathfrak{c}_2 \in \mathcal{O}(1)$ .
- (ii)  $\mathfrak{d}_{\epsilon} < 1$  and  $L \in \mathcal{O}(\operatorname{poly}(m))$ .

where  $\mathfrak{c}_2$  and  $\mathfrak{d}_{\epsilon}$  are contraction coefficients defined below in Definition 1.

Theorem 2 is based on the displacement propagation algorithm for estimating characteristic functions, explained in Section V.

Finally, we consider the problem of estimating quadratures expectation values. Namely, measuring operators of the form

$$\operatorname{Tr}\left[\hat{r}_{j}^{k}\mathcal{U}(\rho_{0})\right],$$
 (13)

for  $\hat{r}=\hat{q},\hat{p}$  and k=1,2. The runtime in this case includes an additional dependency on the moments of the local energy operators  $\hat{N}_j:=\frac{1}{2}\left(\hat{p}_j^2+\hat{q}_j^2\right)$ . For convenience, we introduce the following parameter:

$$E := \max_{j \in [m]} \left( \max \left( \operatorname{Tr} \left[ \hat{N}_j^3 \mathcal{U}(\rho_0) \right], \operatorname{Tr} \left[ \hat{N}_j^2 \mathcal{U}(\rho_0) \right] \right) \right). \tag{14}$$

**Theorem 3** (Classically estimating quadratures under gate-based noise). Given an initial m-mode quantum state  $\rho_0$  evolving under the bosonic circuit described by Eq. (9), and given  $\hat{O} = \hat{p}_j, \hat{q}_j, \hat{p}_j^2$ , or  $\hat{q}_j^2$  for some  $j \in [m]$ , the expectation value

$$\operatorname{Tr}\left[\hat{O}\mathcal{U}(\rho_0)\right],$$
 (15)

can be estimated classically with precision  $\epsilon$  and success probability  $1 - \delta$  in time  $\mathcal{O}(\text{poly}(m, \epsilon, E) \log(1/\delta))$  in the following three regimes:

- (i)  $\mathfrak{c}_2 < 1$  and  $L \in \mathcal{O}(\operatorname{poly}(m))$ .
- (iii)  $L \in \mathcal{O}(\log(m))$  for arbitrary  $\mathfrak{c}_2 \in \mathcal{O}(1)$ .
- (ii)  $\mathfrak{d}_{\epsilon} < 1$  and  $L \in \mathcal{O}(\operatorname{poly}(m))$ .

where  $\mathfrak{c}_2$  and  $\mathfrak{d}_{\epsilon}$  are contraction coefficients defined below in Definition 1.

Theorem 3 combines Lemmas G.7 and G.9 from the Supplementary Material and is also based on our displacement propagation algorithm and a new technical result connecting quadrature moments to finite differences of characteristic functions (Lemma D.2).

Note that the evaluation of  $\hat{q}_j^2, \hat{p}_j^2, \forall j \in \{1, ..., m\}$  also allows for calculating the expectation value of the number operator  $\hat{N} := \sum_{j=1}^m \frac{\hat{q}_j^2 + \hat{p}_j^2}{2}$  and thus estimating the energy.

# B. The interplay of quantum resources and noise

Contraction coefficients. The contraction coefficients  $\mathfrak{c}_1, \mathfrak{c}_2$  and  $\mathfrak{d}_\epsilon$  play a pivotal role in Theorems 1, 2 and 3, determining the regimes of trivial quantum computations and efficient classical simulability. In this section, we provide the formal definition of these coefficients and use them to explore the interplay between noise and different quantum computational resources.

**Definition 1** (Contraction coefficients). Given a bosonic circuit defined by Eq. (9), we define the associated contraction coefficients given by

$$c_1 = \frac{\Gamma(1/4)}{\sigma_{\min} \eta^{1/4} \sqrt{24\pi \gamma_{\min}} ((1/2 + \bar{n})(1 - \eta))^{1/4}},$$
 (16)

$$\mathfrak{c}_2 = \frac{\Gamma(1/4)}{(\sigma^{-1})_{\min} \eta^{1/2} \sqrt{24\pi \gamma_{\min}} ((1/2 + \bar{n})(1 - \eta))^{1/4}}, \quad (17)$$

$$\mathfrak{d}_{\epsilon} = \sqrt{\frac{M}{\epsilon}} \exp\left[-\left(\frac{1}{2} + \bar{n}\right)(1 - \eta)\frac{\epsilon^2}{36M^2 \gamma_{\max}^2}\right], \qquad (18)$$

where

$$\gamma_{\min} = \min_{j} |\gamma_{j}|, \quad \gamma_{\max} = \max_{j} |\gamma_{j}|, \quad \sigma_{\min} = \min_{j} |(S_{j})_{q_{1}, p_{1}}|,$$

$$(\sigma^{-1})_{\min} = \min_{j} |(S_{j}^{-1})_{q_{1}, p_{1}}|,$$
(19)

$$M = \max_{j} \max_{\mathbf{r}' \in \mathbb{R}^{2m}} \left| \left\{ \frac{\partial^2}{\partial^2 p_1} \chi_j(\mathbf{r}) \right\}_{\mathbf{r} = \mathbf{r}'} \right|, \tag{20}$$

where  $\chi_j$  is the characteristic function of the quantum state evolved under j noisy circuit layers, i.e.  $\rho_j := C_j \circ \Lambda_{\bar{n},\eta} \circ U_{j-1} \circ ... \circ U_1(\rho_0)$ .

The  $\sigma$  component can be intuitively understood as the minimum amount by which the Gaussian gates are mixing the position quadrature with the momentum quadrature on the modes on which the cubic phase gates act, i.e. the minimum symplectic coherence with respect to those modes of the Gaussian gates of the given circuit [27]. By our convention, all cubic phase gates act on the first mode hence the dependence on  $q_1$  and  $p_1$  in Eq. (19).

On the other hand,  $\gamma_{\min}$  and  $\gamma_{\max}$  can be intuitively seen as the maximum and minimum strength of the non-Gaussian gates present in the quantum system, while non-Gaussianity itself is captured by the number L of such gates in the circuit. Finally, as we show in the Supplementary Material (see Lemma D.1), M can be bounded in terms of the second and fourth moments of local quadrature operators evaluated on partially evolved states, and can thus be interpreted as a global upper bound on the energy throughout the computation.

The key role of these contraction coefficients in Theorems 1, 2 and 3 mirrors that central role played by contraction coefficients in DV quantum information, where they provide a rigorous framework for characterizing the action of noise and, in particular, its interplay with unitary dynamics. They have been employed in several recent results on the limitations of noisy quantum devices [50, 54–57], including bounds on error-mitigation protocols [52] and regimes of classical simulability [15, 18, 19, 58].

In the DV case, analyses of the role of quantum resources and noise in delineating the boundary between non-trivial quantum computation and efficient classical simulation often treat these resources largely independently. This typically leads to relatively simple functional relationships, where the ratio between noise strength and a single resource suffices to determine classical simulability. For example, Ref. [18] identifies regimes of classical simulability by examining the interplay between the noise rate and the rate at which magic is injected by non-Clifford gates. Even more strikingly, Ref. [24] shows that in noiseless circuits the injection rate of magic alone already suffices to determine regimes of classical simulability. A further

example is provided by the analyses of Refs. [56, 59, 60], which rely on contraction of the quantum Wasserstein distance. In these latter works, noise-induced concentration is characterized by the rate at which noise suppresses the non-local interactions generated by the unitary gates.

Computational phase transitions in bosonic systems. In noisy bosonic circuits, in contrast to the DV case, the effects of quantum resources are intrinsically intertwined, leading to far more intricate phase diagrams (see Figure 3). While the effect of the average thermal photons is straightforward (increasing temperature makes the bosonic system classical), the interplay between the other resources is more subtle, with the cubicity parameters  $\gamma_j$  never appearing in isolation in the computational complexity of our algorithms, but always in combination with either the rate at which the Gaussian gates inject symplectic coherence (captured by  $\sigma$  in  $\mathfrak{c}_1$  and  $\mathfrak{c}_2$ ) or with the energy of partially evolved states (captured by M in  $\mathfrak{d}_{\epsilon}$ ).

By analyzing phase diagrams for  $\mathfrak{c}_1,\mathfrak{c}_2$  and  $\mathfrak{d}_\epsilon$ , we find that cubicity and symplectic coherence play vastly different roles, which we explain below. Note that the contraction coefficients  $\mathfrak{c}_1$  and  $\mathfrak{c}_2$  have similar expressions, up to a factor of  $1/\eta^{1/4}$  and different notions of symplectic coherence,  $\sigma_{min}$  vs  $(\sigma^{-1})_{\min}$ , therefore the interplay of resources leading to classical simulable phases characterized by  $\mathfrak{c}_1 < 1$  and  $\mathfrak{c}_2 < 1$  is qualitatively the same and we group them together:

- (i) Combined with high symplectic coherence, large cubicity makes noisy bosonic computations easier to simulate classically. This is shown in the top and middle row of Figure 3, where for all values of noise parameters  $\eta$  and  $\bar{n}$ , increasing the value of the quantum resources  $\sqrt{\gamma_{\min}}\sigma$  ( $\sqrt{\gamma_{\min}}\sigma^{-1}$ ) decreases  $\mathfrak{c}_1$  ( $\mathfrak{c}_2$ ) to a value less than one and brings the bosonic system to a regime of efficient classical simulation. This is rather surprising, since higher values of symplectic coherence are associated with increasing complexity of simulation in the noiseless case [27]. Here we observe that for noisy computations, a higher value of a quantum computational resource can lead to efficient classical simulation algorithms for the system.
- (ii) In contrast, when the energy generated throughout the circuit remains sufficiently small, low cubicity values instead render the computation easier to simulate classically. This is also shown in the bottom row of Figure 3 where for given value of M and desired precision  $\epsilon$ , decreasing the value of  $\gamma$  takes the contraction coefficient  $\mathfrak{d}_{\epsilon}$  below one, so that system becomes classically simulable. This result is closer to expectations, since universal bosonic circuits where the value of the cubicity of the cubic phase gates is very small can be thought of as "near-Gaussian" circuits

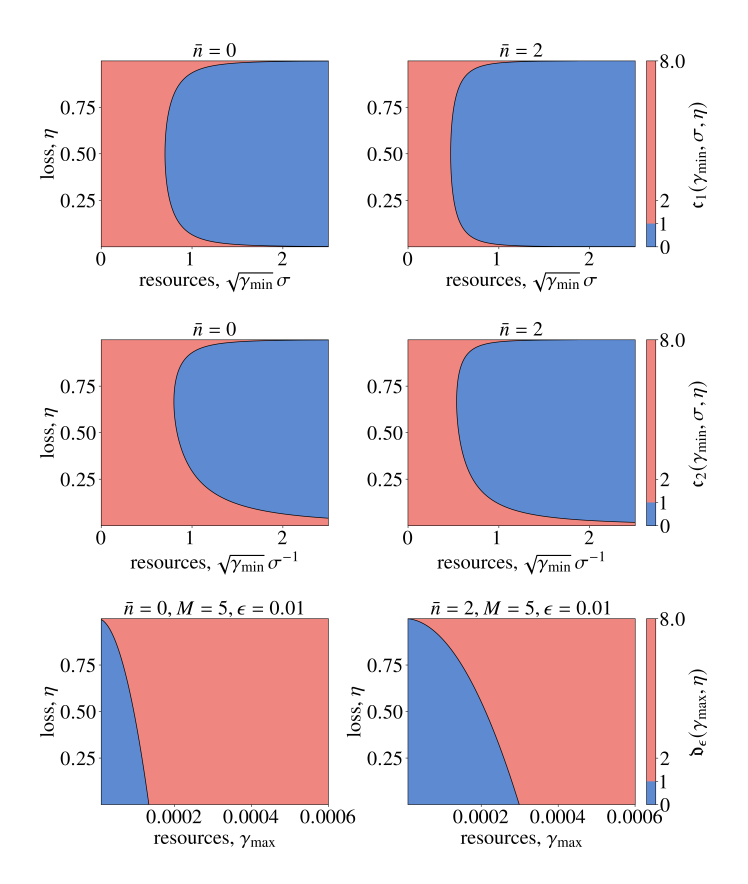


Figure 3. Top and middle row: Contraction coefficients  $\mathfrak{c}_1$  and  $\mathfrak{c}_2$  as a function of photon loss  $\eta$  and quantum resources  $\sqrt{\gamma_{\min}}\sigma$  (for  $\mathfrak{c}_1$ ) and  $\sqrt{\gamma_{\min}}\sigma^{-1}$  for different values of average thermal photons  $\bar{n}$ .  $\forall \eta, \bar{n}$ , increasing the quantum resources leads us to the efficiently classically simulable phase (marked by the blue/green region). Bottom row: Contraction coefficient  $\mathfrak{d}_{\epsilon}$  as a function of  $\gamma$  for different values of  $\bar{n}$ , with fixed M and  $\epsilon$ . Decreasing the value of  $\gamma$  (approaching near-Gaussian circuits) leads us to the efficiently classically simulable phase of the noisy bosonic computations (marked by the violet region).

and would be expected to be classically simulable [44].

In both cases, the runtime of our classical simulation algorithms grows (at least) exponentially with circuit depth whenever  $\mathfrak{c}_1,\mathfrak{c}_2,\mathfrak{d}_{\epsilon}>1$ , thereby leaving room for substantial quantum speed-ups. In contrast, when  $\mathfrak{c}_1,\mathfrak{c}_2,\mathfrak{d}_{\epsilon}\leqslant 1$ , the simulation can be carried out in polynomial time, and in some regimes the dynamics even become computationally trivial: expectation values are exponentially suppressed, severely restricting the potential for quantum advantage in estimating observables.

# V. METHODS: THE DISPLACEMENT PROPAGATION ALGORITHM

In this section we briefly present the displacement propagation simulation framework that we developed to obtain our theoretical results above. This framework should be understood both as a theoretical tool for identifying regimes for quantum advantage as well as a new practical tool for simulating bosonic systems.

The displacement propagation algorithm follows from the optical equivalence theorem for the CV characteristic function: given an operator  $\hat{O}$  and an output state  $\mathcal{U}(\rho_0)$ , the expectation value of  $\hat{O}$  over  $\mathcal{U}(\rho_0)$  is given by

$$\operatorname{Tr}\left[\mathcal{U}(\rho_{0})\hat{O}\right] = \frac{1}{\pi^{m}} \int_{\mathbb{R}^{2m}} d^{2m} \boldsymbol{r} \operatorname{Tr}\left[\hat{O}\hat{D}(\boldsymbol{r})\right] \times \operatorname{Tr}\left[\mathcal{U}(\rho_{0})\hat{D}^{\dagger}(\boldsymbol{r})\right],$$

$$= \frac{1}{\pi^{m}} \int_{\mathbb{R}^{2m}} d^{2m} \boldsymbol{r} \chi_{\hat{O}}(\boldsymbol{r}) \chi_{\mathcal{U}(\rho_{0})}^{*}(\boldsymbol{r}), \tag{21}$$

where  $\mathbf{r} = \{q_1, p_1, \dots, q_m, p_m\}$ . Defining the Fourier 1-norm of  $\hat{O}$  as  $\|\hat{O}\|_{\mathbb{F},1} := \int_{\mathbb{R}^{2m}} d\mathbf{r} \left| \frac{\text{Tr}[\hat{O}D(\mathbf{r})]}{\pi^m} \right|$ , and defining the probability density function

$$p_{\hat{o}}(\mathbf{r}) = \frac{|\chi_{\hat{O}}(\mathbf{r})|}{\pi^m \|\hat{O}\|_{\mathbb{F},1}},\tag{22}$$

this can be written as

$$\operatorname{Tr}\left[\mathcal{U}(\rho_0)\hat{O}\right] = \|\hat{O}\|_{\mathbb{F},1} \int_{\mathbb{R}^{2m}} d^{2m} \boldsymbol{r} p_{\hat{o}}(\boldsymbol{r}) \chi_{\mathcal{U}(\rho_0)}^*(\boldsymbol{r}) \operatorname{arg}(\chi_{\hat{O}}(\boldsymbol{r})),$$
(23)

where  $\arg(z)$  denotes the phase of the complex number z. Therefore,  $\operatorname{Tr}\left[\mathcal{U}(\rho_0)\hat{O}\right]$  can be estimated by sampling a phase-space point  $\boldsymbol{r}$  from the probability distribution  $p_{\hat{o}}(\boldsymbol{r})$  and estimating  $\chi_{\mathcal{U}(\rho)}^*(\boldsymbol{r})\arg(\chi_{\hat{O}}(\boldsymbol{r}))$  at that point. A similar technique can be applied repeatedly via a Markov Chain sampling argument.

This technique is closely related to randomized versions of the Pauli propagation algorithm [18, 61] and it is similar to the sampling techniques with quasi-probability distribution commonly used in CV quantum information [28–33], with the key difference being that using characteristic function for the estimation is less common, with only a few works for noiseless computations [62, 63]. The main reason is that characteristic function are complex and not always normalizable to use as a probability distribution. However for

$$\hat{O} = \left(\bigotimes_{i=1}^{k} |\alpha_i\rangle\langle\alpha_i|\right) \otimes \mathbb{I}^{\otimes m-k},\tag{24}$$

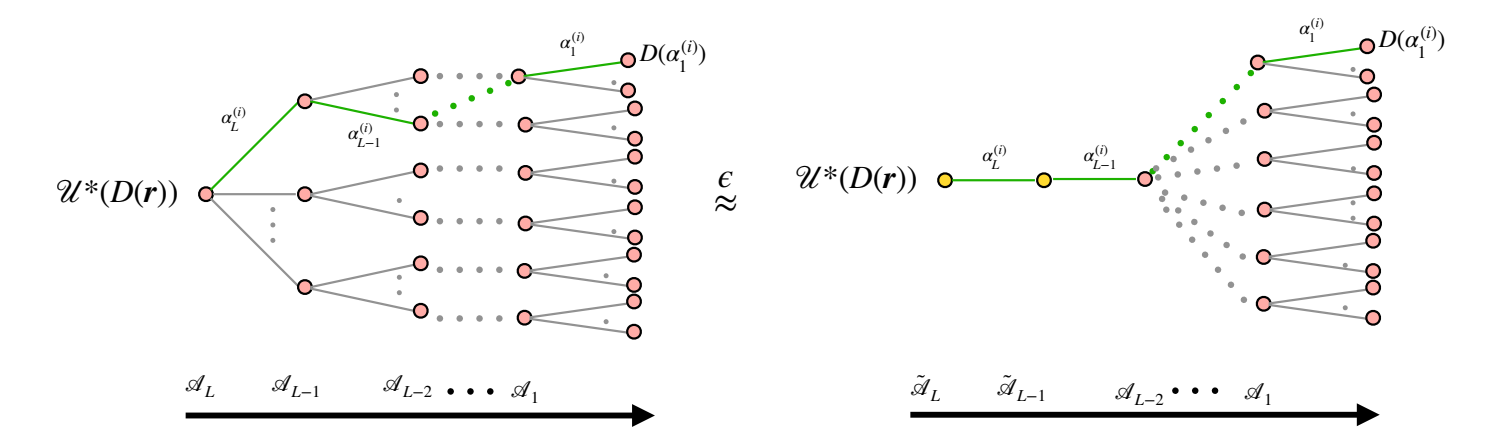


Figure 4. Intuition behind the displacement propagation algorithm. To evaluate the characteristic function  $\text{Tr}\left[\mathcal{U}^*(\hat{D}(\mathbf{r}))\rho_0\right]$ , we build a Markov chain by decomposing  $\mathcal{U}^*$  into L possibly non-physical quantum maps  $\mathcal{A}_1 \circ \cdots \circ \mathcal{A}_L$  and for each of the L layers, we sample a phase space point  $\alpha_i$  according to a probability distribution that depends on both the properties of the current layer and the previously sampled phase-space point. At the end of the L'th layer, we obtain a phase space point  $\alpha_1 \in \mathbb{C}^m$  at which we estimate the characteristic function  $\text{Tr}\left[\rho_0\hat{D}(\alpha_1)\right]$  (assuming that the characteristic function of the input state is efficiently computable). By carefully choosing the quantum channels, we ensure that the statistical average of N such characteristic functions approximates  $\text{Tr}\left[\mathcal{U}^*(\hat{D}(\mathbf{r}))\rho_0\right]$  to arbitrary precision using a polynomial number of samples. This process is illustrated by the tree on the left and formalized in Algorithm 1 in the Supplementary Material. However, for certain regions of phase space, efficient sampling at every layer may not be feasible, particularly due to the non-linearity introduced by non-Gaussian cubic-phase gates. In these cases, we employ adaptive simulation algorithms, in which the layer  $\mathcal{A}_j$  is replaced by an approximate map  $\hat{\mathcal{A}}_j$  (the modification is designed so that the corresponding sampled phase-space point becomes deterministic; see Section F 2 of the Supplementary Material). This procedure ensures that the resulting Markov chain approximates the target characteristic function with only a negligible bias. This adaptive approach is depicted by the tree on the right and formalized in Algorithm 2 in the Supplementary Material.

the modulus of characteristic function is given as

$$|\chi_{\hat{O}}(\boldsymbol{r})| = \left(\prod_{i=1}^{k} \exp\left(-(q_i^2 + p_i^2)/2\right)\right) \left(\prod_{j=k+1}^{m} \delta(q_j)\delta(p_j)\right) \tag{25}$$

which is normalizable and hence can be used as a probability distribution. Another problem is that the calculation of the characteristic function of the evolved state might not be straightforward.

The main technical contribution of this work is to provide techniques to efficiently estimate this characteristic function for universal bosonic computations with noisy cubic phase gates in the specified regimes, by applying Monte Carlo Markov Chain sampling algorithms over carefully constructed Markov chains, obtained through suitable channel decompositions. We call this sampling algorithm the "displacement propagation algorithm". The key idea is to express noisy circuit layers as sequences of (possibly unphysical) linear maps and to model their action on displacement operators by chaining together biased and unbiased estimators, chosen adaptively throughout the procedure. This is detailed in Appendix G and a visual intuition for the displacement propagation algorithm is given in Figure

4

The methods for efficiently computing the characteristic function can also be extended to estimating commutative quadrature operators. In particular, as we show in Lemma D.2, expectation values of single-mode quadratures can be approximated as follows using a first-order Taylor expansion

$$\operatorname{Tr}[\rho \hat{q}_{j}] = -\frac{i}{\delta} \left( \operatorname{Tr} \left[ \rho \hat{D}_{j}(0, \delta) \right] - 1 \right) + \mathcal{O} \left( \delta \operatorname{Tr} \left[ \rho \hat{N}_{j}^{2} \right] \right), \tag{26}$$

$$\operatorname{Tr}[\rho \hat{p}_{j}] = -\frac{i}{\delta} \left( 1 - \operatorname{Tr} \left[ \rho \hat{D}_{j}(\delta, 0) \right] \right) + \mathcal{O} \left( \delta \operatorname{Tr} \left[ \rho \hat{N}_{j}^{2} \right] \right). \tag{27}$$

Importantly, the value of  $\delta$  has to be chosen such that  $\delta \ll \text{Tr}\left[\rho\hat{N}_{j}^{2}\right]$  and in practice the state  $\rho$  in Eq. (26) will be the state evolved under the noisy circuit, i.e.  $\rho := \mathcal{U}(\rho_{0})$ . While this approximation enables the estimation of quadrature expectation values from characteristic functions, it comes at the cost of increasing the variance of the classical estimator by a factor of order  $\delta^{-2}$ . Since this factor must

be larger than  $\text{Tr}\left[\rho\hat{N}_{j}^{2}\right]$ , the classical simulation overhead grows with the energy of the system. Analogous expression can be derived also for higher order polynomials (We give the expression for the second moment of quadratures in terms of characteristic functions in Lemma D.2). These observations underlie Theorem 3.

### VI. CONCLUSION

In this work, we have developed classical simulation algorithms to estimate expectation values of observables at the output of noisy bosonic computations, for both uniform and gate-dependent noise models. We uncover a rich interplay between noise and computational resources, identifying regimes where circuits of different depths can be simulated efficiently on classical hardware.

Our results help pinpoint the boundary for bosonic quantum computational advantage under noise, where quantum error correction becomes mandatory to maintain an edge over classical computers. Whether the same interplay of resources also determines efficient classical simulation beyond expectation values (e.g., sampling) represents an interesting research direction. Another promising direction is to investigate the classical simulability of bosonic circuits with different non-Gaussian gates, such as the Kerr gate, or with different noise models such as phase noise or partial distinguishability, and understand the interplay of resources leading to computational phase transitions.

Our main tool is the *displacement propagation* formalism, a new, powerful framework which combines classi-

cal Monte Carlo Markov Chain sampling algorithms with the optical equivalence theorem for CV characteristic functions, generalizing to the bosonic setting the Pauli propagation formalism [14–17]. While in this manuscript we have focused on use of displacement propagation as a tool to study the simulability of noisy bosonic circuits we foresee it also finding use as a practical simulation algorithm in regimes beyond that for which we currently have guarantees (as has been seen in the case of Pauli propagation [20, 21, 23]). A particularly interesting test case would be the simulation of bosonic error correction codes [13].

Another interesting direction for future research is to see whether the displacement propagation framework can be hybridized with Pauli propagation, or other classical simulation methods for simulating spin systems, to simulate hybrid spin-boson systems. Such hybrid algorithms could be applied to simulate open quantum systems. In particular, they might open up new methods for exploring the strong coupling limit and non-Markovian environments. We leave these research directions for future work.

## ACKNOWLEDGEMENTS

UC acknowledges inspiring discussions with G. Ferrini, A. Leverrier, A. Debray, M. Frigerio and M. Walschaers. AA acknowledges inspiring discussions with F. A. Mele and M. S. Rudolph. VU and UC acknowledge funding from the European Union's Horizon Europe Framework Programme (EIC Pathfinder Challenge project Veriqub) under Grant Agreement No. 101114899. ZH and AA acknowledge support from the Sandoz Family Foundation-Monique de Meuron program for Academic Promotion.

- [1] D. Gottesman, A. Kitaev, and J. Preskill, Encoding a qubit in an oscillator, Phys. Rev. A 64, 012310 (2001).
- [2] E. Knill, R. Laflamme, and G. Milburn, A scheme for efficient quantum computation with linear optics, Nature 409, 46 (2001).
- [3] N. C. Menicucci, P. van Loock, M. Gu, C. Weedbrook, T. C. Ralph, and M. A. Nielsen, Universal quantum computation with continuous-variable cluster states, Phys. Rev. Lett. 97, 110501 (2006).
- [4] L. S. Madsen, F. Laudenbach, M. F. Askarani, F. Rortais, T. Vincent, J. F. Bulmer, F. M. Miatto, L. Neuhaus, L. G. Helt, M. J. Collins, et al., Quantum computational advantage with a programmable photonic processor, Nature 606, 75 (2022).
- [5] Y. Liu, S. Singh, K. C. Smith, E. Crane, J. M. Martyn, A. Eickbusch, A. Schuckert, R. D. Li, J. Sinanan-Singh, M. B. Soley, et al., Hybrid oscillator-qubit quantum processors: Instruction set architectures, abstract machine

- models, and applications, arXiv preprint arXiv:2407.10381(2024).
- [6] S. Yokoyama, R. Ukai, S. C. Armstrong, C. Sornphiphatphong, T. Kaji, S. Suzuki, J.-i. Yoshikawa, H. Yonezawa, N. C. Menicucci, and A. Furusawa, Ultra-large-scale continuous-variable cluster states multiplexed in the time domain, Nature Photonics 7, 982 (2013).
- [7] M. Larsen, J. Bourassa, S. Kocsis, J. Tasker, R. Chadwick, C. González-Arciniegas, J. Hastrup, C. Lopetegui-González, F. Miatto, A. Motamedi, et al., Integrated photonic source of gottesman-kitaev-preskill qubits, Nature, 1 (2025).
- [8] M. H. Michael, M. Silveri, R. Brierley, V. V. Albert, J. Salmilehto, L. Jiang, and S. M. Girvin, New class of quantum error-correcting codes for a bosonic mode, Physical Review X 6, 031006 (2016).
- [9] B. M. Terhal, J. Conrad, and C. Vuillot, Towards scalable bosonic quantum error correction, Quantum Science and

- Technology 5, 043001 (2020).
- [10] W. Cai, Y. Ma, W. Wang, C.-L. Zou, and L. Sun, Bosonic quantum error correction codes in superconducting quantum circuits, Fundamental Research 1, 50 (2021).
- [11] V. Sivak, A. Eickbusch, B. Royer, S. Singh, I. Tsioutsios, S. Ganjam, A. Miano, B. Brock, A. Ding, L. Frunzio, et al., Real-time quantum error correction beyond breakeven, Nature 616, 50 (2023).
- [12] H. Putterman, K. Noh, C. T. Hann, G. S. MacCabe, S. Aghaeimeibodi, R. N. Patel, M. Lee, W. M. Jones, H. Moradinejad, R. Rodriguez, et al., Hardware-efficient quantum error correction via concatenated bosonic qubits, Nature 638, 927 (2025).
- [13] V. V. Albert, Bosonic coding: introduction and use cases, in *Quantum Fluids of Light and Matter* (IOS Press, 2025) pp. 79–107.
- [14] D. Aharonov, X. Gao, Z. Landau, Y. Liu, and U. Vazirani, A polynomial-time classical algorithm for noisy random circuit sampling, Proceedings of the 55th Annual ACM Symposium on Theory of Computing, 945 (2023).
- [15] T. Schuster, C. Yin, X. Gao, and N. Y. Yao, A polynomial-time classical algorithm for noisy quantum circuits, arXiv preprint arXiv:2407.12768 https://doi.org/10.48550/arXiv.2407.12768 (2024).
- [16] E. Fontana, M. S. Rudolph, R. Duncan, I. Rungger, and C. Cîrstoiu, Classical simulations of noisy variational quantum circuits (2023), arXiv:2306.05400 [quant-ph].
- [17] A. Angrisani, A. Schmidhuber, M. S. Rudolph, M. Cerezo, Z. Holmes, and H.-Y. Huang, Classically estimating observables of noiseless quantum circuits, arXiv preprint arXiv:2409.01706 (2024).
- [18] P. Rall, D. Liang, J. Cook, and W. Kretschmer, Simulation of qubit quantum circuits via pauli propagation, Physical Review A 99, 062337 (2019).
- [19] G. González-García, J. I. Cirac, and R. Trivedi, Pauli path simulations of noisy quantum circuits beyond average case, arXiv preprint arXiv:2407.16068 (2024).
- [20] T. Begušić, J. Gray, and G. K.-L. Chan, Fast and converged classical simulations of evidence for the utility of quantum computing before fault tolerance, Science Advances 10, 10.1126/sciadv.adk4321 (2024).
- [21] M. S. Rudolph, E. Fontana, Z. Holmes, and L. Cincio, Classical surrogate simulation of quantum systems with LOWESA, arXiv preprint arXiv:2308.09109 (2023).
- [22] Y. Shao, F. Wei, S. Cheng, and Z. Liu, Simulating noisy variational quantum algorithms: A polynomial approach, Physical Review Letters 133, 120603 (2024).
- [23] T. Begušić and G. K.-L. Chan, Real-time operator evolution in two and three dimensions via sparse pauli dynamics, PRX Quantum 6, 020302 (2025).
- [24] S. Lerch, R. Puig, M. Rudolph, A. Angrisani, T. Jones, M. Cerezo, S. Thanasilp, and Z. Holmes, Efficient quantum-enhanced classical simulation for patches of quantum landscapes, arXiv preprint arXiv:2411.19896 10.48550/arXiv.2411.19896 (2024).
- [25] P. Bermejo, B. Aizpurua, and R. Orús, Improving gradient methods via coordinate transformations: Applications to

- quantum machine learning, Physical Review Research 6, 023069 (2024).
- [26] M. S. Rudolph, T. Jones, Y. Teng, A. Angrisani, and Z. Holmes, Pauli propagation: A computational framework for simulating quantum systems, arXiv preprint arXiv:2505.21606 (2025).
- [27] V. Upreti and U. Chabaud, Interplay of resources for universal continuous-variable quantum computing, arXiv preprint arXiv:2502.07670 https://doi.org/10.48550/arXiv.2502.07670 (2025).
- [28] V. Veitch, C. Ferrie, D. Gross, and J. Emerson, Negative quasi-probability as a resource for quantum computation, New Journal of Physics 14, 113011 (2012).
- [29] A. Mari and J. Eisert, Positive Wigner functions render classical simulation of quantum computation efficient, Physical Review Letters 109, 230503 (2012).
- [30] H. Pashayan, J. J. Wallman, and S. D. Bartlett, Estimating outcome probabilities of quantum circuits using quasiprobabilities, Physical Review Letters 115, 070501 (2015).
- [31] S. Rahimi-Keshari, T. C. Ralph, and C. M. Caves, Sufficient conditions for efficient classical simulation of quantum optics, Phys. Rev. X 6, 021039 (2016).
- [32] U. Chabaud, R. Ghobadi, S. Beigi, and S. Rahimi-Keshari, Phase-space negativity as a computational resource for quantum kernel methods, Quantum 8, 1519 (2024).
- [33] M. Frigerio, A. Debray, N. Treps, and M. Walschaers, Simulability of non-classical continuous-variable quantum circuits (2024), arXiv:2410.09226 [quant-ph].
- [34] A. Lund, S. Rahimi-Keshari, and T. Ralph, Exact boson sampling using gaussian continuous-variable measurements, Physical Review A 96, 022301 (2017).
- [35] J. J. Renema, A. Menssen, W. R. Clements, G. Triginer, W. S. Kolthammer, and I. A. Walmsley, Efficient classical algorithm for boson sampling with partially distinguishable photons, Phys. Rev. Lett. 120, 220502 (2018).
- [36] R. García-Patrón, J. J. Renema, and V. Shchesnovich, Simulating boson sampling in lossy architectures, Quantum 3, 169 (2019).
- [37] J. J. Renema, Simulability of partially distinguishable superposition and gaussian boson sampling, Phys. Rev. A 101, 063840 (2020).
- [38] H. Qi, D. J. Brod, N. Quesada, and R. García-Patrón, Regimes of classical simulability for noisy gaussian boson sampling, Phys. Rev. Lett. 124, 100502 (2020).
- [39] C. Oh, K. Noh, B. Fefferman, and L. Jiang, Classical simulation of lossy boson sampling using matrix product operators, Physical Review A 104, 022407 (2021).
- [40] M. Liu, C. Oh, J. Liu, L. Jiang, and Y. Alexeev, Simulating lossy gaussian boson sampling with matrix-product operators, Physical Review A 108, 052604 (2023).
- [41] C. Oh, M. Liu, Y. Alexeev, et al., Classical algorithm for simulating experimental gaussian boson sampling, Nature Physics 20, 1461 (2024).
- [42] C. Oh, Classical simulability of constant-depth linearoptical circuits with noise, npj Quantum Information 11, 126 (2025).

- [43] M. Walschaers, Non-gaussian quantum states and where to find them, PRX quantum 2, 030204 (2021).
- [44] S. D. Bartlett, B. C. Sanders, S. L. Braunstein, and K. Nemoto, Efficient classical simulation of continuous variable quantum information processes, Physical Review Letters 88, 097904 (2002).
- [45] S. Lloyd and S. L. Braunstein, Quantum computation over continuous variables, Phys. Rev. Lett. 82, 1784 (1999).
- [46] S. Sefi and P. van Loock, How to decompose arbitrary continuous-variable quantum operations, Phys. Rev. Lett. 107, 170501 (2011).
- [47] F. Arzani, R. I. Booth, and U. Chabaud, Can effective descriptions of bosonic tems considered complete?, arXiv:2501.13857 https://doi.org/10.48550/arXiv.2501.13857 (2025).
- [48] D. Aharonov, M. Ben-Or, R. Impagliazzo, and N. Nisan, Limitations of noisy reversible computation, arXiv preprint quant-ph/9611028 (1996).
- [49] A. Müller-Hermes, D. Stilck França, and M. M. Wolf, Relative entropy convergence for depolarizing channels, Journal of Mathematical Physics 57, 022202 (2016).
- [50] C. Hirche, C. Rouzé, and D. Stilck França, On contraction coefficients, partial orders and approximation of capacities for quantum channels, Quantum 6, 862 (2022).
- [51] S. Wang, E. Fontana, M. Cerezo, K. Sharma, A. Sone, L. Cincio, and P. J. Coles, Noise-induced barren plateaus in variational quantum algorithms, Nature Communications 12, 1 (2021).
- [52] Y. Quek, D. Stilck França, S. Khatri, J. J. Meyer, and J. Eisert, Exponentially tighter bounds on limitations of quantum error mitigation, Nature Physics 20, 1648 (2024).
- [53] If a cubic phase gate acted on a different mode, it could equivalently be represented as a cubic gate acting on the first mode, preceded and followed by swap gates. Since swaps are Gaussian operations, they can be absorbed into the surrounding Gaussian unitaries  $\mathcal{G}_j$ .
- [54] D. Stilck França and R. Garcia-Patron, Limitations of optimization algorithms on noisy quantum devices, Nature Physics 17, 1221 (2021).
- [55] G. De Palma, M. Marvian, C. Rouzé, and D. Stilck França, Limitations of variational quantum algorithms: a quantum optimal transport approach, PRX Quantum 4, 010309 (2023).
- [56] A. A. Mele, A. Angrisani, S. Ghosh, S. Khatri, J. Eisert, D. Stilck França, and Y. Quek, Noise-induced shallow circuits and absence of barren plateaus, arXiv preprint arXiv:2403.13927 (2024).
- [57] R. Ibarrondo and D. Stilck França, Average contraction coefficients of quantum channels, arXiv preprint arXiv:2508.08214 10.48550/arXiv.2508.08214 (2025).
- [58] A. Angrisani, A. A. Mele, M. S. Rudolph, M. Cerezo, and Z. Holmes, Simulating quantum circuits with arbitrary local noise using pauli propagation, arXiv preprint arXiv:2501.13101 10.48550/arXiv.2501.13101 (2025).
- [59] G. De Palma, M. Marvian, D. Trevisan, and S. Lloyd, The quantum wasserstein distance of order 1, IEEE Transactions on Information Theory 67, 6627 (2021).

- [60] C. Hirche, C. Rouzé, and D. Stilck França, Quantum differential privacy: An information theory perspective, IEEE Transactions on Information Theory 69, 5771 (2023).
- [61] V. Martinez, A. Angrisani, E. Pankovets, O. Fawzi, and D. Stilck França, Efficient simulation of parametrized quantum circuits under nonunital noise through pauli backpropagation, Physical Review Letters 134, 250602 (2025).
- [62] Y. Lim and C. Oh, Efficient classical algorithms for linear optical circuits (2025), arXiv:2502.12882 [quant-ph].
- [63] C. Oh and Y. Lim, Classical algorithms for measurementadaptive gaussian circuits (2025), arXiv:2509.00746 [quantph].
- [64] B. Baumgartner, An inequality for the trace of matrix products, using absolute values, arXiv preprint arXiv:1106.6189 (2011).
- [65] U. Chabaud, T. Douce, F. Grosshans, E. Kashefi, and D. Markham, Building trust for continuous variable quantum states, in 15th Conference on the Theory of Quantum Computation, Communication and Cryptography (2020) arXiv:1905.12700.
- [66] M. A. Nielsen and I. L. Chuang, Quantum Computation and Quantum Information: 10th Anniversary Edition (Cambridge University Press, New York, NY, USA, 2011).
- [67] S. L. Braunstein and P. van Loock, Quantum information with continuous variables, Rev. Mod. Phys. 77, 513 (2005).
- [68] A. Ferraro, S. Olivares, and M. G. Paris, Gaussian states in continuous variable quantum information (Bibliopolis, Napoli, 2005).
- [69] C. Weedbrook, S. Pirandola, R. García-Patrón, N. J. Cerf, T. C. Ralph, J. H. Shapiro, and S. Lloyd, Gaussian quantum information, Rev. Mod. Phys. 84, 621 (2012).
- [70] A. Serafini, Quantum Continuous Variables: A Primer of Theoretical Methods (CRC Press, Taylor & Francis Group, Boca Raton, USA, 2017).
- [71] N. Budinger, A. Furusawa, and P. van Loock, All-optical quantum computing using cubic phase gates, Phys. Rev. Res. 6, 023332 (2024).

# Supplementary Material

# Table of Contents

A	Notation	13
В	Mathematical preliminaries  1 Useful technical results	<b>13</b>
	2 Monte Carlo methods	17
$\mathbf{C}$	Bosonic quantum information	19
	1 Evolution of displacement operators under the effect of bosonic channels	22
	2 Coherent state projectors as probability distributions	26
$\mathbf{D}$	Technical lemmas for bosonic operators	27
	1 Curvature bound for the noisy characteristic function	27
	2 Estimating first and second moment of quadratures	29
	3 Useful decompositions of bosonic channels	31
$\mathbf{E}$	m up: Overlap decay under uniform noise 33	
$\mathbf{F}$	Sampling from the Fourier-Weyl spectrum	34
	1 Unbiased oracles	35
	2 Biased oracle	38
$\mathbf{G}$	Classical simulation of noisy bosonic circuits	40
	Noise-induced concentration in estimation of global observables	40
	2 Unbiased estimator	44
	3 Adaptive algorithms	47

# Appendix A: Notation

Symbol	Definition
$\mathbb{R}$	Set of real numbers
$\mathbb{R}^*$	Set of real numbers excluding zero
$\mathbb{C}$	Set of complex numbers
$\mathbb{C}^*$	Set of complex numbers excluding zero
$\mathbb{N}$	Set of natural numbers
$\mathbb{N}^*$	Set of natural numbers excluding zero
$A \succeq B$	The operator $A - B$ is positive semidefinite
$\Gamma(\cdot)$	Gamma function, $\Gamma(n+\frac{1}{2}) = \binom{n-\frac{1}{2}}{n} n! \sqrt{\pi}$ for $n \in \mathbb{N}$
$\delta(\cdot)$	Dirac delta function
$\mathcal{N}(\mu, \sigma^2)$	Normal distribution with mean $\mu$ and variance $\sigma^2$
$Gamma(\alpha, \lambda)$	Gamma distribution with shape $\alpha$ and rate $\lambda$
m	Number of modes of a bosonic system
$\mathbb{I}$	Infinite-dimensional identity operator
Ω	Standard symplectic form, $\Omega := \bigoplus_{j=1}^{m} \begin{bmatrix} 0 & 1 \\ -1 & 0 \end{bmatrix}$
r	2 <i>m</i> -dimensional quadrature vector, i.e. $\mathbf{r} = (q_1, p_1, q_2, p_2, \dots, q_m, p_m) \in \mathbb{R}^{2m}$
$\hat{D}(m{r})$	Fourier–Weyl operator associated to the displacement $m{r}$
r angle	Coherent state associated to the displacement $r$ , $ r\rangle \coloneqq \hat{D}(r) 0\rangle$
$ \hbar $	Reduced Planck constant, we adopt the convention $\hbar = 2$ throughout this work
$ \hat{a},\hat{a}^{\dagger} $	Annihilation $(\hat{a})$ and creation $(\hat{a}^{\dagger})$ operators, satisfying $[\hat{a}, \hat{a}^{\dagger}] = \mathbb{I}$
$ \hat{p},\hat{q} $	Position $(\hat{q} := \hat{a} + \hat{a}^{\dagger})$ and momentum $\hat{p} := -i(\hat{a} - \hat{a}^{\dagger})$ operators, satisfying $[\hat{q}, \hat{p}] = 2i \mathbb{I}$
$ \hat{n} $	Single-mode particle number operator, $\hat{n} \coloneqq \hat{a}^{\dagger} \hat{a} = \frac{1}{4} \left( \hat{p}^2 + \hat{q}^2 - 2\mathbb{I} \right)$
$\ f\ _{L_p}$	$p$ -norm of an $L^p$ -integrable function $f: \mathcal{X} \to \mathbb{C}$ , $  f  _p \coloneqq \left(\int_{x \in \mathcal{X}} dx  f(x) ^p\right)^{\frac{1}{p}}$
$ \chi_{\hat{O}} $	characteristic function of the operator $\hat{O}$ , $\chi_{\hat{O}}(r) := \text{Tr}[OD(r)]$
$\begin{split} \ \hat{O}\ _p \\ \ \hat{O}\ _{\mathbb{F},p} \end{split}$	Schatten <i>p</i> -norm, i.e. $\ \hat{O}\ _p := \text{Tr}\left[\left \hat{O}\right ^p\right]^{\frac{1}{p}}$ , where $ \hat{O}  = \sqrt{\hat{O}^{\dagger}\hat{O}}$
$\ \hat{O}\ _{\mathbb{F},p}$	Fourier p-norm (Def. C.1). If $\chi_{\hat{O}}$ is $L^p$ -integrable, then $\ O\ _{\mathbb{F},p} \coloneqq \left(\int_{\mathbb{R}^{2m}} d\mathbf{r} \left  \frac{\chi_{\hat{O}}(\mathbf{r})}{\pi^m} \right ^p \right)^{\frac{1}{p}}$

# Appendix B: Mathematical preliminaries

We start by giving the mathematical preliminaries that will be repeatedly used throughout the paper. We begin with a few technical lemmas concerning measure theory, norm inequalities, and approximation bounds, and then recall some standard results from probability theory that underlie our Monte Carlo methods.

# 1. Useful technical results

The following result will be useful for deriving simple upper bounds on high-dimensional integrals.

**Lemma B.1.** The volume of the 2m-dimensional ball of radius  $\tau$  equals  $\frac{\pi^m}{m!}\tau^{2m}$ .

The following Lemma provides a standard result on the manipulation of multi-dimensional integrals.

**Lemma B.2** (Fubini-Tonelli's theorem). Let  $f: \mathbb{R}^2 \to [0, \infty)$  be an integrable function. Then the following identities hold

$$\int_{\mathbb{R}^2} f(x, y) dx dy = \int_{\mathbb{R}} \left( \int_{\mathbb{R}} f(x, y) dy \right) dx = \int_{\mathbb{R}} \left( \int_{\mathbb{R}} f(x, y) dx \right) dy.$$
 (B1)

We then have the following result for a special type of integral that will be important for the work:

**Lemma B.3.** Given  $a, b \in \mathbb{R}, A \in \mathbb{R}^+$ , then

$$I = \int_{\mathbb{R}} dx \frac{e^{-A(ax+b)^2}}{\sqrt{|ax+b|}} = \frac{\Gamma(1/4)}{Aa^{1/4}}.$$
 (B2)

*Proof.* Given the integral

$$\int_{\mathbb{R}} dx \frac{e^{-A(ax+b)^2}}{\sqrt{|ax+b|}} = \int_{\mathbb{R}} dx \frac{e^{-A(|a|x + \text{sgn}(a)b)^2}}{\sqrt{||a|x + \text{sgn}(a)b|}},$$
(B3)

we first make the substitution

$$u = |a|x + \operatorname{sgn}(a)b,$$
  

$$du = |a|dx,$$
(B4)

to get

$$I = \frac{1}{|a|} \int_{\mathbb{R}} du \frac{e^{-Au^2}}{\sqrt{|u|}}.$$
 (B5)

Again, making the substitution

$$a = \sqrt{A}u,$$

$$da = \sqrt{A}du.$$
 (B6)

We get

$$I = \frac{1}{|a|A^{1/4}} \int_{\mathbb{R}} da \frac{e^{-a^2}}{\sqrt{|a|}} = \frac{2}{aA^{1/4}} \int_{\mathbb{R}^+} da \frac{e^{-a^2}}{\sqrt{|a|}} = \frac{4\Gamma(5/4)}{|a|A^{1/4}} = \frac{\Gamma(1/4)}{|a|A^{1/4}}.$$
 (B7)

We next recall a classical expansion formula that will be useful when approximating integrals and operator-valued functions.

**Theorem B.1** (Taylor's remainder theorem). Let  $f: \mathbb{R} \to \mathbb{R}$  be k+1 times differentiable on the open interval between a and x with  $f^{(k)}$  continuous on the closed interval between a and x. Then

$$f(x) = \sum_{j=0}^{k} \frac{f^{(j)}(a)}{j!} (x - a)^{j} + \frac{f^{k+1}(y)}{(k+1)!} (x - a)^{k+1},$$
(B8)

for some y between a and x, with  $k \ge 1$ .

As an immediate application of Taylor's theorem, we state the following Lemma for approximating oscillatory integrals:

Lemma B.4 (Integral approximation). Given integral

$$I(f, x') = \frac{e^{-i\pi/4}}{\sqrt{\pi\sigma}} \int dx \exp\left(i\frac{(x - x')^2}{\sigma}\right) f(x).$$
 (B9)

It holds that

$$|I(f, x') - f(x')| \leqslant \frac{|\sigma|}{4} \max_{\xi \in \mathbb{R}} |f''(\xi)|. \tag{B10}$$

*Proof.* We first note that the integral can be rewritten as

$$I(f, x') = \frac{e^{-i\pi/4}e^{\epsilon x'^2}}{\sqrt{\pi\sigma}} \int dx \exp\left(-\left(\epsilon - \frac{i}{\sigma}\right)(x - x')^2\right) e^{\epsilon x^2 - 2\epsilon xx'} f(x)$$
(B11)

for some  $\epsilon > 0$ . We denote  $g_{\epsilon}(x) := e^{\epsilon x^2 - 2\epsilon xx'} f(x)$  and using Taylor's remainder theorem (Theorem B.1) on g(x)

$$g_{\epsilon}(x) = g_{\epsilon}(x') + (x - x')g_{\epsilon}'(x') + \frac{(x - x')^2}{2!}g_{\epsilon}''(\xi)$$
(B12)

for some  $\xi \in \mathbb{R}$ , possibly dependent on  $\epsilon$ . Using the fact that

$$\frac{e^{-i\pi/4} e^{\epsilon x'^2}}{\sqrt{\pi \sigma}} \int dx \exp\left(-(\epsilon - i/\sigma)(x - x')^2\right) = \frac{e^{-i\pi/4} e^{\epsilon x'^2}}{\sqrt{\pi \sigma}} \times \sqrt{\frac{\pi}{\epsilon - i/\sigma}} = e^{-i\pi/4 + \epsilon x'^2} \sqrt{\frac{1}{(\epsilon \sigma - i)}},$$
(B13)

$$\frac{e^{-i\pi/4} e^{\epsilon x'^2}}{\sqrt{\pi \sigma}} \int dx \exp\left(-(\epsilon - i/\sigma)(x - x')^2\right) (x - x') = 0 \text{ (Odd function)}, \tag{B14}$$

$$\frac{e^{-i\pi/4} e^{\epsilon x'^2}}{\sqrt{\pi \sigma}} \int dx \exp\left(-(\epsilon - i/\sigma)(x - x')^2\right) (x - x')^2 = \frac{e^{-i\pi/4} e^{\epsilon x'^2}}{\sqrt{\pi \sigma}} \times \frac{\sqrt{\pi}}{2(\epsilon - i/\sigma)^{3/2}} = \frac{e^{-i\pi/4 + \epsilon x'^2}}{2} \frac{\sigma}{(\epsilon \sigma - i)^{3/2}}.$$
 (B15)

We get, for all  $\epsilon > 0$ 

$$I(f,x') = g_{\epsilon}(x')e^{-i\pi/4 + \epsilon x'^2} \sqrt{\frac{1}{(\epsilon \sigma - i)}} + \frac{e^{-i\pi/4 + \epsilon x'^2}}{2} \frac{\sigma}{(\epsilon \sigma - i)^{3/2}} \frac{g_{\epsilon}''(\xi)}{2!}.$$
 (B16)

Taking the one-sided limit  $\epsilon \to 0^+$ , we find that

$$I(f, x') = \lim_{\epsilon \to 0^+} g_{\epsilon}(x') e^{-i\pi/4 + \epsilon x'^2} \sqrt{\frac{1}{(\epsilon \sigma - i)}} + \lim_{\epsilon \to 0^+} \frac{e^{-i\pi/4 + \epsilon x'^2}}{2} \frac{\sigma}{(\epsilon \sigma - i)^{3/2}} \frac{g_{\epsilon}''(\xi_{\epsilon})}{2!}$$
(B17)

$$= f(x') + \lim_{\epsilon \to 0^+} \frac{e^{-i\pi/4 + \epsilon x'^2}}{2} \frac{\sigma}{(\epsilon \sigma - i)^{3/2}} \frac{g''(\xi_{\epsilon})}{2!}, \tag{B18}$$

and therefore,

$$|I(f,x') - f(x')| \leqslant \max_{\xi \in \mathbb{R}} \left| \lim_{\epsilon \to 0^+} \frac{e^{-i\pi/4 + \epsilon x'^2}}{2} \frac{\sigma}{(\epsilon \sigma - i)^{3/2}} \frac{g_{\epsilon}''(\xi)}{2!} \right|.$$
 (B19)

$$= \frac{|\sigma|}{4} \max_{\xi \in \mathbb{R}} \left| \lim_{\epsilon \to 0^+} g_{\epsilon}''(\xi) \right|. \tag{B20}$$

Let us evaluate the second derivative of  $g_{\epsilon}$  and compute the one-sided limit.

$$g_{\epsilon}''(x) = e^{\epsilon(x^2 - 2xx')} \left[ f''(x) + 4\epsilon(x - x')f'(x) + 2\epsilon \left( 1 + 2\epsilon(x - x')^2 \right) f(x) \right] \xrightarrow{\epsilon \to 0^+} f''(x).$$
 (B21)

We now recall some fundamental definitions and inequalities that will be central for handling operator norms.

**Definition B.1** (Schatten p-norms). Let  $\mathcal{H}$  be a (possibly infinite-dimensional) Hilbert space and let O be a compact operator on  $\mathcal{H}$ . For  $p \in [1, \infty)$ , the Schatten p-norm of O is defined as

$$||O||_p := (\operatorname{Tr}[|O|^p])^{\frac{1}{p}},$$
 (B22)

whenever the trace is finite. For  $p = \infty$ , the Schatten  $\infty$ -norm coincides with the operator norm:

$$||O||_{\infty} := \sup_{\rho:||\rho||_1=1} \text{Tr}[O\rho], \tag{B23}$$

where the supremum is taken over all trace-class operators  $\rho$  with unit trace norm.

One of the key tools associated with Schatten norms is Hölder's inequality, which we state next in the operator setting.

**Lemma B.5** (Hölder's inequality [64]). Let  $p, q \in [1, \infty]$  such that  $\frac{1}{p} + \frac{1}{q} = 1$ , and let A, B be two operators such that  $\|A\|_p$  and  $\|B\|_q$  are finite. Then,

$$|\text{Tr}[AB]| \leqslant ||A||_n ||B||_q. \tag{B24}$$

Finally, we provide a simple but useful inequality relating the expectation value of an operator to its symmetrized second moment.

**Lemma B.6** (Tracial second moment). Let A be an operator and  $\rho$  be a quantum state.

$$\left|\operatorname{Tr}[A\rho]\right|^2 \leqslant \frac{1}{2}\operatorname{Tr}\left[\{A, A^{\dagger}\}\rho\right].$$
 (B25)

*Proof.* We decompose A in its Hermitian and anti-Hermitian components:

$$A = A_1 + iA_2, \tag{B26}$$

$$A_1 = \frac{A + A^{\dagger}}{2},\tag{B27}$$

$$A_2 = \frac{A - A^{\dagger}}{2i},\tag{B28}$$

where  $A_1$  and  $A_2$  are both Hermitian, and therefore  $iA_2$  is anti-Hermitian. We have that

$$|\text{Tr}[A\rho]|^2 = |\text{Tr}[A_1\rho] + i \,\text{Tr}[A_2\rho]|^2 = \text{Tr}[A_1\rho]^2 + \text{Tr}[A_2\rho]^2,$$
 (B29)

where we used the fact that  $|x+iy|^2 = x^2 + y^2$  for  $x, y \in \mathbb{R}$ . Moreover, for any hermitian operator H, the variance  $\text{Tr}[H^2\rho] - \text{Tr}[H\rho]^2$  is always non-negative, hence

$$\operatorname{Tr}[A_1 \rho]^2 \leqslant \operatorname{Tr}[A_1^2 \rho] = \frac{1}{4} \operatorname{Tr}[(A^2 + (A^{\dagger})^2 + \{A, A^{\dagger}\})\rho],$$
 (B30)

$$\operatorname{Tr}[A_2 \rho]^2 \leqslant \operatorname{Tr}[A_2^2 \rho] = \frac{1}{4} \operatorname{Tr}[(-A^2 - (A^{\dagger})^2 + \{A, A^{\dagger}\})\rho].$$
 (B31)

Putting all together, we find that

$$|\text{Tr}[A\rho]|^2 \leqslant \frac{1}{2} \,\text{Tr}[\{A, A^{\dagger}\}\rho].$$
 (B32)

#### 2. Monte Carlo methods

The simulation algorithms presented in the paper build on the Monte Carlo sampling techniques. Here, we present an overview of these techniques. In their essence, these sampling techniques consists of approximating the value of a given integral by sampling a random variable from an appropriately defined probability distribution and computing the value of an estimator function at that point, such that the expectation value of the estimator function over the probability distribution gives the value of this integral. Finally, we take the average of the N such sampled values of the estimator function and the statistical sampling error depends on the range of this estimator function.

We say that a real-valued random variable X is distributed with respect to a probability density function (PDF)  $f_X(x)$  if for all  $a, b \in \mathbb{R}, a \leq b$ ,

$$\Pr[a \leqslant X \leqslant b] = \int_{a}^{b} f_X(x) dx. \tag{B33}$$

Equivalently, the distribution of X can be entirely described by the associated cumulative distribution function (CDF)  $F_X(x) = \int_{-\infty}^x f_X(t)dt$ :

$$\Pr[a \leqslant X \leqslant b] = F_X(b) - F_X(a). \tag{B34}$$

Here, we will give some results that will help us in building Monte Carlo methods for our expectation value estimation problem in the subsequent sections.

**Lemma B.7** (Chernoff-Hoeffding bound [65]). Let  $\lambda > 0$ , let  $n \ge 1$ , let  $z_1, \ldots, z_n$  be i.i.d. complex random variables from a probability density  $\mathcal{D}$  over  $\mathbb{R}$ , and let  $f: \mathbb{C} \mapsto \mathbb{R}$  such that  $|f(z)| \le M$ , for M > 0 and all  $z \in \mathbb{C}$ . Then

$$\Pr\left[\left|\frac{1}{n}\sum_{i=1}^{n}f(z_{i})-\mathbb{E}_{z\sim D}[f(z)]\right|\geqslant\lambda\right]\leqslant2\exp\left[-\frac{n\lambda^{2}}{2M^{2}}\right].$$
(B35)

The following two Lemmas construct the probability distributions and estimator functions for approximating values of two different types of integrals, which will enable the development of simulation algorithms in our subsequent work.

**Lemma B.8** (Integral approximation via shifted–Gaussian samples). Let  $a,b \in \mathbb{R}$ , A > 0, and  $G : \mathbb{R} \to \mathbb{C}$  satisfy  $\|G\|_{L_{\infty}} \leq 1$ . Define

$$I = \int_{\mathbb{R}} e^{-A(ay+b)^2} G(y) dy.$$
 (B36)

If we draw

$$Y \sim \mathcal{N}\left(\mu, \sigma^2\right), \quad \mu = -\frac{b}{a}, \quad \sigma^2 = \frac{1}{2Aa^2},$$
 (B37)

then the importance-sampling estimator

$$X = \frac{e^{-A(aY+b)^2}}{p(Y)}G(Y), \tag{B38}$$

where

$$p(y) = \frac{1}{\sqrt{2\pi}\sigma} \exp\left(-\frac{(y-\mu)^2}{2\sigma^2}\right) = \sqrt{\frac{A}{\pi}} a \exp\left[-A(ay+b)^2\right],$$
 (B39)

satisfies

$$\mathbb{E}[X] := \mathbb{E}_{Y \sim p}[X(Y)] = I, \quad |X| \le \frac{\sqrt{\pi/A}}{|a|}.$$
 (B40)

In particular, X is unbiased and uniformly bounded in magnitude by  $\sqrt{\pi/A}/|a|$ .

*Proof.* We choose  $Y \sim \mathcal{N}(\mu, \sigma^2)$  with

$$\mu = -\frac{b}{a}, \qquad \sigma^2 = \frac{1}{2A a^2}.$$
 (B41)

Its density is

$$p(y) = \frac{1}{\sqrt{2\pi}\sigma} \exp\left(-\frac{(y-\mu)^2}{2\sigma^2}\right) = \sqrt{\frac{A}{\pi}} \ a \ \exp\left[-A (ay+b)^2\right]. \tag{B42}$$

Notice that p(y) is proportional to the Gaussian kernel in the integrand.

$$I = \int_{\mathbb{R}} e^{-A(ay+b)^2} G(y) \, dy = \int_{\mathbb{R}} \underbrace{\frac{e^{-A(ay+b)^2}}{p(y)}}_{=X(y)} G(y) \, p(y) \, dy = \mathbb{E}_{Y \sim p}[X(Y)], \tag{B43}$$

one obtains the unbiased estimator

$$X = \frac{e^{-A(aY+b)^2}}{p(Y)}G(Y).$$
 (B44)

Since by construction  $p(Y) = \sqrt{\frac{A}{\pi}} a e^{-A(aY+b)^2}$ , the weight simplifies to

$$\frac{e^{-A(aY+b)^2}}{p(Y)} = \frac{1}{\sqrt{\frac{A}{\pi}} a} = \frac{\sqrt{\pi/A}}{a}.$$
 (B45)

Hence

$$X = \frac{\sqrt{\pi/A}}{a} G(Y), \qquad |X| \le \frac{\sqrt{\pi/A}}{|a|} \|G\|_{L_{\infty}} \le \frac{\sqrt{\pi/A}}{|a|}.$$
 (B46)

Thus X is an unbiased estimator of I, with the simple deterministic bound

$$|X| \le \frac{\sqrt{\pi/A}}{|a|},\tag{B47}$$

as claimed.  $\Box$ 

**Lemma B.9** (Integral approximation via Gamma-distributed samples). Let  $a,b \in \mathbb{R}$  and  $A,B \in \mathbb{R}^+$ . Let  $G: \mathbb{R} \to \mathbb{C}$  such that  $\|G\|_{L_{\infty}} \leq 1$ . Consider the integral

$$I = \int_{\mathbb{R}} \frac{e^{-A(ay+b)^2}}{B\sqrt{|ay+b|}} G(y) dy.$$
 (B48)

Then, using only draws from the Gamma distribution  $\operatorname{Gamma}(\frac{1}{4}, A)$ , one may generate a random variable X such that

$$\mathbb{E}[X] = I \qquad and \qquad |X| \leqslant \frac{\Gamma(\frac{1}{4})A^{-\frac{1}{4}}}{aB}. \tag{B49}$$

*Proof.* We start by performing the change of variable defined by the linear map  $y \mapsto t = ay + b$ . Then dy = dt/a and

$$I = \int_{\mathbb{R}} \frac{e^{-At^2}}{aB\sqrt{|t|}} G\left(\frac{t-b}{a}\right) dt = I_- + I_+, \tag{B50}$$

$$I_{-} = \int_{-\infty}^{0} \frac{e^{-At^2}}{aB\sqrt{|t|}} G\left(\frac{t-b}{a}\right) dt, \tag{B51}$$

$$I_{+} = \int_{0}^{\infty} \frac{e^{-At^{2}}}{aB\sqrt{|t|}} G\left(\frac{t-b}{a}\right) dt \tag{B52}$$

We further perform the changes of variable  $t \mapsto -\sqrt{u}$  and  $t \mapsto \sqrt{u}$  respectively in the integrals  $I_-$  and  $I_+$ :

$$I_{-} = \int_{0}^{\infty} \frac{e^{-Au}}{2aBu^{\frac{3}{4}}} G\left(\frac{-\sqrt{u} - b}{a}\right) du \tag{B53}$$

$$I_{+} = \int_{0}^{\infty} \frac{e^{-Au}}{2aBu^{\frac{3}{4}}} G\left(\frac{\sqrt{u} - b}{a}\right) du$$
(B54)

Recall the Gamma( $\alpha, \beta$ ) probability density function with shape  $\alpha$  and rate  $\beta$  is

$$f(u) = \frac{\beta^{\alpha}}{\Gamma(\alpha)} u^{\alpha - 1} e^{-\beta u}.$$
 (B55)

For  $\alpha = \frac{1}{4}$ ,  $\beta = A$ , this is

$$f(u) = \frac{A^{1/4}}{\Gamma(\frac{1}{4})} u^{-3/4} e^{-Au}.$$
 (B56)

Hence the integral I can be rewritten as

$$I = \frac{1}{2} \int_0^\infty f(u) H_-(u) du + \frac{1}{2} \int_0^\infty f(u) H_+(u) du,$$
 (B57)

where  $H_{\pm}(u) = \frac{\Gamma(\frac{1}{4})}{aA^{1/4}B}G\left(\frac{\pm\sqrt{u}-b}{a}\right)$ . Thus, given  $U \sim \text{Gamma}(\frac{1}{4},A)$ , we define the derived random variable "sgn" which equals – with probability 1/2 and + with probability 1/2. Lets denote this 50-50 probability distribution for "sgn" by  $p_{\text{flip}}$ . Then

$$\mathbb{E}[X] = \mathbb{E}_{U \sim \text{Gamma}(\frac{1}{4}, A), \text{sgn} \sim p_{\text{flip}}} [H_{\text{sgn}}(U)] = I.$$
(B58)

$$\text{Moreover, } |X|\leqslant \|H\|_{L_\infty}\leqslant \frac{\Gamma\left(\frac{1}{4}\right)}{aA^{1/4}B}\|G\|_{L_\infty}\leqslant \frac{\Gamma\left(\frac{1}{4}\right)}{aA^{1/4}B}.$$

## Appendix C: Bosonic quantum information

This paper deals with bosonic or continuous variable (CV) quantum information, and this section aims to provide a brief overview of the relevant background information needed to understand the work. We refer the reader to [66] for background on quantum information theory and to [67–70] for detailed CV quantum information material.

Bosonic modes and quadratures. In CV quantum information, a mode refers to a degree of freedom associated with a specific quantum field of a CV quantum system, such as a single spatial or frequency mode of light, and is the equivalent of qubit in the CV regime. In this paper,  $m \in \mathbb{N}^*$  denotes the number of modes in the system. Hereafter,  $\{|n\rangle\}_{n\in\mathbb{N}}$  denote the single-mode Fock basis, with  $|0\rangle$  being the vacuum state, and  $\hat{a}$  and  $\hat{a}^{\dagger}$  refer to the single-mode

annihilation and creation operator, respectively, satisfying  $[\hat{a}, \hat{a}^{\dagger}] = \mathbb{I}$ . These are related to the position and momentum quadrature operators as

$$\hat{q} = \hat{a} + \hat{a}^{\dagger}, \quad \hat{p} = -i(\hat{a} - \hat{a}^{\dagger}), \tag{C1}$$

with the convention  $\hbar = 2$ . Furthermore,  $\hat{q}$  and  $\hat{p}$  satisfy the commutation relation  $[\hat{q}, \hat{p}] = 2i \mathbb{I}$ . The particle number operator is given as  $\hat{n} = \hat{a}^{\dagger}\hat{a}$ , whereas the energy operator is denoted by

$$\hat{N} = \sum_{j=1}^{m} \hat{N}_j = \sum_{j=1}^{m} \frac{\hat{q}_j^2 + \hat{p}_j^2}{2}.$$
 (C2)

Gaussian unitaries and states. Product of unitary operations generated by Hamiltonians that are quadratic in the quadrature operators of the modes are called Gaussian unitary operations, and states produced by applying a Gaussian unitary operation to the vacuum state are Gaussian states. The action of an m-mode Gaussian unitary operation  $\hat{G}$  on the vector of quadratures  $\mathbf{\Gamma} = [\hat{q}_1, \dots, \hat{q}_m, \hat{p}_1, \dots, \hat{p}_m]$  is given by

$$\hat{G}^{\dagger} \Gamma \hat{G} = S \Gamma + d, \tag{C3}$$

where S is a  $2m \times 2m$  symplectic matrix and  $\mathbf{d} \in \mathbb{R}^{2m}$  is a displacement vector, associated to the Gaussian unitary gate  $\hat{G}$ . Single-mode displacement operator can be written in terms of creation operators as

$$\hat{D}(\alpha) = e^{\alpha \hat{a}^{\dagger} - \alpha^* a} \tag{C4}$$

where  $\alpha \in \mathbb{C}$ , or in terms of the position and momentum operators as

$$\hat{D}(q,p) = e^{ip\hat{q} - iq\hat{p}}.$$
(C5)

where  $q_i, p_i \in \mathbb{R}$ , with  $q_i = \text{Re}(\alpha)$  and  $p_i = \text{Im}(\alpha)$ . Note that with our convention, we are writing the multimode displacement operator as

$$\hat{D}(\mathbf{r}) = \exp(i\hat{R}^T \Omega \mathbf{r}),\tag{C6}$$

with  $\mathbf{r} = \{q_1, p_1, \dots, q_m, p_m\}, \ \alpha_j = (q_j + ip_j)/2, \forall j, \ \hat{R} = [\hat{q}_1, \hat{p}_1, \dots, \hat{q}_m, \hat{p}_m] \ \text{and where}$ 

$$\Omega = \bigoplus_{i=1}^{m} \begin{bmatrix} 0 & 1 \\ -1 & 0 \end{bmatrix}. \tag{C7}$$

Finally, the single-mode state produced by the action of the displacement operator on the vacuum is called the coherent state,  $|\alpha\rangle = \hat{D}(\alpha)|0\rangle$ .

Displacement operator basis and characteristic functions. The set of displacement operators forms an operator basis, and therefore for any operator  $\hat{O}$  living in the *m*-mode Hilbert space  $\mathcal{H}^{\otimes m}$ , we can write

$$\hat{O} = \frac{1}{\pi^m} \int_{\alpha \in \mathbb{C}^m} d^{2m} \alpha \chi_{\hat{O}}(\alpha) \hat{D}^{\dagger}(\alpha), \tag{C8}$$

where  $\hat{D}(\boldsymbol{\alpha}) = \hat{D}(\boldsymbol{\alpha}_1) \otimes ... \otimes \hat{D}(\boldsymbol{\alpha}_m)$  is the multi-mode displacement operator, and  $\chi_{\hat{O}}(\boldsymbol{\alpha})$  is referred to as the *characteristic function* of the operator  $\hat{O}$ , and is given by

$$\chi_{\hat{O}}(\boldsymbol{\alpha}) = \text{Tr} \left[ \rho \hat{D}(\boldsymbol{\alpha}) \right].$$
 (C9)

As an example, the characteristic function of the single-mode coherent state  $|\beta\rangle$  (which would be useful later) is given by

$$\chi_{|\beta\rangle\langle\beta|}(\alpha) = \text{Tr}\left[|\beta\rangle\langle\beta|\,\hat{D}(\alpha)\right] = \langle\beta|\,\hat{D}(\alpha)\,|\beta\rangle = \exp(i\text{Im}(\alpha\beta^*))\,\langle\beta|\alpha + \beta\rangle$$
$$= \exp(i\text{Im}(\alpha\beta^*))\exp\left(-\frac{1}{2}|\beta|^2 - \frac{1}{2}|\alpha + \beta|^2 + \beta^*(\alpha + \beta)\right). \tag{C10}$$

Further in terms of characteristic function,

$$\operatorname{Tr}\left[\rho\hat{O}\right] = \frac{1}{\pi^m} \int_{\boldsymbol{\alpha} \in \mathbb{C}^m} d^{2m} \boldsymbol{\alpha} \chi_{\rho}^*(\boldsymbol{\alpha}) \chi_{\hat{O}}(\boldsymbol{\alpha}), \tag{C11}$$

where the identity follows from combining Eqs. C8 and C9 and interchanging the order of the trace and the integral by linearity. Finally the magnitude of the characteristic function of a quantum state  $\rho$ ,

$$\left| \operatorname{Tr} \left[ \rho \hat{D}(\boldsymbol{r}) \right] \right| \leqslant 1.$$
 (C12)

 $\forall \boldsymbol{r} \in \mathbb{R}^{2m}$ . This follows since

$$\left| \operatorname{Tr} \left[ \rho \hat{D}(\boldsymbol{r}) \right] \right| \leq \|\rho\|_1 \|\hat{D}(\boldsymbol{r})\|_{\infty} \leq 1 \times 1 = 1.$$
 (C13)

The first inequality follows from the Hölder's inequality (Lemma B.5) whereas the second inequality follows from the fact that for a quantum state  $\|\rho\|_1 = 1$  and that  $\forall \boldsymbol{r} \in \mathbb{R}^{2m}$ ,  $\|\hat{D}(\boldsymbol{r})\|_{\infty} = 1$  since the displacement operator is a unitary operator.

Fourier norms and operator inequalities. In order to study the properties of (noisy) bosonic systems, we introduce the following notion, which serves as a metric for the complexity of bosonic operators and directly reflects the cost of classically simulating expectation values.

**Definition C.1** (Fourier p-norms). Let  $\hat{O}$  be an operator whose characteristic function  $\chi_{\hat{O}}$  is in  $L^p$  (i.e. the p-th power of the absolute value of  $\chi_{\hat{O}}$  is Lebesgue integrable). Then the Fourier p-norm of  $\hat{O}$  is the defined as the p-norm of  $\chi_{\hat{O}}/\pi^m$ :

$$\|\hat{O}\|_{\mathbb{F},p} := \left( \int_{\mathbb{C}^m} d^{2m} \boldsymbol{\alpha} \left| \frac{\chi_{\hat{O}}(\boldsymbol{\alpha})}{\pi^m} \right|^p \right)^{\frac{1}{p}}. \tag{C14}$$

Moreover, if  $\hat{O}$  has a discrete spectrum in the displacement operator basis, i.e.  $\hat{O} := \sum_{i \in \mathbb{N}} c_i \hat{D}(\boldsymbol{\alpha}_i)$ , then the Fourier 1-norm of  $\hat{O}$  is defined as follows:

$$||O||_{\mathbb{F},p} := \left(\sum_{i \in \mathbb{N}} |c_i|^p\right)^{\frac{1}{p}}.$$
 (C15)

We also prove the following relation between the Fourier 1-norm and the operator norm (i.e. the Schatten  $\infty$ -norm), which can be regarded as a quantum extension of the Hausdorff-Young inequality.

**Lemma C.1** (Quantum Hausdorff–Young inequality). Let  $\hat{O}$  be an operator with finite Fourier 1-norm. Then it holds that

$$\|\hat{O}\|_{\infty} \leqslant \|\hat{O}\|_{\mathbb{F},1}.\tag{C16}$$

*Proof.* The result readily follows from the definition of Fourier 1-norm. If  $\chi_{\hat{O}}$  is  $L^1$  integrable, we have that

$$\|\hat{O}\|_{\infty} = \sup_{\rho:\|\rho\|_{1}=1} \left| \operatorname{Tr} \left[ \hat{O}\rho \right] \right| = \sup_{\rho:\|\rho\|_{1}=1} \left| \frac{1}{\pi^{m}} \int_{\boldsymbol{\alpha} \in \mathbb{C}^{m}} d^{2m} \boldsymbol{\alpha} \chi_{\hat{O}}(\boldsymbol{\alpha}) \operatorname{Tr} \left[ \hat{D}(-\boldsymbol{\alpha})\rho \right] \right|$$
(C17)

$$\leqslant \left(\frac{1}{\pi^m} \int_{\boldsymbol{\alpha} \in \mathbb{C}^m} d^{2m} \boldsymbol{\alpha} \left| \chi_{\hat{O}} \right| \right) \sup_{\substack{\rho : \|\rho\|_1 = 1, \\ \boldsymbol{\alpha} \in \mathbb{C}^m}} \left| \operatorname{Tr} \left[ \hat{D}(-\boldsymbol{\alpha}) \rho \right] \right| \leqslant \|\hat{O}\|_{\mathbb{F}, 1} \sup_{\boldsymbol{\alpha} \in \mathbb{C}^m} \|\hat{D}(\boldsymbol{\alpha})\|_{\infty} = \|\hat{O}\|_{\mathbb{F}, 1}, \tag{C18}$$

where we applied Minkowski's inequality in the second-to-last step and Hölder's inequality in the last step, and we noted that  $\|\hat{D}(\alpha)\|_{\infty} = 1$  Similarly, if  $\hat{O}$  is a weighted sum of displacement operators, we have that

$$\|\hat{O}\|_{\infty} = \sup_{\rho:\|\rho\|_{1}=1} \left| \operatorname{Tr} \left[ \hat{O}\rho \right] \right| = \sup_{\rho:\|\rho\|_{1}=1} \left| \sum_{i \in \mathbb{N}} c_{i} \operatorname{Tr} \left[ D(\boldsymbol{\alpha}_{i})\rho \right] \right| \leq \left( \sum_{i \in \mathbb{N}} |c_{i}| \right) \sup_{\substack{\rho:\|\rho\|_{1}=1\\\boldsymbol{\alpha} \in \mathbb{C}^{m}}} \left| \operatorname{Tr} \left[ \hat{D}(\boldsymbol{\alpha})\rho \right] \right|$$
(C19)

$$\leq \|\hat{O}\|_{\mathbb{F},1} \sup_{\boldsymbol{\alpha} \in \mathbb{C}^m} \|\hat{D}(\boldsymbol{\alpha})\|_{\infty} = \|\hat{O}\|_{\mathbb{F},1}, \tag{C20}$$

where we applied again Minkowski's inequality in the second-to-last step and Hölder's inequality in the last step, and we noted again that  $\|\hat{D}(\boldsymbol{\alpha})\|_{\infty} = 1$ .

Non-Gaussian operations. Non-Gaussian operations are necessary for enabling quantum advantage since Gaussian gates acting on Gaussian states and followed by Gaussian measurements can be classically simulated efficiently [44]. One prominent example of a non-Gaussian gate is the cubic phase gate  $e^{i\gamma\hat{q}^3}$  [1], whose action on the quadratures is given by [71]

$$e^{-i\gamma\hat{q}^3}\hat{q}e^{i\gamma\hat{q}^3} = \hat{q}, \quad e^{-i\gamma\hat{q}^3}\hat{p}e^{i\gamma\hat{q}^3} = \hat{p} + 6\gamma\hat{q}^2.$$
 (C21)

A standard model of universal CV quantum computation (CVQC) is defined by a vacuum state input into a circuit with Gaussian unitaries and cubic phase gates [45–47].

**Thermal loss channel.** Thermal loss arises from the interaction of our system with the thermal state of a finite-temperature environment. We model its effect using a quantum channel  $\Lambda_{\bar{n},\eta}(\cdot)$ , where the action on a single-mode density matrix  $\rho$  is given by:

$$\Lambda_{\bar{n},\eta}(\rho) = \text{Tr}_E[\hat{B}_{\eta}\rho \otimes \rho_{\bar{n}}\hat{B}_{\eta}^{\dagger}], \tag{C22}$$

where  $\rho_{\bar{n}}$  is the thermal state of the environment with mean photon number  $\bar{n}$ , given by

$$\rho_{\bar{n}} = \frac{1}{1+\bar{n}} \sum_{n=0}^{\infty} \left(\frac{\bar{n}}{\bar{n}+1}\right)^n |n\rangle\langle n|$$

$$= \frac{1}{\pi} \int_{\mathbb{C}} d^2\alpha \exp\left(-\left(\bar{n}+\frac{1}{2}\right)|\alpha|^2\right) D(-\alpha), \tag{C23}$$

whereas  $\hat{B}_{\eta}$  is the two-mode Gaussian unitary gate beam splitter whose associated displacement vector is zero and its associated symplectic matrix is given by

$$\begin{bmatrix} \sqrt{\eta} & \sqrt{1-\eta} & 0 & 0\\ -\sqrt{1-\eta} & \sqrt{\eta} & 0 & 0\\ 0 & 0 & \sqrt{\eta} & \sqrt{1-\eta}\\ 0 & 0 & -\sqrt{1-\eta} & \sqrt{\eta} \end{bmatrix}.$$
 (C24)

Note that the thermal loss channel for  $\bar{n} = 0$  is known as the photon loss channel.

### 1. Evolution of displacement operators under the effect of bosonic channels

Evolution of displacement operators under the effect of Gaussian gates. The evolution of the displacement operator under the Gaussian channel  $(\mathcal{G}_j(\cdot) = \hat{G}_j^{\dagger}(\cdot)\hat{G}_j)$  is defined via its action on the displacement operator basis as follows [70]

$$\mathcal{G}_{j}(D(\mathbf{r})) = e^{-i\mathbf{d}_{j}^{\mathsf{T}}\Omega S_{j}\mathbf{r}}D(S_{j}\mathbf{r}), \tag{C25}$$

$$\mathcal{G}_j^*(D(\mathbf{r})) = e^{i\mathbf{d}_j^\top \Omega \mathbf{r}} D(S_j^{-1} \mathbf{r}). \tag{C26}$$

In the next sections, we give the expression of the evolution of the Displacement operator under the other two relevant channels in this work, the cubic phase gate and thermal loss channel.

Evolution of displacement operator under the effect of cubic phase gate The following Lemma gives the evolution of the displacement operator under the effect of the cubic phase gate:

**Lemma C.2** (Displacement operators under the action of cubic phase gate). Given the m-mode displacement operator  $\hat{D}(\mathbf{r})$  for  $\mathbf{r} = \{r_1, \dots, r_m\} \in \mathbb{R}^{2m}$ , with  $r_i = \{q_i, p_i\}, \forall i \in \{1, \dots, m\}$ , the evolution of the displacement operator under the action of the cubic phase gate  $e^{i\gamma\hat{q}_1^3}$  is given by

$$e^{-i\gamma\hat{q}_1^3}\hat{D}(\boldsymbol{r})e^{i\gamma\hat{q}_1^3} = e^{-i\frac{\pi}{4}}\sqrt{\frac{1}{24\pi\gamma q_1}}\exp\left(-4i\gamma q_1^3\right)\int dp_1'\exp\left(i\frac{(p_1-p_1')^2}{24\gamma q_1}\right)\hat{D}(q_1,p_1')\otimes\hat{D}(r_2)\otimes\ldots\otimes\hat{D}(r_m). \tag{C27}$$

*Proof.* We first focus on the effect of the cubic phase gate on a single mode displacement operator  $\hat{D}(\alpha)$ , with  $r_1 = q_1 + ip_1$ . Expanding  $e^{-i\gamma\hat{q}^3}\hat{D}(r)e^{i\gamma\hat{q}^3}$  in the displacement operator basis,

$$e^{-i\gamma\hat{q}^3}\hat{D}(r)e^{i\gamma\hat{q}^3} = \frac{1}{\pi} \int_{\mathbb{R}^2} \text{Tr}\Big[e^{-i\gamma\hat{q}^3}\hat{D}(r)e^{i\gamma\hat{q}^3}\hat{D}(\beta)\Big]\hat{D}^{\dagger}(\beta)d^2\beta, \qquad (C28)$$

where

$$\beta := q_{\beta} + ip_{\beta} \,. \tag{C29}$$

From [33, Eq. (54)],

$$\operatorname{Tr}\left[e^{-i\gamma\hat{q}^{3}}\hat{D}(r)e^{i\gamma\hat{q}^{3}}\hat{D}(\beta)\right] = e^{-i\frac{\pi}{4}}\delta(q_{1}, -q_{\beta})\sqrt{\frac{\pi}{24\gamma q_{1}}}\exp\left(i\frac{(p_{1} + p_{\beta})^{2}}{24\gamma q_{1}} - 4i\gamma q_{1}^{3}\right). \tag{C30}$$

Therefore,

$$e^{-i\gamma\hat{q}^{3}}\hat{D}(r)e^{i\gamma\hat{q}^{3}} = e^{-i\frac{\pi}{4}}\sqrt{\frac{1}{24\pi\gamma q_{1}}}\exp\left(-4i\gamma q_{1}^{3}\right)\int dp_{\beta}\exp\left(i\frac{(p_{1}+p_{\beta})^{2}}{24\gamma q_{1}}\right)\hat{D}(q_{1},-p_{\beta})$$

$$= e^{-i\frac{\pi}{4}}\sqrt{\frac{1}{24\pi\gamma q_{1}}}\exp\left(-4i\gamma q_{1}^{3}\right)\int dp_{\beta}\exp\left(i\frac{(p_{1}-p_{\beta})^{2}}{24\gamma q_{1}}\right)\hat{D}(q_{1},p_{\beta}). \tag{C31}$$

Now, for the *m*-mode displacement operator  $\hat{D}(r_1) \otimes ... \otimes \hat{D}(r_m)$ :

$$e^{-i\gamma\hat{q}_{1}^{3}}\hat{D}(r_{1})\otimes\ldots\otimes\hat{D}(r_{m})e^{i\gamma\hat{q}_{1}^{3}} = e^{-i\gamma\hat{q}_{1}^{3}}\hat{D}(r_{1})e^{i\gamma\hat{q}_{1}^{3}}\otimes\ldots\otimes\hat{D}(r_{m})$$

$$= e^{-i\frac{\pi}{4}}\sqrt{\frac{1}{24\pi\gamma q_{1}}}\exp\left(-4i\gamma q_{1}^{3}\right)\int dp_{1}'\exp\left(i\frac{(p_{1}-p_{1}')^{2}}{24\gamma q_{1}}\right)\hat{D}(q_{1},p_{1}')\otimes\hat{D}(r_{2})\otimes\ldots\otimes\hat{D}(r_{m}).$$
(C32)

Evolution of displacement operator under the effect of thermal loss The following Lemma gives the evolution of the displacement operator under the thermal loss channel and is the more general version of [32, Appendix C] where the evolution of the displacement operator under photon loss was given.

**Lemma C.3** (Evolution of characteristic function under thermal loss channel). Given a thermal loss channel  $\Lambda_{\bar{n},\eta}$  with efficiency  $\eta$  and thermal photon number  $\bar{n}$ , the evolution of the single-mode displacement operator  $\hat{D}(r_1)$  with  $r_1 = \{q_1, p_1\}$  under the effect of the thermal noise channel and its adjoint is given by:

$$\Lambda_{\bar{n},\eta}(\hat{D}(r_1)) = \frac{1}{\eta} \exp\left(-(1+2\bar{n})\left(\frac{1}{\eta}-1\right)\frac{q_1^2+p_1^2}{2}\right)\hat{D}(r_1/\sqrt{\eta}),$$

$$\Lambda_{\bar{n},\eta}^*(\hat{D}(r_1)) = \exp\left(-(1+2\bar{n})(1-\eta)\frac{q_1^2+p_1^2}{2}\right)\hat{D}(r_1\sqrt{\eta}).$$
(C33)

*Proof.* First, we describe the effect of thermal loss channel on coherent states:

$$\Lambda_{\bar{n},\eta}(|\alpha\rangle\langle\alpha|) = \operatorname{Tr}_{E}[B_{\eta}|\alpha\rangle\langle\alpha|\otimes\lambda B_{\eta}^{\dagger}] 
= \int d^{2}\beta \frac{e^{-|\beta|^{2}/\bar{n}}}{\pi\bar{n}} \operatorname{Tr}_{E}[B_{\eta}|\alpha\rangle\langle\alpha|\otimes|\beta\rangle\langle\beta|_{E} B_{\eta}^{\dagger}] 
= \int d^{2}\beta \frac{e^{-|\beta|^{2}/\bar{n}}}{\pi\bar{n}} 
\operatorname{Tr}_{E}\left[\left|\alpha\sqrt{\eta} - \beta\sqrt{1-\eta}\right\rangle\langle\alpha\sqrt{\eta} - \beta\sqrt{1-\eta}\right|\otimes\left|\alpha\sqrt{1-\eta} + \beta\sqrt{\eta}\right\rangle\langle\alpha\sqrt{1-\eta} + \beta\sqrt{\eta}\Big|_{E}\right] 
= \int d^{2}\beta \frac{e^{-|\beta|^{2}/\bar{n}}}{\pi\bar{n}} \left|\alpha\sqrt{\eta} - \beta\sqrt{1-\eta}\right\rangle\langle\alpha\sqrt{\eta} - \beta\sqrt{1-\eta}\right|,$$
(C34)

where we have used the fact that the thermal state  $\lambda$  can be represented in the coherent state basis as

$$\lambda = \int d^2 \beta \frac{e^{-|\beta|^2/\bar{n}}}{\pi \bar{n}} |\beta\rangle \langle\beta| \tag{C35}$$

and that a beamsplitter with efficiency  $\eta$  acts on a tensor product of coherent states as

$$\hat{B}_{\eta}(|\alpha\rangle \otimes |\beta\rangle) = \left|\alpha\sqrt{\eta} - \beta\sqrt{1-\eta}\right\rangle \otimes \left|\alpha\sqrt{1-\eta} + \beta\sqrt{\eta}\right\rangle.$$
 (C36)

Therefore,

$$\Lambda_{\bar{n},\eta}(\hat{D}(r_1)) = \frac{1}{\pi} e^{|r_1|^2/2} \int d^2 \alpha e^{r_1 \alpha^* - r_1^* \alpha} \Lambda_{\bar{n},\eta}(|\alpha\rangle \langle \alpha|) 
= \frac{1}{\pi} e^{r_1^2/2} \int d^2 \alpha e^{r_1 \alpha^* - r_1^* \alpha} \int d^2 \beta \frac{e^{-|\beta|^2/\bar{n}}}{\pi \bar{n}} \left| \alpha \sqrt{\eta} - \beta \sqrt{1 - \eta} \right\rangle \left\langle \alpha \sqrt{\eta} - \beta \sqrt{1 - \eta} \right|.$$
(C37)

Writing  $\left|\alpha\sqrt{\eta}-\beta\sqrt{1-\eta}\right>=e^{i\phi(\alpha,\beta)}\hat{D}(-\beta\sqrt{1-\eta})\left|\alpha\sqrt{\eta}\right>$  and noting that we can cancel out the phases obtained by

decomposition of  $|\alpha\sqrt{\eta} - \beta\sqrt{1-\eta}\rangle$  and  $\langle\alpha\sqrt{\eta} - \beta\sqrt{1-\eta}|$  into  $\hat{D}(-\beta\sqrt{1-\eta}) |\alpha\sqrt{\eta}\rangle$ , we get

$$\begin{split} &\Lambda_{\bar{n},\eta}(D(r_{1})) = \int d^{2}\beta \frac{e^{-|\beta|^{2}/\bar{n}}}{\pi\bar{n}} \hat{D}(-\beta\sqrt{1-\eta}) \left(\frac{1}{\pi}e^{|r_{1}|^{2}/2} \int d^{2}\alpha e^{r_{1}\alpha^{*} - r_{1}^{*}\alpha} |\alpha\sqrt{\eta}\rangle \langle\alpha\sqrt{\eta}|\right) \hat{D}^{\dagger}(-\beta\sqrt{1-\eta}) \\ &= \int d^{2}\beta \frac{e^{-|\beta|^{2}/\bar{n}}}{\pi\bar{n}} \hat{D}(-\beta\sqrt{1-\eta}) \frac{1}{\eta} \exp\left(-\left(\frac{1}{\eta} - 1\right) \frac{q_{1}^{2} + p_{1}^{2}}{2}\right) \hat{D}(r_{1}/\sqrt{\eta}) \hat{D}^{\dagger}(-\beta\sqrt{1-\eta}) \\ &= \frac{1}{\eta} \exp\left(-\left(\frac{1}{\eta} - 1\right) \frac{q_{1}^{2} + p_{1}^{2}}{2}\right) \int d^{2}\beta \frac{e^{-|\beta|^{2}/\bar{n}}}{\pi\bar{n}} \hat{D}(-\beta\sqrt{1-\eta}) \hat{D}(r_{1}/\sqrt{\eta}) \hat{D}^{\dagger}(-\beta\sqrt{1-\eta}) \\ &= \frac{1}{\eta} \exp\left(-\left(\frac{1}{\eta} - 1\right) \frac{q_{1}^{2} + p_{1}^{2}}{2}\right) \\ &\qquad \times \int d^{2}\beta \frac{e^{-|\beta|^{2}/\bar{n}}}{\pi\bar{n}} \exp\left(i \operatorname{Im}\left(-\beta\sqrt{1-\eta} \frac{(q_{1} - ip_{1})}{\sqrt{\eta}}\right)\right) \hat{D}\left(-\beta\sqrt{1-\eta} + \frac{q_{1} + ip_{1}}{\sqrt{\eta}}\right) \hat{D}^{\dagger}(-\beta\sqrt{1-\eta}) \\ &= \frac{1}{\eta} \exp\left(-\left(\frac{1}{\eta} - 1\right) \frac{q_{1}^{2} + p_{1}^{2}}{2}\right) \hat{D}(r_{1}/\sqrt{\eta}) \\ &\qquad \times \int d^{2}\beta \frac{e^{-|\beta|^{2}/\bar{n}}}{\pi\bar{n}} \exp\left(i \operatorname{Im}\left(-\beta\sqrt{1-\eta} \frac{(q_{1} - ip_{1}))}{\sqrt{\eta}}\right)\right) \exp\left(i \operatorname{Im}\left(\left(-\beta\sqrt{1-\eta} + \frac{q_{1} + ip_{1}}{\sqrt{\eta}}\right) (\beta^{*}\sqrt{1-\eta})\right)\right) \\ &= \frac{1}{\eta} \exp\left(-\left(\frac{1}{\eta} - 1\right) \frac{q_{1}^{2} + p_{1}^{2}}{2}\right) \hat{D}(r_{1}/\sqrt{\eta}) \int d^{2}\beta \frac{e^{-|\beta|^{2}/\bar{n}}}{\pi\bar{n}} \exp\left(2i \operatorname{Im}\left(\frac{\sqrt{1-\eta}}{\sqrt{\eta}}\beta^{*}(q_{1} + ip_{1})\right)\right)\right) \\ &:= \frac{1}{\eta} \exp\left(-\left(\frac{1}{\eta} - 1\right) \frac{q_{1}^{2} + p_{1}^{2}}{2}\right) \hat{D}(r_{1}/\sqrt{\eta}) f(\eta, \bar{n}, q_{1}, p_{1}), \end{split}$$
(C38)

where the second line follows from [32, Eqn. 55]. To find the value of  $f(\eta, \bar{n}, \xi)$ , substitute  $\beta^* = x + iy$  and  $a = 2\sqrt{\frac{1-\eta}{\eta}(q_1+ip_1)}$ .

$$f(\eta, \bar{n}, \xi) = \frac{1}{\pi \bar{n}} \int dx dy \exp\left(-\frac{x^2 + y^2}{\bar{n}}\right) \exp\left(i\operatorname{Im}((a_R + ia_I)(x + iy))\right)$$

$$= \frac{1}{\pi \bar{n}} \int dx \exp\left(-\left(\frac{x^2}{\bar{n}} - ia_I x\right)\right) \int dy \exp\left(-\left(\frac{y^2}{\bar{n}} - ia_R y\right)\right)$$

$$= \frac{1}{\pi \bar{n}} \exp\left(\frac{1}{\bar{n}} - \frac{\bar{n}^2 a_I^2}{4}\right) \sqrt{\pi \bar{n}} \exp\left(\frac{1}{\bar{n}} - \frac{\bar{n}^2 a_R^2}{4}\right) \sqrt{\pi \bar{n}}$$

$$= \exp\left(-\frac{\bar{n}}{4}|a|^2\right)$$

$$= \exp\left(-\bar{n}\left(\frac{1}{\eta} - 1\right)(q_1^2 + p_1^2)\right). \tag{C39}$$

Putting the value of  $f(\eta, \bar{n}, \xi)$  back into equation C38,

$$\Lambda_{\bar{n},\eta}(D(r_1)) = \frac{1}{n} \exp\left(-(1+2\bar{n})\left(\frac{1}{n}-1\right) \frac{q_1^2 + p_1^2}{2}\right) \hat{D}(r_1/\sqrt{\eta}). \tag{C40}$$

Now,

$$\operatorname{Tr}\left[\Lambda_{\bar{n},\eta}(\hat{D}(r_{1}))\hat{D}(\alpha)\right] = \frac{1}{\eta} \exp\left(-(1+2\bar{n})\left(\frac{1}{\eta}-1\right)\frac{q_{1}^{2}+p_{1}^{2}}{2}\right) \operatorname{Tr}\left[D(r_{1}/\sqrt{\eta})\hat{D}(\alpha)\right]$$

$$= \frac{1}{\eta} \exp\left(-(1+2\bar{n})\left(\frac{1}{\eta}-1\right)\frac{q_{1}^{2}+p_{1}^{2}}{2}\right) \pi \delta^{2}(r_{1}/\sqrt{\eta}+\alpha)$$

$$= \exp\left(-(1+2\bar{n})\left(\frac{1}{\eta}-1\right)\frac{q_{1}^{2}+p_{1}^{2}}{2}\right) \pi \delta^{2}(r_{1}+\alpha\sqrt{\eta})$$

$$= \exp\left(-(1+2\bar{n})\left(1-\eta\right)\frac{|\alpha|^{2}}{2}\right) \pi \delta^{2}(r_{1}+\alpha\sqrt{\eta})$$

$$= \exp\left(-(1+2\bar{n})\left(1-\eta\right)\frac{|\alpha|^{2}}{2}\right) \operatorname{Tr}\left[\hat{D}(r_{1})\hat{D}(\alpha\sqrt{\eta})\right]$$
(C41)

Since  $\operatorname{Tr}\left[\Lambda_{\bar{n},\eta}(\hat{D}(\xi))\hat{D}(\chi)\right] = \operatorname{Tr}\left[\hat{D}(\xi)\Lambda_{\bar{n},\eta}^*(\hat{D}(\chi))\right]$ , therefore

$$\Lambda_{\bar{n},\eta}^*(\hat{D}(\alpha)) = \exp\left(-(1+2\bar{n})(1-\eta)\frac{|\alpha|^2}{2}\right)\hat{D}(\alpha\sqrt{\eta}). \tag{C42}$$

Note that for  $\bar{n} = 0$ , the thermal loss channel corresponds to the photon loss, and we recover the expression of the action on the photon loss channel and its adjoint given in [32, Appendix C].

## 2. Coherent state projectors as probability distributions.

When trying to estimate the overlap of the output of noisy bosonic circuit with the local coherent state projectors, we will use the (renormalized) magnitude of characteristic function of these local coherent state projectors as probability distributions. In this section, we explain how this can be done. Given the output operator

$$\hat{O} = \left(\bigotimes_{i=1}^{k} |\alpha_i\rangle \langle \alpha_i|\right) \otimes \mathbb{I}^{\otimes m-k},\tag{C43}$$

for  $r \in \mathbb{R}^{2m}$ , its characteristic function is given as

$$\chi_{\hat{O}}(\mathbf{r}) = \text{Tr}\left[\hat{O}\hat{D}(\mathbf{r})\right] = \left(\Pi_{i=1}^{k}(\text{Tr}\left[|\alpha_{i}\rangle\langle\alpha_{i}|\hat{D}(r_{i})\right]) \times \Pi_{i=k+1}^{m}(\text{Tr}[D(r_{j})])\right). \tag{C44}$$

Now

$$Tr[D(r_j)] = \pi \delta^2(r_j) \tag{C45}$$

 $\forall j \in \{k+1, \dots, m\} \text{ and } r_j = (q_j, p_j) \text{ Further, for two single coherent states } |\alpha\rangle \text{ and } |\beta\rangle,$ 

$$\langle \alpha | \beta \rangle = \exp\left(-\frac{1}{2}|\alpha|^2 - \frac{1}{2}|\beta|^2 + \alpha^*\beta\right),$$
 (C46)

and therefore

$$\operatorname{Tr}\left[\left|\alpha_{i}\right\rangle\left\langle\alpha_{i}\right|\hat{D}(r_{i})\right] = \exp(i\operatorname{Im}(\alpha_{i}r_{i}^{*}))\left\langle\alpha_{i}\right|\alpha_{i} + r_{i}\right\rangle = \exp\left(-\frac{1}{2}|\alpha_{i}|^{2} - \frac{1}{2}|\alpha_{i} + r_{i}|^{2} + \alpha_{i}^{*}(\alpha_{i} + r_{i})\right). \tag{C47}$$

This gives

$$\chi_{\hat{O}}(\mathbf{r}) = \left( \Pi_{i=1}^k \exp\left( -\frac{1}{2} |\alpha_i|^2 - \frac{1}{2} |\alpha_i + r_i|^2 + \alpha_i^* (q_i + ip_i) \right) \right) \times \pi^{m-k} (\Pi_{j=k+1}^m \delta^2(r_j)).$$
 (C48)

For the Dirac delta functions (that would appear whenever we are dealing with operators which are not acting on all the modes), instead of taking the modulus (which is not well defined since Dirac delta is not a proper function), we simply define it as the probability distribution with probability one at the point (0,0) and zero everywhere else. With this consideration and the fact that

$$|\langle \alpha_i | \alpha_i + r_i \rangle| = \exp\left(-\frac{1}{2}|\alpha_i + r_i - \alpha_i|^2\right) = \exp\left(-\frac{q_i^2 + p_i^2}{2}\right),\tag{C49}$$

we get that

$$\|\hat{O}\|_{\mathbb{F},1} = \frac{1}{\pi^m} \int_{\mathbb{R}^{2m}} d^{2m} \mathbf{r} |\chi_{\hat{O}}(\mathbf{r})| = \frac{1}{\pi^k} \prod_{i=1}^k \int_{\mathbb{R}^2} dq_i dp_i \exp\left(-\frac{q_i^2 + p_i^2}{2}\right) = 2^k.$$
 (C50)

Therefore the magnitude of the characteristic function of the local coherent state projectors can be used as a probability distribution by multiplying and dividing it by the normalizing constant  $2^k$ .

#### Appendix D: Technical lemmas for bosonic operators

This section details additional technical tools that are specific to our expectation value estimation problems. The results mentioned in this section will be referenced later when we detail our estimation algorithm and its efficiency.

## 1. Curvature bound for the noisy characteristic function

In this work, we make the assumption that our noisy bosonic circuit is such that the magnitude of double derivative with respect to the momentum coordinate of the first mode of the expectation value of the displacement operator under the noisy evolved state after each layer of quantum channel in the circuit is bounded. The following Lemma connects this rather non-intuitive quantity to a much more commonly considered quantity, the quadrature moments:

**Lemma D.1** (Curvature bound for noisy characteristic function). Given a quantum state  $\rho$ , displacement operator  $\hat{D}(\mathbf{r})$ , with  $r_1 = q_1 + ip_1$ , we have that

$$\max_{p_1 \in \mathbb{R}} \left| \frac{\partial^2}{\partial^2 p_1} \operatorname{Tr}[D(\boldsymbol{r}) \Lambda_{\bar{n}, \eta}(\rho)] \right| \leqslant f_{\rho, \alpha}(\hat{q}), \tag{D1}$$

where  $f_{\rho,\alpha}(\hat{q})$  is a function depending on the expectation value of the first four moments of position quadrature of the first mode  $\hat{q}_1$ .

*Proof.* First we write,

$$Tr[D(\alpha)\Lambda_{\bar{n},\eta}(\rho)] = Tr\left[\Lambda_{\bar{n},\eta}^*(D(\alpha))\rho\right]. \tag{D2}$$

Now, from Lemma C.3,

$$\Lambda_{\bar{n},\eta}^*(D(\alpha)) = \exp\left(-(1/2 + \bar{n})(1 - \eta)(q_1^2 + p_1^2)\right) D(\sqrt{\eta}\alpha) 
= \exp\left(-(1/2 + \bar{n})(1 - \eta)(q_1^2 + p_1^2)\right) \exp\left(i\sqrt{\eta}p_1\hat{q} - i\sqrt{\eta}q_1\hat{p}\right).$$
(D3)

Therefore, taking the double derivative with respect to the momentum coordinate,

$$\frac{\partial^2}{\partial^2 p_1} \Lambda_{\bar{n},\eta}^*(D(\alpha)) = (-(1+2\bar{n})(1-\eta) + (1-\eta)^2 (1+2\bar{n})^2 p_1^2 - \eta \hat{q}^2 + 2ip_1(1+2\bar{n})(1-\eta)\sqrt{\eta}\hat{q})\Lambda_{\bar{n},\eta}^*(D(\alpha)), \tag{D4}$$

and

$$\operatorname{Tr}\left[\frac{\partial^{2}}{\partial^{2}p_{1}}\Lambda_{\bar{n},\eta}^{*}(D(\alpha))\rho\right] = \left((-(1+2\bar{n})(1-\eta)+(1-\eta)^{2}(1+2\bar{n})^{2}p_{1}^{2})\exp\left(-(1/2+\bar{n})(1-\eta)(q_{1}^{2}+p_{1}^{2})\right)\chi_{\rho}(\sqrt{\eta}\alpha)\right) + \operatorname{Tr}\left[(-\eta\hat{q}^{2}-2ip_{1}(1+2\bar{n})(1-\eta)\sqrt{\eta}\hat{q})\hat{D}(\sqrt{\eta}\alpha)\rho\right]\right) \times \exp\left(-\left(\frac{1}{2}+\bar{n}\right)(1-\eta)(q_{1}^{2}+p_{1}^{2})\right)(D5)$$

We know that the magnitude of characteristic function is less than equal to 1 (Derived in Section C). To bound the second term, we use the inequality (Lemma B.6)

$$|\text{Tr}[A\rho]|^2 \leqslant \frac{1}{2} \text{Tr}[\{A, A^{\dagger}\}\rho],$$
 (D6)

with  $A = (-\eta \hat{q}^2 - 2ip_1(1 + 2\bar{n})(1 - \eta)\sqrt{\eta}\hat{q})\hat{D}(\sqrt{\eta}\alpha)$ . Now,

$$\{A, A^{\dagger}\} = \eta^2 \hat{q}^4 + 4p_1^2 (2\bar{n} + 1)^2 (1 - \eta)^2 \eta \hat{q}^2 + D^{\dagger} (\sqrt{\eta}\alpha) (\eta \hat{q}^4 + 4p_1^2 (2\bar{n} + 1)^2 (1 - \eta)^2 \eta \hat{q}^2) D(\sqrt{\eta}\alpha). \tag{D7}$$

Therefore, using the triangle's inequality,

$$\left| \operatorname{Tr} \left[ \frac{\partial^{2}}{\partial^{2} p_{1}} \Lambda_{\bar{n}, \eta}^{*}(D(\alpha)) \rho \right] \right| \leq \left( \left| -(1 + 2\bar{n})(1 - \eta) + (1 - \eta)^{2}(1 + 2\bar{n})^{2} p_{1}^{2} \right| \\
+ \frac{1}{\sqrt{2}} \sqrt{\left( \eta^{2} (\operatorname{Tr}[\rho \hat{q}^{4}] + \operatorname{Tr} \left[ \hat{D}(\sqrt{\eta} \alpha) \rho \hat{D}^{\dagger}(\sqrt{\eta} \alpha) \hat{q}^{4} \right] \right) + 4 p_{1}^{2} (2\bar{n} + 1)^{2} (1 - \eta)^{2} \eta (\operatorname{Tr}[\rho \hat{q}^{4}] + \operatorname{Tr} \left[ \hat{D}(\sqrt{\eta} \alpha) \rho \hat{D}^{\dagger}(\sqrt{\eta} \alpha) \hat{q}^{4} \right]) \right)} \right) \\
\times \exp \left( - \left( \frac{1}{2} + \bar{n} \right) (1 - \eta) (q_{1}^{2} + p_{1}^{2}) \right) \\
\leq \left( \left| -(1 + 2\bar{n})(1 - \eta) + (1 - \eta)^{2} (1 + 2\bar{n})^{2} p_{1}^{2} \right| \\
+ \frac{1}{\sqrt{2}} \sqrt{\left( \eta^{2} \left( \operatorname{Tr}[\rho \hat{q}^{4}] + \sum_{k=0}^{4} \left( \binom{n}{k} (2q_{1})^{4-k} \operatorname{Tr}[\rho \hat{q}^{k}] \right) \right) + 4 p_{1}^{2} (2\bar{n} + 1)^{2} (1 - \eta)^{2} \eta \left( \operatorname{Tr}[\rho \hat{q}^{4}] + \sum_{k=0}^{4} \left( \binom{n}{k} (2\sqrt{\eta} q_{1})^{4-k} \operatorname{Tr}[\rho \hat{q}^{k}] \right) \right) \right)} \\
\times \exp \left( - \left( \frac{1}{2} + \bar{n} \right) (1 - \eta) (q_{1}^{2} + p_{1}^{2}) \right) \\
= f_{\rho, \alpha}(\hat{q}), \tag{D8}$$

Therefore, bounding the second and fourth moment of the position quadrature throughout the circuit guarantees that  $\left| \text{Tr} \left[ \frac{\partial^2}{\partial^2 p^{(1)}} \Lambda_{n,\eta}^*(D(\boldsymbol{r})) \rho \right] \right|$  is bounded throughout the circuit,  $\forall \boldsymbol{r} \in \mathbb{R}^{2m}$ . Further, defining the total energy operator

$$\hat{N} = \sum_{j=1}^{m} \hat{N}_{j} = \sum_{j=1}^{m} \frac{\hat{q}_{j}^{2} + \hat{p}_{j}^{2}}{2}, \tag{D9}$$

we have for each mode j

$$\hat{N}^2 \succeq \hat{N}_j^2 \succeq \frac{1}{4} \hat{q}_j^4, \tag{D10}$$

and therefore for any state  $\rho$  (with Tr  $\rho = 1$ )

$$\operatorname{Tr}(\rho \,\hat{q}_i^4) \le 4 \,\operatorname{Tr}(\rho \,\hat{N}^2). \tag{D11}$$

Moreover, by Hölder (or standard moment inequalities), for any integer k with  $0 \le k \le 4$ ,

$$\left|\operatorname{Tr}(\rho\,\hat{q}_{i}^{k})\right| \le \left(\operatorname{Tr}(\rho\,\hat{q}_{i}^{4})\right)^{k/4} \le \left(4\operatorname{Tr}(\rho\,\hat{N}^{2})\right)^{k/4}.\tag{D12}$$

Hence a uniform bound on the second moment of the energy operator  $\text{Tr}(\rho \hat{N}^2)$  throughout the circuit implies uniform bounds on the first four moments of each quadrature  $\hat{q}_j$ . We refer to this assumption as the *bounded energy* condition in the main text.

## 2. Estimating first and second moment of quadratures

In this section, we explain how estimating the characteristic function of a quantum state enables the estimation of quadrature moments. The key observation is that position and momentum operators can be written as partial derivatives of displacement operators and can therefore be approximated by finite differences of displacement operators through a Taylor expansion. However, this approximation is valid only under suitable energy bounds, since position and momentum operators (and their powers) are unbounded. These assumptions ensure that Taylor's theorem can be applied consistently and that the corresponding expectation values remain finite.

**Lemma D.2.** Given a quantum state  $\rho$ , it holds that  $\forall j \in \{1, ..., m\}$ :

$$\left| \operatorname{Tr} \left[ \rho \hat{q}_{j} \right] - \frac{\operatorname{Tr} \left[ \rho \hat{D}_{j}(0, \delta) \right] - 1}{i \delta} \right| \leq \delta \operatorname{Tr} \left[ \rho \hat{q}_{j}^{4} \right],$$

$$\left| \operatorname{Tr} \left[ \rho \hat{q}_{j}^{2} \right] - \frac{2}{\delta^{2}} \left( \left( 1 - \operatorname{Tr} \left[ \rho \hat{D}_{j}(0, \delta) \right] \right) + \frac{1}{\delta} \left( \operatorname{Tr} \left[ \rho \hat{D}_{j}(0, \delta^{2}) \right] - 1 \right) \right) \right| \leq \frac{2}{3} \delta \operatorname{Tr} \left[ \rho \hat{q}_{j}^{6} \right] + 2\delta \operatorname{Tr} \left[ \rho \hat{q}_{j}^{4} \right],$$

$$\left| \operatorname{Tr} \left[ \rho \hat{p}_{j} \right] - \frac{1 - \operatorname{Tr} \left[ \rho \hat{D}_{j}(\delta, 0) \right]}{i \delta} \right| \leq \delta \operatorname{Tr} \left[ \rho \hat{p}_{j}^{4} \right],$$

$$\left| \operatorname{Tr} \left[ \rho \hat{p}_{j}^{2} \right] - \left( \frac{2}{\delta^{2}} \left( 1 - \operatorname{Tr} \left[ \rho \hat{D}_{j}(\delta, 0) \right] \right) + \frac{2}{\delta^{3}} \left( \operatorname{Tr} \left[ \rho \hat{D}_{j}(\delta^{2}, 0) \right] - 1 \right) \right) \right| \leq \frac{2}{3} \delta \operatorname{Tr} \left[ \rho \hat{p}_{j}^{6} \right] + 2\delta \operatorname{Tr} \left[ \rho \hat{p}_{j}^{4} \right],$$
(D13)

where  $\hat{D}_{j}(q_{i}, p_{j})$  is the jth mode displacement operator.

*Proof.* We will prove the result for the position quadratures, and the results for the momentum quadratures can be similarly proven. The j'th mode displacement operator of the first mode is given by

$$\hat{D}_j(q,p) = \exp(ip\hat{q}_j - iq\hat{p}_j). \tag{D14}$$

Therefore,

$$\hat{D}_j(0,p) = \exp(ip\hat{q}_j),\tag{D15}$$

and hence

$$\left. \frac{\partial}{\partial p} \hat{D}_j(0, p) \right|_{p=0} = i\hat{q}_j. \tag{D16}$$

By Taylor's remainder theorem (Theorem B.1),

$$\hat{D}_{j}(0,\delta) = \hat{D}_{j}(0,0) + \delta \frac{\partial}{\partial p} \hat{D}_{j}(0,p) \Big|_{p=0} + \frac{\delta^{2}}{2!} \frac{\partial^{2}}{\partial p^{2}} \hat{D}_{j}(0,p) \Big|_{p=\xi}$$

$$= \hat{D}_{j}(0,0) + i\delta \hat{q}_{1} + \frac{\delta^{2}}{2!} \frac{\partial^{2}}{\partial p^{2}} \hat{D}_{j}(0,p) \Big|_{p=\xi} \tag{D17}$$

for some  $\xi \in (0, \delta)$ . Therefore,

$$\operatorname{Tr}[\rho \hat{q}_{j}] = \frac{\operatorname{Tr}\left[\rho \hat{D}_{j}(0,\delta)\right] - 1}{i\delta} + i\frac{\delta}{2}\operatorname{Tr}\left[\rho \frac{\partial^{2}}{\partial p^{2}}\hat{D}_{j}(0,p)\Big|_{p=\xi}\right]. \tag{D18}$$

Now

$$\left| \operatorname{Tr} \left[ \rho \frac{\partial^2}{\partial p^2} \hat{D}_j(0, p) \right] \right| = \left| \operatorname{Tr} \left[ \rho \hat{q}_j^2 \hat{D}_j(0, p) \right] \right| \leq \left| \operatorname{Tr} \left[ \rho \{ \hat{q}_j^2 \hat{D}_j(0, p), \hat{D}_j^{\dagger}(0, p), \hat{q}_j^2 \} \right] \right| = 2 \operatorname{Tr} \left[ \rho \hat{q}_j^4 \right],$$

where the inequality follows from Lemma B.6. Therefore, we get

$$\left| \operatorname{Tr}[\rho \hat{q}_j] - \frac{\operatorname{Tr}\left[\rho \hat{D}_j(0,\delta)\right] - 1}{i\delta} \right| \leqslant \delta \operatorname{Tr}\left[\rho \hat{q}_j^4\right]. \tag{D19}$$

To estimate  $\operatorname{Tr}\left[\rho\hat{q}_{j}^{2}\right]$ , notice that

$$\left. \frac{\partial^2}{\partial p^2} \hat{D}_j(0, p) \right|_{p=0} = -\hat{q}_j^2. \tag{D20}$$

Therefore, using Taylor's remainder theorem (Theorem B.1) and expanding up to the third order term,

$$\hat{D}_{j}(0,\delta) = \hat{D}_{j}(0,0) + \delta \frac{\partial}{\partial p} \hat{D}_{j}(0,p) \Big|_{p=0} + \frac{\delta^{2}}{2!} \frac{\partial^{2}}{\partial p^{2}} \hat{D}_{j}(0,p) \Big|_{p=0} + \frac{\delta^{3}}{3!} \frac{\partial^{3}}{\partial p^{3}} \hat{D}(0,p) \Big|_{p=\xi}$$

$$= \hat{D}_{j}(0,0) + i\delta \hat{q}_{j} - \frac{\delta^{2}}{2!} \hat{q}_{j}^{2} + \frac{\delta^{3}}{3!} \frac{\partial^{3}}{\partial p^{3}} \hat{D}_{j}(0,p) \Big|_{p=\xi} \tag{D21}$$

for some  $\xi \in (0, \delta)$ . Therefore,

$$\operatorname{Tr}\left[\rho\hat{q}_{j}^{2}\right] = \frac{2}{\delta^{2}}\left(1 - \operatorname{Tr}\left[\rho\hat{D}_{j}(0,\delta)\right]\right) + \frac{2i}{\delta}\operatorname{Tr}\left[\rho\hat{q}_{j}\right] + \frac{\delta}{3}\operatorname{Tr}\left[\rho\frac{\partial^{3}}{\partial\rho^{3}}\hat{D}_{j}(0,p)\Big|_{p=\xi}\right]. \tag{D22}$$

Now,

$$\left|\operatorname{Tr}\left[\rho\frac{\partial^3}{\partial p_1^3}\hat{D}(0,p_1)\right]\right| = \left|\operatorname{Tr}\left[\rho\hat{q}_1^3\hat{D}(0,p_1)\right]\right| \\ \leqslant \left|\operatorname{Tr}\left[\rho\{\hat{q}_1^3\hat{D}(0,p_1),\hat{D}^{\dagger}(0,p_1),\hat{q}_1^3\}\right]\right| \\ = 2\operatorname{Tr}\left[\rho\hat{q}_1^6\right].$$

Where the inequality follows from Lemma B.6. Also from the previous discussion,

$$\operatorname{Tr}[\rho \hat{q}_j] = \frac{\operatorname{Tr}\left[\rho \hat{D}_j(0, \delta^2)\right] - 1}{i\delta^2} \pm Error,\tag{D23}$$

where  $|Error| \leq \delta^2 \operatorname{Tr} \left[ \rho \hat{q}^4 \right]$ . Therefore, using the Triangle's inequality, we get

$$\left| \operatorname{Tr} \left[ \rho \hat{q}_{j}^{2} \right] - \frac{2}{\delta^{2}} \left( \left( 1 - \operatorname{Tr} \left[ \rho \hat{D}_{j}(0, \delta) \right] \right) + \frac{1}{\delta} \left( \operatorname{Tr} \left[ \rho \hat{D}_{j}(0, \delta^{2}) \right] - 1 \right) \right) \right| \leqslant \frac{2}{3} \delta \operatorname{Tr} \left[ \rho \hat{q}_{j}^{6} \right] + 2\delta \operatorname{Tr} \left[ \rho \hat{q}_{j}^{4} \right]. \tag{D24}$$

Therefore, given guarantees on the moments of quadrature up to the sixth order on the evolved output state, we can approximate the first two quadrature moments with the characteristic function of the output state up to arbitrary precision. This Lemma will be useful after we detail simulation algorithm to estimate the characteristic function. Since  $\hat{N}_j^2 \succeq \hat{q}_j^4, \hat{N}_j^3 \succeq \hat{q}_j^6, \forall j \in (1, ..., m)$  for the energy operator  $\hat{N}$  (Eq. C2), the condition of bounded fourth and sixth quadrature moments on the output state are expressed as condition on boundedness of second and third moments of  $\hat{N}_j$  in the main text.

Note that similar techniques allow us to estimate higher and higher quadrature moments in terms of characteristic functions. However, this requires guarantees on magnitudes of higher and higher moments (because we need to expand the Taylor's remainder theorem up to higher and higher order terms), making the estimation impractical.

### 3. Useful decompositions of bosonic channels

As detailed in the preliminaries in Section C, this work deals with noisy bosonic circuits consisting of Gaussian unitary gates and cubic phase gates and we model interaction with the environment using the thermal loss channel.

In what follows, we the cubic phase gate  $(e^{i\gamma\hat{q}^3})$  and Gaussian gate  $(\hat{G})$  by the quantum channels  $\mathcal{C}$  and  $\mathcal{G}$ , such that their action is given by:

$$\mathcal{C}(\cdot) = e^{i\gamma\hat{q}^3}(\cdot)e^{-i\gamma\hat{q}^3},$$

$$\mathcal{C}^*(\cdot) = e^{-i\gamma\hat{q}^3}(\cdot)e^{i\gamma\hat{q}^3},$$

$$\mathcal{G}(\cdot) = \hat{G}(\cdot)\hat{G}^{\dagger},$$

$$\mathcal{G}^*(\cdot) = \hat{G}^{\dagger}(\cdot)\hat{G}.$$
(D25)

Here we give the decomposition of the cubic gate and thermal loss channel into (non-physical) quantum channels such that the composition of these channels describes the action of the cubic phase gate and thermal loss channel on the displacement operator.

Cubic phase gates. For convenience, we decompose each cubic phase gate C with cubicity  $\gamma$  into two consecutive linear maps:

$$C^* = C_{\sigma}^* \circ C_{\mathfrak{D}}^*, \qquad C = C_{\mathfrak{D}} \circ C_{\mathfrak{C}}, \tag{D26}$$

where  $\mathfrak{D}$  stands for "discrete" and  $\mathfrak{C}$  stands for "continuous". The action of the maps in the displacement operator basis is given by:

$$C_{\mathfrak{D}}^*(D(\mathbf{r})) := \begin{cases} \sqrt{\frac{1}{24\pi\gamma q_1}} D(\mathbf{r}) & \text{if } q_1 \neq 0, \\ D(\mathbf{r}) & \text{if } q_1 = 0, \end{cases}$$
(D27)

$$\mathcal{C}_{\mathfrak{C}}^{*}(D(\boldsymbol{r})) := \begin{cases}
\int_{\mathbb{R}} d\bar{p}_{1} e^{i \left[\frac{(p_{1} - \bar{p}_{1})^{2}}{24\gamma q_{1}} - 4\gamma q_{1}^{3} - \frac{\pi}{4}\right]} D(\bar{\boldsymbol{r}}), & \text{if } q_{1} \neq 0, \\
D(\boldsymbol{r}) & \text{if } q_{1} = 0,
\end{cases} \tag{D28}$$

where  $\bar{r} = (q_1, -\bar{p}_1, q_2, p_2, \dots, q_m, p_m)$ . Note that the composition correctly describes the action of the cubic phase gate on the displacement operator according to Lemma C.2.

We also define an analogous decomposition for the channel itself:

$$C_{\mathfrak{D}}(D(\mathbf{r})) := \begin{cases} \sqrt{\frac{1}{24\pi\gamma q_1}} D(\mathbf{r}) & \text{if } q_1 \neq 0, \\ D(\mathbf{r}) & \text{if } q_1 = 0, \end{cases}$$
(D29)

$$\mathcal{C}_{\mathfrak{C}}(D(\boldsymbol{r})) := \begin{cases}
\int_{\mathbb{R}} d\bar{p}_1 e^{i\left[-\frac{(p_1 - \bar{p}_1)^2}{24\gamma q_1} + 4\gamma q_1^3 + \frac{\pi}{4}\right]} D(\bar{\boldsymbol{r}}), & \text{if } q_1 \neq 0, \\
D(\boldsymbol{r}) & \text{if } q_1 = 0,
\end{cases} \tag{D30}$$

with  $\tilde{r} = (q_1, q_2, \dots, q_m, p_1, p_2, \dots, p_m).$ 

**Thermal channels.** We introduce the following linear map, which we dub depolarizing map with noise rate p:

$$\mathcal{N}_p := \exp\left(-p|\xi|^2\right) D(\xi) \tag{D31}$$

The thermal channel can be re-expressed as follows:

$$\Lambda_{\bar{n},\eta}(D(\xi)) = \Lambda_{0,\eta} \circ \mathcal{N}_{\bar{n}(1/\eta - 1)}(D(\xi)), \tag{D32}$$

$$\Lambda_{\bar{n},\eta}^*(D(\xi)) = \Lambda_{0,\eta}^* \circ \mathcal{N}_{\bar{n}(1-\eta)}(D(\xi)), \tag{D33}$$

such that the composition of these maps describe the action of thermal loss channel and its adjoint on the displacement operator according to Lemma C.3. Similarly, we also decompose the thermal loss channel into three simple linear maps:

$$\Lambda_{\bar{n},\eta} = \Lambda_{\bar{n},\eta}^{\text{(shift)}} \circ \Lambda_{\bar{n},\eta}^{\text{(Im)}} \circ \Lambda_{\bar{n},\eta}^{\text{(Re)}}, \tag{D34}$$

$$\Lambda_{\bar{n},\eta} = \Lambda_{\bar{n},\eta}^{\text{(shift)}} \circ \Lambda_{\bar{n},\eta}^{\text{(Im)}} \circ \Lambda_{\bar{n},\eta}^{\text{(Re)}},$$

$$\Lambda_{\bar{n},\eta}^* = \Lambda_{\bar{n},\eta}^{\text{(Re)},*} \circ \Lambda_{\bar{n},\eta}^{\text{(Im)},*} \circ \Lambda_{\bar{n},\eta}^{\text{(shift)},*}.$$
(D34)

Their explicit action in the displacement basis is:

$$\Lambda_{\bar{n},\eta}^{(\mathrm{Im})}(D(\xi)) = \exp\left(-(1+2\bar{n})\left(\frac{1}{\eta}-1\right)\frac{p_{\xi}^2}{2}\right)D(\xi),\tag{D36}$$

$$\Lambda_{\bar{n},\eta}^{(\text{Re})}(D(\xi)) = \exp\left(-(1+2\bar{n})\left(\frac{1}{\eta}-1\right)\frac{q_{\xi}^{2}}{2}\right)D(\xi),\tag{D37}$$

$$\Lambda_{\bar{n},\eta}^{\text{(shift)}}(D(\xi)) = \frac{1}{\eta} D\left(\frac{\xi}{\sqrt{\eta}}\right). \tag{D38}$$

and for their adjoints:

$$\Lambda_{\bar{n},\eta}^{(\text{Im}),*}(D(\xi)) = \exp\left(-(1+2\bar{n})(1-\eta)\frac{p_{\xi}^{2}}{2}\right)D(\xi), \tag{D39}$$

$$\Lambda_{\bar{n},\eta}^{(\mathrm{Re}),*}(D(\xi)) = \exp\left(-(1+2\bar{n})(1-\eta)\frac{q_{\xi}^{2}}{2}\right)D(\xi), \tag{D40}$$

$$\Lambda_{\bar{n},\eta}^{(\text{shift}),*}(D(\xi)) = D(\sqrt{\eta}\,\xi). \tag{D41}$$

Commutativity of linear maps. When acting on the displacement operator, the cubic phase gate commutes with the "real" part of the thermal loss channel:

$$\Lambda_{\bar{n},\eta} \circ \mathcal{C}_{\gamma} = \Lambda_{\bar{n},\eta}^{(\text{shift})} \circ \Lambda_{\bar{n},\eta}^{(\text{Im})} \circ \Lambda_{\bar{n},\eta}^{(\text{Re})} \circ \mathcal{C}_{\gamma}$$
(D42)

$$= \Lambda_{\bar{n},\eta}^{\text{(shift)}} \circ \Lambda_{\bar{n},\eta}^{\text{(Im)}} \circ \mathcal{C}_{\gamma} \circ \Lambda_{\bar{n},\eta}^{\text{(Re)}}. \tag{D43}$$

Analogously, for the adjoints:

$$\mathcal{C}_{\gamma}^{*} \circ \Lambda_{\bar{n},\eta}^{*} = \mathcal{C}_{\gamma}^{*} \circ \Lambda_{\bar{n},\eta}^{(\mathrm{Re}),*} \circ \Lambda_{\bar{n},\eta}^{(\mathrm{Im}),*} \circ \Lambda_{\bar{n},\eta}^{(\mathrm{shift}),*} 
= \Lambda_{\bar{n},\eta}^{(\mathrm{Re}),*} \circ \mathcal{C}_{\gamma}^{*} \circ \Lambda_{\bar{n},\eta}^{(\mathrm{Im}),*} \circ \Lambda_{\bar{n},\eta}^{(\mathrm{shift}),*}.$$
(D44)

$$= \Lambda_{\bar{n},\eta}^{(\text{Re}),*} \circ \mathcal{C}_{\gamma}^{*} \circ \Lambda_{\bar{n},\eta}^{(\text{Im}),*} \circ \Lambda_{\bar{n},\eta}^{(\text{shift}),*}. \tag{D45}$$

This is because both the cubic phase gate and the "real" part of the thermal loss channel leaves the position quadrature of the mode unchanged, therefore they can be inter-changably applied. Although these decomposed channels are unphysical, expressing them in this way is crucial: it enables us to devise efficient classical simulation algorithms, as explained in the following sections.

Before detailing our main simulation algorithm, as a warm-up demonstration, we explain how a stronger noise model of uniform layer of thermal loss channel can render the calculation of overlap of two quantum states trivial.

# Appendix E: Warm up: Overlap decay under uniform noise

We analyze the effect of a uniform layer of thermal noise acting on all modes of a bosonic circuit (Figure 1). This setting, while strong, provides a clean and illustrative case where overlap quantum states decays rapidly under noise. As a preliminary technical step, we show that the purity of an operator evolved under the (unphysical) depolarizing map introduced in the previous section decay exponentially with the number of modes.

**Lemma E.1** (Purity decay under depolarizing map). Let H be a trace-class operator on m modes, and  $\mathcal{N}_p^{\otimes m}$  denote the depolarizing map with parameter p. For any  $\tau \geqslant 0$ , it holds that

$$\|\mathcal{N}_{p}^{\otimes m}(H)\|_{2}^{2} \leqslant \left(\frac{\tau^{m}}{m!}\right) \|H\|_{1}^{2} + \exp(-2p\tau) \|H\|_{1}^{2}. \tag{E1}$$

In particular, if  $p \in \Omega(1)$ , then it holds that

$$\|\mathcal{N}_{p}^{\otimes m}(H)\|_{2}^{2} \in \exp\left(-\Omega(m \cdot \min\{1, p\})\right) \|H\|_{1}^{2}. \tag{E2}$$

*Proof.* Expressing the Schatten 2-norm of  $\mathcal{N}_p^{\otimes m}(H)$  in the displacement operator basis, we find that

$$\|\mathcal{N}_p^{\otimes m}(H)\|_2^2 = \frac{1}{\pi^m} \int_{\mathbb{C}^m} d^{2m} \boldsymbol{\alpha} \left| \text{Tr} \left[ H \mathcal{N}_p^{\otimes m}(D(\boldsymbol{\alpha})) \right] \right|^2$$
 (E3)

$$= \underbrace{\frac{1}{\pi^m} \int_{\substack{\mathbb{C}^m : \\ \|\boldsymbol{\alpha}\|_2^2 \leqslant \tau}} d^{2m} \boldsymbol{\alpha} \left| \operatorname{Tr} \left[ H \mathcal{N}_p^{\otimes m} (D(\boldsymbol{\alpha})) \right] \right|^2}_{:=I_{\text{low}}} + \underbrace{\frac{1}{\pi^m} \int_{\substack{\mathbb{C}^m : \\ \|\boldsymbol{\alpha}\|_2^2 \geqslant \tau}} d^{2m} \boldsymbol{\alpha} \left| \operatorname{Tr} \left[ H \mathcal{N}_p^{\otimes m} (D(\boldsymbol{\alpha})) \right] \right|^2}_{:=I_{\text{high}}}, \tag{E4}$$

where in the first step we used the fact that the depolarizing map and its adjoint coincide, i.e.  $\mathcal{N}_p^* = \mathcal{N}_p$ . We now upper bound  $I_{\text{low}}$  and  $I_{\text{high}}$  separately. The integral  $I_{\text{low}}$  can be upper bounded as follows

$$I_{\text{low}} = \frac{1}{\pi^m} \int_{\substack{\mathbb{C}^m:\\ \|\boldsymbol{\alpha}\|_2^2 \leqslant \tau}} d^{2m} \boldsymbol{\alpha} \left| \text{Tr} \left[ H \mathcal{N}_p^{\otimes m} (D(\boldsymbol{\alpha})) \right] \right|^2$$
 (E5)

$$\leq \max_{\alpha} \left\{ \exp\left(-2p|\alpha|^{2}\right) |\operatorname{Tr}[HD(\alpha)]|^{2} \right\} \times \left( \frac{1}{\pi^{m}} \int_{\substack{\mathbb{C}^{m}:\\ \|\alpha\|_{s}^{2} \leq \tau}} d^{2m} \alpha \right)$$
 (E6)

$$\leq \|H\|_{1}^{2} \max_{\alpha} \|D(\alpha)\|_{\infty}^{2} \frac{\tau^{m}}{m!} = \frac{\tau^{m}}{m!} \|H\|_{1}^{2},$$
 (E7)

where in the second inequality we use Hölder's inequality and then we noted that  $||D(\alpha)||_{\infty} = 1$  since the displacement operators are unitary. Moreover, we also used the fact that the volume of the 2m-dimensional ball of radius  $\tau$  is  $\pi^m \tau^m / m!$  (Fact B.1). As for  $I_{\text{high}}$ , we have that

$$I_{\text{high}} = \frac{1}{\pi^m} \int_{\substack{\mathbb{C}^m:\\ \|\boldsymbol{\alpha}\|_2^2 \geqslant \tau}} d^{2m} \boldsymbol{\alpha} \operatorname{Tr} \left[ H \mathcal{N}_p^{\otimes m} (D(\boldsymbol{\alpha})) \right]^2$$
 (E8)

$$= \frac{1}{\pi^m} \int_{\substack{\mathbb{C}^m:\\ \|\boldsymbol{\alpha}\|_2^2 \geqslant \tau}} d^{2m} \boldsymbol{\alpha} \exp\left(-2p\|\boldsymbol{\alpha}\|_2^2\right) |\operatorname{Tr}[HD(\boldsymbol{\alpha})]|^2 \leqslant \exp(-2p\tau) \int_{\substack{\mathbb{C}^m:\\ \|\boldsymbol{\alpha}\|_2^2 \geqslant \tau}} d^{2m} \boldsymbol{\alpha} |\operatorname{Tr}[HD(\boldsymbol{\alpha})]|^2$$
(E9)

$$\leq \exp(-2p\tau) \int_{\mathbb{C}^m} d^{2m} \boldsymbol{\alpha} |\text{Tr}[HD(\boldsymbol{\alpha})]|^2 = \exp(-2p\tau) \|H\|_2^2$$
(E10)

$$\leq \exp(-2p\tau)\|H\|_1^2,\tag{E11}$$

where for the last inequality, we have used the property of Schatten norms that  $||H||_2 \leq ||H||_1$ . Putting everything together, we obtain the first part of the Lemma:

$$\|\mathcal{N}_{p}^{\otimes m}(H)\|_{2}^{2} \leqslant \left(\frac{\tau^{m}}{m!} + \exp(-2p\tau)\right) \|H\|_{1}^{2}.$$
 (E12)

In order to prove the second part of the Lemma, we employ the inequality  $\frac{1}{m!} \leqslant \frac{e^m}{m^m}$  and we choose  $\tau = 0.9e^{-1}m$ :

$$\|\mathcal{N}_{p}^{\otimes m}(H)\|_{2}^{2} \leqslant \left(\frac{e^{m}\tau^{m}}{m^{m}} + \exp(-2p\tau)\right) \|H\|_{1}^{2}$$
 (E13)

$$= 2\left(0.9^{m} + \exp\left(-m(1.8e^{-1}p)\right)\right) \|H\|_{1}^{2} \tag{E14}$$

$$\in \exp(-\Omega(m)) \|H\|_{1}^{2} + \exp(-\Omega(mp)) \|H\|_{1}^{2}$$
 (E15)

$$\subseteq \exp(-\Omega(m \cdot \min\{1, p\})) \|H\|_1^2, \tag{E16}$$

where in the second-to-last step we noted that  $1.8e^{-1}p \in \Omega(p)$  and  $0.9^m \in \exp(-\Omega(m))$ .

Building on Lemma E.1, which establishes exponential purity decay under the depolarizing map, we can now lift this result to the physical thermal loss channel, leading to the following Theorem.

**Theorem E.1** (Overlap decay under thermal channel). Given two quantum states  $\rho$  and  $\sigma$  and the m-mode thermal loss channel  $\Lambda_{\bar{n},\eta}^{\otimes m}$  satisfying  $\bar{n}(1-\eta) \in \Omega(1)$ 

$$\left| \operatorname{Tr} \left[ \Lambda_{\bar{n}, \eta}^{\otimes m}(\rho) \sigma \right] \right| = \left| \operatorname{Tr} \left[ \rho \Lambda_{\bar{n}, \eta}^{\otimes m*}(\sigma) \right] \right| \in \exp(-\Omega(\bar{n}(1 - \eta)m)). \tag{E17}$$

*Proof.* Decomposing each of the thermal loss channels as  $\Lambda_{\bar{n},\eta}^*$  as  $\Lambda_{\bar{n},\eta}^* = \Lambda_{0,\eta}^* \circ \mathcal{N}_{\bar{n}(1-\eta)}$ , we get

$$\left| \operatorname{Tr} \left[ \rho \Lambda_{\bar{n},\eta}^{\otimes m*}(\sigma) \right] \right| = \left| \operatorname{Tr} \left[ \Lambda_{0,\eta}^{\otimes m}(\rho) \mathcal{N}_{\bar{n}(1-\eta)}^{\otimes m}(\sigma) \right] \right| \leq \|\Lambda_{0,\eta}^{\otimes m}(\rho)\|_2 \|\mathcal{N}_{\bar{n}(1-\eta)}^{\otimes m}(\sigma)\|_2$$
 (E18)

$$\in \exp(-\Omega(m \cdot \min\{1, \bar{n}(1-\eta))\}) \subseteq \exp(-\Omega(\bar{n}(1-\eta)m)), \tag{E19}$$

Here we first used Hölder's inequality (Lemma B.5) with p=q=2, the facts that  $\Lambda_{0,\eta}^{\otimes m}(\rho)$  is a quantum state and therefore its purity  $\|\Lambda_{0,\eta}^{\otimes m}(\rho)\|_2^2$  is at most 1, together with Lemma E.1. Finally, in the last step we used that  $\bar{n}(1-\eta) \in \Omega(1)$ .

This Theorem demonstrates that for a uniform layer of thermal loss channel, the overlap of two states exponentially in m concentrates to zero and hence the simulation of such overlaps becomes trivial.

Before establishing classical simulation results for a weaker noise model, we need a few more technical results, which we detail in the upcoming section.

### Appendix F: Sampling from the Fourier-Weyl spectrum

As stated earlier, our simulation algorithm is an instance of Markov chain Monte Carlo methods, where we are sampling a point from an appropriate probability distribution and evaluating the estimator function at that point. In order to formalize our algorithm and our results, we first define a sampling oracle:

**Definition F.1** (Sampling Oracle). Let O be an m-mode operator and let S be a set of m-mode operators. Given  $\epsilon, A \geq 0$ , we define the Sampling Oracle Sample<sup>(S)</sup>(O) with bias  $\epsilon$  and magnitude A. When queried, Sample<sup>(S)</sup>(O) returns independent draws  $(Z, \mathbf{r}) \in \mathbb{C} \times \mathbb{R}^{2m}$  such that for any fixed operator  $\sigma \in S$  independent of  $(Z, \mathbf{r})$ , it holds that:

$$|Z| \le A \quad and \quad |\mathbb{E}[Z\operatorname{Tr}[D(r)\sigma]] - \operatorname{Tr}[O\sigma]| \le \epsilon.$$
 (F1)

When S is the entire set of m-mode operators, we drop the superscript and simply write Sample(O).

The sampling oracle can be thought of as a randomized procedure that outputs a displacement operator (weighted by a prefactor), allowing the estimation of expectation values. The *bias* quantifies the systematic error introduced by the oracle, while the *magnitude* controls the maximum variance of its outputs. Together, these parameters allow us to rigorously track how approximation errors accumulate when combining many oracles in a simulation algorithm, as detailed in the following lemma.

**Lemma F.1** (Chained Sampling). Let  $\mathcal{L}$  be a linear map and O be an operator. Assume we have access to the oracle  $\mathsf{Sample}^{(\mathcal{S})}(O)$  with bias  $\epsilon_1$  and magnitude  $A_1$  and also to the oracle  $\mathsf{Sample}^{(\mathcal{S})}(\mathcal{L}(D(\mathbf{r})))$  with bias  $\epsilon_2$  and magnitude  $A_2$  for all  $\mathbf{r} \in \mathbb{R}^{2m}$ . Moreover, we assume that  $\sigma \in \mathcal{S} \implies \mathcal{L}^*(\sigma) \in \mathcal{S}$ . Then we can simulate the oracle  $\mathsf{Sample}^{(\mathcal{S})}(\mathcal{L}(O))$  with bias  $\epsilon_1 + A_1\epsilon_2$  and magnitude  $A_1A_2$ .

*Proof.* Let  $(Z_1, r_1)$  be drawn from the oracle  $\mathsf{Sample}^{(\mathcal{S})}(O)$ . Then it holds that

$$\forall \sigma \in \mathcal{S} : \left| \mathbb{E}_{Z_1, \mathbf{r}_1} \left[ Z_1 \operatorname{Tr} \left[ D(\mathbf{r}_1) \mathcal{L}^*(\sigma) \right] \right] - \operatorname{Tr} \left[ O \mathcal{L}^*(\sigma) \right] \right| \leqslant \epsilon_1.$$
 (F2)

By the definition of adjoint map, it follows that

$$\left| \mathbb{E}_{Z_1, \mathbf{r}_1} \left[ Z_1 \operatorname{Tr} \left[ \mathcal{L}(D(\mathbf{r}_1)) \sigma \right] \right] - \operatorname{Tr} \left[ \mathcal{L}(O) \sigma \right] \right| \leqslant \epsilon_1.$$
 (F3)

Moreover, given  $(Z_2, \mathbf{r}_2)$  drawn from the oracle  $\mathsf{Sample}^{(\mathcal{S})}(\mathcal{L}(D(\mathbf{r}_1)))$ , it holds that

$$\forall \sigma \in \mathcal{S} : \left| \mathbb{E}_{Z_2, r_2} \left[ Z_2 \operatorname{Tr} \left[ D(r_2) \sigma \right] \right] - \operatorname{Tr} \left[ \mathcal{L}(D(r_1)) \sigma \right] \right| \leqslant \epsilon_2.$$
 (F4)

Thus, for all  $\sigma \in \mathcal{S}$  it holds that

$$\mathbb{E}_{Z_1, \boldsymbol{r}_1, Z_2, \boldsymbol{r}_2} \left\{ Z_1 Z_2 \operatorname{Tr} \left[ D(\boldsymbol{r}_2) \sigma \right] \right\} \tag{F5}$$

$$= \mathbb{E}_{Z_1, \mathbf{r}_1} \left\{ Z_1 \mathbb{E}_{Z_2, \mathbf{r}_2 \mid Z_1, \mathbf{r}_1} \left[ Z_2 \operatorname{Tr} \left[ D(\mathbf{r}_2) \sigma \right] \right] \right\}$$
 (F6)

$$= \mathbb{E}_{Z_1, \mathbf{r}_1} \left\{ Z_1 \operatorname{Tr} \left[ \mathcal{L}(D(\mathbf{r}_1)) \sigma \right] \right\} + Z_1 \alpha_2 \tag{F7}$$

$$=\operatorname{Tr}[O\sigma] + \alpha_1 + Z_1\alpha_2,\tag{F8}$$

where  $\alpha_1, \alpha_2 \in \mathbb{C}$  satisfy  $|\alpha_1| \leq \epsilon_1$  and  $|\alpha_2| \leq \epsilon_2$ , reflecting the fact that the corresponding oracles have biases  $\epsilon_1$  and  $\epsilon_2$ , respectively. Rearranging the above equation and using the triangle inequality we find that

$$\left| \mathbb{E}_{Z_1, \mathbf{r}_1, Z_2, \mathbf{r}_2} \left\{ Z_1 Z_2 \operatorname{Tr} \left[ D(\mathbf{r}_2) \sigma \right] \right\} - \operatorname{Tr} [O \sigma] \right| \leqslant \epsilon_1 + A_1 \epsilon_2.$$
 (F9)

As  $Z_1Z_2 \leq |A_1A_2|$ , the above inequality implies that we can simulate the oracle  $\mathsf{Sample}^{(\mathcal{S})}(\mathcal{L}(O))$  with bias  $\epsilon_1 + A_1\epsilon_2$  and magnitude  $A_1A_2$ .

We briefly comment on how errors propagate when simulating circuits layer by layer. At each step, the bias adds linearly, while the magnitude multiplies across layers. Consequently, repeated chaining of oracles can cause the simulation error to grow exponentially with depth, unless the magnitude remains strictly smaller than one. This contractive property will therefore be crucial in identifying efficiently simulable regimes.

Note that when estimating  $\mathbb{E}[Z\operatorname{Tr}[D(r)\sigma]]$  via statistical sampling, we are effectively drawing points from phase space and evaluating the characteristic function at these points. Extending this to a Markov chain by chaining several such sampling oracles corresponds to sampling sequences of displacement operators, or "paths," and evaluating the characteristic function at the endpoint of each path. This perspective motivates the terminology displacement propagation for the simulation algorithm.

#### 1. Unbiased oracles

To develop efficient simulation algorithms, we require unbiased sampling procedures that accurately reproduce the action of noisy circuit layers on displacement operators. This can be achieved by decomposing the noisy cubic gates and thermal channels into simpler linear maps, as detailed in Section D3. Here, we construct sampling oracles whose statistical averages coincide exactly with the desired quantum expectation values. The following Lemmas provide the technical foundation for this construction, presenting explicit recipes for implementing these unbiased estimators.

**Lemma F.2.** For j = 2, 3, ..., L, let  $A_j$  be defined as follows:

$$\mathcal{A}_{j} = \mathcal{C}_{j-1,\mathfrak{D}}^{*} \circ \Lambda_{\bar{n},\eta}^{(\mathrm{Re}),*} \circ \mathcal{G}_{j}^{*} \circ \Lambda_{\bar{n},\eta}^{(\mathrm{shift}),*} \circ \Lambda_{\bar{n},\eta}^{(\mathrm{Im}),*} \circ \mathcal{C}_{j,\mathfrak{C}}^{*}, \tag{F10}$$

Then for all  $\mathbf{r} = (q_1, p_1, \dots, q_m, p_m) \in \mathbb{R}^{2m}$  with  $q_1 \neq 0$  we have that

$$\|\mathcal{A}_{j}(D(r))\|_{\mathbb{F},1} \leqslant \frac{\Gamma(\frac{1}{4})}{(\sigma^{-1})_{j} \sqrt{24\pi} \eta^{1/2} |\gamma_{j-1}|^{1/2}} \times \left\{ \left(\frac{1}{2} + \bar{n}\right) (1 - \eta) \right\}^{-1/4}, \tag{F11}$$

where

$$(\sigma^{-1})_j = |(S_j^{-1})_{q_1, p_1}| \tag{F12}$$

and  $S_j$  is the symplectic matrix associated with the Gaussian channel  $\mathcal{G}_j$ . Moreover, for all  $\mathbf{r} = (q_1, p_1, \dots, q_m, p_m) \in \mathbb{R}^{2m}$  with  $q_1 \neq 0$ , there is a classical randomized algorithm that implements the oracle  $\mathsf{Sample}(\mathcal{A}_j(D(\mathbf{r})))$  with zero bias and magnitude

$$\frac{\Gamma(\frac{1}{4})}{\sigma_i^{-1} \sqrt{24\pi} \eta^{1/2} |\gamma_{j-1}|^{1/2}} \times \left\{ \left(\frac{1}{2} + \bar{n}\right) (1 - \eta) \right\}^{-1/4}.$$
 (F13)

*Proof.* We start by decomposing  $A_j$  into simpler linear maps, and considering its action on a displacement operator:

$$\mathcal{A}_{j}(D(\boldsymbol{r})) = \mathcal{C}_{j-1,\mathfrak{D}}^{*} \circ \Lambda_{\bar{n},\eta}^{(\mathrm{Re}),*} \circ \mathcal{G}_{j}^{*} \circ \Lambda_{\bar{n},\eta}^{(\mathrm{shift}),*} \circ \Lambda_{\bar{n},\eta}^{(\mathrm{Im}),*} \circ \mathcal{C}_{j,\mathfrak{C}}^{*}(D(\boldsymbol{r}))$$

$$= \int_{\mathbb{R}} d\bar{p}_{1} \exp\left[i\left(\frac{(p_{1} - \bar{p}_{1})^{2}}{24\gamma_{j}q_{1}} - 4\gamma_{j}q_{1}^{3} - \frac{\pi}{4} + \boldsymbol{d}_{j}^{T}\Omega\bar{\boldsymbol{r}}\right)\right]$$

$$\times \sqrt{\operatorname{sgn}(\tilde{q}_{1}\gamma_{j-1})} \times \frac{\exp\left(-(1/2 + \bar{n})(1 - \eta)(\tilde{q}_{1}^{2} + \bar{p}_{1}^{2})\right)}{\sqrt{6\pi|\tilde{q}_{1}\gamma_{j-1}|}}D(\tilde{\boldsymbol{r}}), \tag{F14}$$

where

$$\bar{\boldsymbol{r}} = (\bar{q}_1, \bar{p}_1, \dots, \bar{q}_m, \bar{p}_m) = \sqrt{\eta}(q_1, \bar{p}_1, \dots, q_m, p_m), 
\tilde{\boldsymbol{r}} = (\tilde{q}_1, \tilde{p}_1, \dots, \tilde{q}_m, \tilde{p}_m) = S_j^{-1} \bar{\boldsymbol{r}}.$$
(F15)

(F16)

Defining the function  $\Phi_j : \mathbb{R}^{2m+1} \to \mathbb{C}$  such that  $\max_{r,\bar{p}_1} |\Phi_j(r,\bar{p}_1)| \leqslant 1$ ,

$$\Phi_{j}(\boldsymbol{r},\bar{p}_{1}) := \exp\left[i\left(\frac{(p_{1}-\bar{p}_{1})^{2}}{24\gamma_{j}q_{1}} - 4\gamma_{j}q_{1}^{3} - \frac{\pi}{4} + \boldsymbol{d}_{j}^{T}\Omega\bar{\boldsymbol{r}}\right)\right] \times \sqrt{\operatorname{sgn}(\tilde{q}_{1}\gamma_{j-1})} \times \exp\left(-(1/2+\bar{n})(1-\eta)(\bar{p}_{1}^{2})\right) \times \operatorname{Tr}[\rho D(\tilde{\boldsymbol{r}})]$$
(F17)

and the unnormalized density function  $\nu_i : \mathbb{R} \to \mathbb{R}^+$ 

$$\nu_j(\bar{p}_1) := \frac{\exp(-(1/2 + \bar{n})(1 - \eta)\tilde{q}_1^2)}{\sqrt{24\pi|\tilde{q}_1\gamma_{j-1}|}},\tag{F18}$$

where

$$\tilde{q}_1 = -\sqrt{\eta}(S_j^{-1})_{q_1, p_1}\bar{p}_1 + \text{terms depending on } (q_1, p_1, \dots, q_m, p_m).$$
 (F19)

Then we have

$$\operatorname{Tr}[\rho \mathcal{A}_{j}(D(\boldsymbol{r}))] = \int_{\bar{p}_{1}} d\bar{p}_{1} \Phi_{j}(\boldsymbol{r}, \bar{p}_{1}) \nu_{j}(\bar{p}_{1}). \tag{F20}$$

We note that the Fourier-1 norm of  $A_i(D(r))$  can be computed via a Gamma function, as detailed in Lemma B.3

$$\|\mathcal{A}_{j}(D(\boldsymbol{r}))\|_{\mathbb{F},1} = \int_{\mathbb{R}} d\bar{p}_{1}\nu(\bar{p}_{1})|\Phi_{j}(\boldsymbol{r},\bar{p}_{1})| \leq \int_{\mathbb{R}} d\bar{p}_{1}\nu(\bar{p}_{1}) = \frac{\Gamma(\frac{1}{4})}{(\sigma^{-1})_{j}\sqrt{24\pi}\eta^{1/2}|\gamma_{j-1}|^{1/2}} \times \left\{\left(\frac{1}{2} + \bar{n}\right)(1-\eta)\right\}^{-1/4}$$
(F21)

using Lemma B.3. Therefore, we can invoke Lemma B.9 to implement  $Sample(A_i(D(r)))$  with zero bias and magnitude

$$\frac{\Gamma(\frac{1}{4})}{(\sigma^{-1})_j \sqrt{6\pi} \eta^{1/2} |\gamma_{j-1}|^{1/2}} \times \left\{ \left(\frac{1}{2} + \bar{n}\right) (1 - \eta) \right\}^{-1/4}.$$
 (F22)

Lemma F.2 addresses the general case for  $A_j$  with  $j \ge 2$ . We then define a linear map  $A_1$  with a slightly simpler structure and is therefore handled separately in the next result.

**Lemma F.3.** Given the linear map  $A_1$  defined as

$$\mathcal{A}_{1} := \Lambda_{\bar{n},\eta}^{(\text{shift}),*} \circ \Lambda_{\bar{n},\eta}^{(\text{Im}),*} \circ \mathcal{C}_{1,\mathfrak{C}}^{*} \tag{F23}$$

then for all  $\mathbf{r} \in \mathbb{R}^{2m}$ , we have that

$$\|\mathcal{A}_1(D(\mathbf{r}))\|_{\mathbb{F},1} = \sqrt{\pi}((1/2+\bar{n})(1-\eta))^{-1/2}$$
 (F24)

Moreover, for all  $\mathbf{r} \in \mathbb{R}^{2m}$ , there is a classical randomized algorithm that implements the oracle  $\mathsf{Sample}(\mathcal{A}_1(D(\mathbf{r})))$  with zero bias and magnitude

$$\sqrt{\pi}((1/2+\bar{n})(1-\eta))^{-1/2}$$
 (F25)

*Proof.* We start by decomposing  $A_1$  into simpler linear maps, and considering its action on a displacement operator:

$$\mathcal{A}_{1}(D(\boldsymbol{r})) = \Lambda_{\bar{n},\eta}^{(\text{shift}),*} \circ \Lambda_{\bar{n},\eta}^{(\text{Im}),*} \circ \mathcal{C}_{1,\mathfrak{C}}^{*}(D(\boldsymbol{r}))$$

$$= \int_{\mathbb{R}} d\bar{p}_{1} \exp\left(i\left(\frac{(p_{1} + \bar{p}_{1})^{2}}{24\gamma_{1}q_{1}} - 4\gamma_{1}q_{1}^{3} - \frac{\pi}{4}\right)\right)$$

$$\times \exp\left(-(1/2 + \bar{n})(1 - \eta)\bar{p}_{1}^{2}\right)D(\sqrt{\eta}\tilde{\boldsymbol{r}}), \tag{F26}$$

where

$$\tilde{r} = (q_1, \bar{p}_1, q_2, p_2, \dots, q_m, p_m).$$
 (F27)

Defining the function  $\Phi_1: \mathbb{R}^{2m+1} \to \mathbb{C}$  such that  $\max_{\boldsymbol{r},\bar{p}_1} |\Phi_1(\boldsymbol{r},\bar{p}_1)| \leq 1$ ,

$$\Phi_1(\mathbf{r}, \bar{p}_1) = \exp\left(i\left(\frac{(p_1 + \bar{p}_1)^2}{24\gamma_1 q_1} - 4\gamma_1 q_1^3 - \frac{\pi}{4}\right)\right) \hat{\text{Tr}}[\rho D(\sqrt{\eta}\tilde{\mathbf{r}})]$$
 (F28)

and the unnormalized density function  $\nu_1: \mathbb{R} \to \mathbb{R}^+$ 

$$\nu_1(\bar{p}_1) = \exp(-(1/2 + \bar{n})(1 - \eta)\bar{p}_1^2). \tag{F29}$$

Then we have

$$\operatorname{Tr}[\rho \mathcal{A}_{1}(D(\boldsymbol{r}))] = \int_{\mathbb{R}} d\bar{p}_{1} \nu_{1}(\bar{p}_{1}) \Phi_{1}(\boldsymbol{r}, \bar{p}_{1})$$
(F30)

Then the Fourier one norm of  $\mathcal{A}_1(D(r))$  is given by

$$\|\mathcal{A}_1(D(\mathbf{r}))\|_{\mathbb{F},1} = \sqrt{\pi}((1/2 + \bar{n})(1 - \eta))^{-1/2}.$$
 (F31)

Moreover, as  $|\Phi_1(\mathbf{r}, \bar{p}_1)| \leq 1$  and  $\nu_1$  is a Gaussian probability density function, we can invoke Lemma B.8 to implement  $\mathsf{Sample}(\mathcal{A}_1(D(\mathbf{r})))$  with zero bias and magnitude

$$\sqrt{\pi}((1/2+\bar{n})(1-\eta))^{-1/2}$$
. (F32)

These sampling oracles will be used in Section G 2 where we employ unbiased estimator function to estimate characteristic functions.

#### 2. Biased oracle

Noting the expression of displacement operator  $\hat{D}(q_1, p_1) = \exp(ip_1\hat{q} - iq_1\hat{p})$  and the action of the cubic phase gate on the position and momentum quadrature operators (Eq. C21), we see that for  $q_1 \to 0$  or  $\gamma \to 0$ , the action of the cubic phase gate is the identity operation. The following Lemma is based on this intuition: that for  $|q_1\gamma|$  very close to zero, we can approximate the cubic phase gate with the identity operation by introducing a small error. Our approach involves a "biased sampling" from the Fourier-Weyl spectrum of the Heisenberg evolution of  $D(\alpha)$ . Effectively, our method can be thought of as replacing the cubic gate  $C_j$  with a regularized version  $\widetilde{C}_j$ , which acts as follows

$$\widetilde{C}_{j}(O) = \frac{1}{\pi} \int_{\gamma |\alpha_{R}| \leq \tau} \text{Tr}[OD(\alpha)]D(-\alpha) + \frac{1}{\pi} \int_{\gamma |\alpha_{R}| > \tau} \text{Tr}[OD(\alpha)]C_{j}(D(-\alpha)).$$
 (F33)

In doing so, we incur in a regularization error, which depends on the threshold  $\tau$  we chose and on some properties of the state  $\rho_i$ . We formalize this result in the following Lemma:

**Lemma F.4** (Adaptive sampling from noisy cubic gates). Given  $M \ge 0$ , let  $S_M$  be a set of m-mode quantum states such that

$$\max_{\substack{\rho \in \mathcal{S}_M \\ \mathbf{r}' \in \mathbb{R}^{2m}}} \left| \left\{ \frac{\partial^2}{\partial^2 p_1} \operatorname{Tr}[D(\mathbf{r}) \Lambda_{\bar{n}, \eta}(\rho)] \right\}_{\mathbf{r} = \mathbf{r}'} \right| \leqslant M.$$
 (F34)

1. For any  $\mathbf{r} \in \mathbb{R}^{2m}$  and for any  $\rho \in \mathcal{S}_M$ ,

$$\left| \operatorname{Tr}[D(\boldsymbol{r}) \mathcal{C}_{\gamma}(\Lambda_{\bar{n},\eta}(\rho))] - \exp\left(-i4\gamma \left(q_{1}\right)^{3}\right) \operatorname{Tr}[D(\boldsymbol{r})\Lambda_{\bar{n},\eta}(\rho)] \right| \leqslant 6|\gamma q_{1}|M. \tag{F35}$$

2. For any  $r \in \mathbb{R}^{2m}$ , we can implement the oracle  $\mathsf{Sample}^{(\mathcal{S}_M)}(\Lambda_{\bar{n},\eta}^* \circ \mathcal{C}_{\gamma}^*(D(r)))$  with bias  $\epsilon$  and magnitude

$$\frac{1}{2}\sqrt{\frac{M}{\epsilon}}\exp\left[-\left(\frac{1}{2}+\bar{n}\right)(1-\eta)\frac{\epsilon^2}{36M^2\gamma^2}\right]$$
 (F36)

in time  $\mathcal{O}(m)$ .

*Proof.* We begin by expressing the action of the noisy cubic phase gate in the Heisenberg picture, which introduces an oscillatory integral representation involving the displacement operators.

$$\Lambda_{\bar{n},\eta}^* \circ \mathcal{C}_{\gamma}^*(D(\boldsymbol{r})) = \sqrt{\frac{1}{24\pi\gamma q_1}} \int d\bar{p}_1 \exp\left[i\left(\frac{(p_1 + \bar{p}_1)^2}{24\gamma q_1} - 4\gamma q_1^3 - \frac{\pi}{4}\right)\right] \Lambda_{\bar{n},\eta}^*(D(\bar{\boldsymbol{r}})), \tag{F37}$$

where  $\bar{r} = (q_1, -\bar{p}_1, q_2, p_2, \dots, q_m, p_m)$ . To analyze this integral, we consider two distinct regimes depending on the value of the product  $|\gamma q_1|$ . In the first regime, where  $|\gamma q_1|$  is small, we approximate the cubic phase gate by a simple phase factor. In the second regime, where  $|\gamma q_1|$  is large, we explicitly evaluate the contribution of the thermal loss channel.

The presence of a Gaussian damping factor ensures the integral is well-behaved and can be approximated via a Monte Carlo estimator.

Let  $\lambda \geqslant 0$  be a parameter to be optimized.

Case 1:  $|\gamma q_1| \leq \lambda$ . We will approximate the desired value up to a small error, without performing any sampling procedure. We have:

$$I(\mathbf{r},\rho) := \text{Tr}\left[\Lambda_{\bar{n},\eta}^* \circ \mathcal{C}_{\gamma}^*(D(\mathbf{r}))\rho\right] \tag{F38}$$

$$= \sqrt{\frac{1}{24\pi\gamma q_1}} \int d\tilde{p}_1 \exp\left[i\left(\frac{(p_1 - \tilde{p}_1)^2}{24\gamma q_1} - 4\gamma q_1^3 - \frac{\pi}{4}\right)\right] \operatorname{Tr}[(D(\bar{r}))\Lambda_{\bar{n},\eta}(\rho)], \tag{F39}$$

$$= \int d\tilde{p}_1 \frac{1}{\sqrt{\pi \sigma}} \exp\left(i \left(\frac{(p_1 - \tilde{p}_1)^2}{\sigma} - 4\gamma q_1^3 - \frac{\pi}{4}\right)\right) \text{Tr}[D(\bar{r})\Lambda_{\bar{n},\eta}(\rho)], \tag{F40}$$

where in the last line, we set  $\sigma = 24\gamma q_1$  and  $\bar{r} = (q_1, \bar{p}_1, q_2, p_2, \dots, q_m, p_m)$ . Hence by Lemma B.4

$$\left| I(\boldsymbol{r}, \rho) - \exp\left( -4i\gamma \left( q_1 \right)^3 \right) \operatorname{Tr}[D(\boldsymbol{r}') \Lambda_{\bar{n}, \eta}(\rho)] \right| \leqslant \frac{\sigma}{4} \max_{\boldsymbol{r} \in \mathbb{R}^{2m}} \left| \frac{\partial^2}{\partial^2 p_1} \operatorname{Tr}[D(\boldsymbol{r}) \Lambda_{\bar{n}, \eta}(\rho)] \right| \leqslant 6\lambda M. \tag{F41}$$

Case 2:  $|\gamma q_1| > \lambda$ . In this case, we write the action of the noise channel explicitly:

$$I(\boldsymbol{r},\rho) := \sqrt{\frac{1}{24\gamma q_1}} \int d\tilde{p}_1 \exp\left[i\left(\frac{(p_1 + \bar{p}_1)^2}{24\gamma q_1} - 4\gamma q_1^3 - \frac{\pi}{4}\right)\right]$$
 (F42)

$$\times \exp\left[-\left(\frac{1}{2} + \bar{n}\right)(1 - \eta)\left((q_1)^2 + (\bar{p}_1)^2\right)\right] \operatorname{Tr}[D(\sqrt{\eta}\bar{r})\rho], \tag{F43}$$

$$= \int d\bar{p}_1 \exp\left[-\left(\frac{1}{2} + \bar{n}\right)(1 - \eta)\left(\bar{p}_1^2\right)\right] f(\bar{p}_1), \tag{F44}$$

where

$$f(\bar{p}_1) := \sqrt{\frac{1}{24\gamma q_1}} \exp\left[i\left(\frac{(p_1 + \bar{p}_1)^2}{24\gamma q_1} - 4\gamma q_1^3 - \frac{\pi}{4}\right)\right]$$
 (F45)

$$\times \exp\left[-\left(\frac{1}{2} + \bar{n}\right)(1 - \eta)q_1^2\right] \operatorname{Tr}[D(\sqrt{\eta}\tilde{r})\rho]. \tag{F46}$$

We note that the magnitude of  $f(\bar{p}_1)$  can be bounded as follows:

$$|f(\bar{p}_1)| \le \sqrt{\frac{1}{24|\gamma q_1|}} \exp\left[-\left(\frac{1}{2} + \bar{n}\right)(1 - \eta)q_1^2\right]$$
 (F47)

$$\leq \sqrt{\frac{1}{24\lambda}} \exp\left[-\left(\frac{1}{2} + \bar{n}\right)(1 - \eta)\frac{\lambda^2}{\gamma^2}\right].$$
 (F48)

We choose  $\lambda = \epsilon/(6M)$ . Thus the magnitude of the sampling oracle is

$$\frac{1}{2}\sqrt{\frac{M}{\epsilon}}\exp\left[-\left(\frac{1}{2}+\bar{n}\right)(1-\eta)\frac{\epsilon^2}{36M^2\gamma^2}\right]. \tag{F49}$$

This concludes the proof, showing that expectation values involving noisy cubic gates can be efficiently approximated either by direct approximation in the small-cubicity regime or by Monte Carlo sampling in the large-cubicity regime.

We use this biased oracle in two ways: (i) by combining it with the unbiased estimator (previous section) for when the characteristic function to be estimated has a small  $q_1$  (Section G3a), (ii) for "near Gaussian" circuits where the cubicity of the cubic phase gates is very small throughout the circuit (Section G3b).

Having detailed the necessary preliminaries, we are now ready to introduce the main bosonic circuit considered in this work, consisting of Gaussian unitary gates and cubic phase gates, with environmental interaction modeled by a single-mode thermal loss channel preceding the cubic phase gates (i.e. universal bosonic circuits with noisy cubic phase gates).

#### Appendix G: Classical simulation of noisy bosonic circuits

Having detailed all the required technical results, we are now ready to provide simulation algorithms for simulation of expectation values at the output of a *L*-layered noisy bosonic circuit of the following form:

$$\mathcal{U} := \mathcal{U}_L \circ \mathcal{U}_{L-1} \circ \dots \circ \mathcal{U}_1 \tag{G1}$$

with

$$\mathcal{U}_{j} := \mathcal{C}_{j} \circ \Lambda_{\bar{n},\eta} \circ \mathcal{G}_{j}, \tag{G2}$$

where  $C_j$  is a cubic phase gate with cubicity  $\gamma_j$ ,  $G_j$  is the Gaussian unitary gate with associate symplectic matrix  $S_j$  and displacment vector  $\mathbf{d}_j$ , and  $\Lambda_{\bar{n},\eta}$  is the thermal loss channel (Figure 2).

As a first step, we identify a regime where the simulation of global observables becomes classically efficient in this noisy bosonic circuit.

#### 1. Noise-induced concentration in estimation of global observables

In this section, we prove concentration bounds for expectation values under noisy bosonic evolutions. Our strategy is to establish norm decay properties of linear maps acting on displacement operators and to propagate these through circuit layers. The first step is to quantify how the Fourier 1-norm of an operator evolves under noisy channels. This allows us to characterize the contractive behavior of noisy dynamics and is summarized in the following general Lemma:

**Lemma G.1** (1-norm decay in the Fourier-Weyl basis). Let  $\mathcal{L}$  be a linear map such that  $\|\mathcal{L}(D(r))\|_{\mathbb{F},1} \leq \chi$  for almost every  $r \in \mathbb{R}^{2m}$  (i.e., for all  $r \in \mathbb{R}^{2m}$  except on a subset of measure zero) Let O be an operator whose characteristic function  $\chi_O$  is an  $L^1$ -integrable function. Then the characteristic function of  $\mathcal{L}(O)$  is an  $L^1$ -integrable function, and moreover

$$\|\mathcal{L}(O)\|_{\mathbb{F},1} \leqslant \chi \|O\|_{\mathbb{F},1}. \tag{G3}$$

*Proof.* We start by expanding  $\mathcal{L}(O)$  in the Fourier-Weyl basis

$$\mathcal{L}(O) = \frac{1}{\pi^m} \int_{\mathbb{R}^{2m}} d\mathbf{r} \operatorname{Tr}[OD(\mathbf{r})] \mathcal{L}(D(-\mathbf{r}))$$
 (G4)

$$= \frac{1}{\pi^{2m}} \int_{\mathbb{R}^{4m}} d\mathbf{r} d\mathbf{r}' \operatorname{Tr}[OD(\mathbf{r})] \operatorname{Tr}[\mathcal{L}(D(-\mathbf{r}))D(\mathbf{r}')] \mathcal{D}(-\mathbf{r}'), \tag{G5}$$

where in the second line, we have again expanded  $\mathcal{L}(D(-r))$  in the displacement operator basis. Then by Fubini-Tonelli theorem's (Lemma B.2), the characteristic function of  $\mathcal{L}(O)$  is an  $L^1$ -integrable function, and moreover we can upper

bound the norm  $\|\mathcal{L}(O)\|_{\mathbb{F},1}$  as follows

$$\|\mathcal{L}(O)\|_{\mathbb{F},1} = \frac{1}{\pi^{2m}} \int_{\mathbb{P}^{4m}} d\mathbf{r} d\mathbf{r}' \left| \text{Tr}[OD(\mathbf{r})] \text{Tr}[\mathcal{L}(D(-\mathbf{r}))D(\mathbf{r}')] \right|$$
(G6)

$$= \frac{1}{\pi^m} \int_{\mathbb{R}^{2m}} |\text{Tr}[OD(\boldsymbol{r})]| \left( \frac{1}{\pi^m} \int_{\mathbb{R}^{2m}} \left| \text{Tr}[\mathcal{L}(D(-\boldsymbol{r}))D(\boldsymbol{r}')] \right| d\boldsymbol{r}' \right) d\boldsymbol{r}$$
 (G7)

$$= \frac{1}{\pi^m} \int_{\mathbb{R}^{2m}} |\text{Tr}[OD(\boldsymbol{r})]| \|\mathcal{L}(D(-\boldsymbol{r}))\|_{\mathbb{F},1} d\boldsymbol{r}$$
(G8)

$$\leq \chi \left(\frac{1}{\pi} \int_{\mathbb{R}^{2m}} |\text{Tr}[OD(\boldsymbol{r})]| d\boldsymbol{r}\right) = \chi \|O\|_{\mathbb{F},1},\tag{G9}$$

where the second line follows from Fubini-Tonelli's theorem (Lemma B.2) and the inequality follows from the fact that  $\|\mathcal{L}(D(r))\|_{\mathbb{F},1} \leq \chi$  for almost every  $r \in \mathbb{R}^{2m}$ .

Having established a generic 1-norm decay bound, we now analyze how individual noisy circuit layers act on displacement operators. Specifically, we introduce the maps  $\mathcal{B}_j$  describing the combination of cubic, Gaussian, and noisy evolutions, upper bound their Fourier 1-norm and ultimately show that they admit a strong contraction property for sufficiently strong noise.

**Lemma G.2.** For for j = 2, ..., t-1, we consider the linear map  $\mathcal{B}_j$  defined as follows

$$\mathcal{B}_{j} = \mathcal{C}_{j,\mathfrak{D}} \circ \Lambda_{\bar{n},\eta} \circ \mathcal{G}_{j} \circ \mathcal{C}_{j-1,\mathfrak{C}} \tag{G10}$$

For all  $\mathbf{r} = (q_1, p_1, \dots, q_m, p_m) \in \mathbb{R}^{2m}$  such that  $q_1 \neq 0$ , it holds that

$$\|\mathcal{B}_{j}(D(\mathbf{r}))\|_{\mathbb{F},1} \leqslant \frac{\Gamma(1/4)}{\sqrt{24\pi}\sigma_{j}|\gamma_{j}|^{1/2}\eta^{1/4}} \times ((1/2+\bar{n})(1-\eta))^{-1/4},\tag{G11}$$

where

$$\sigma_j = |(S_j)_{q_1, p_1}|.$$
 (G12)

*Proof.* The evolved operator  $\mathcal{B}_i(D(r))$  can be expressed as follows:

$$\mathcal{B}_{j}(D(\mathbf{r})) = \frac{1}{\sqrt{\eta}} \int_{\mathbb{R}} d\bar{p}_{1} \frac{\exp\left(i\left(-\frac{(p_{1}+\bar{p}_{1})^{2}}{24\gamma_{j-1}q_{1}} + 4\gamma_{j-1}q_{1}^{3} + \pi/4 - \mathbf{d}_{j}^{T}\Omega S_{j}\bar{\mathbf{r}}\right)\right) \exp\left(-(1/2+\bar{n})(1/\eta - 1)(\tilde{q}_{1}^{2} + \tilde{p}_{1}^{2})\right)}{\sqrt{24\pi\gamma_{j}\tilde{q}_{1}}} D\left(\tilde{r}/\sqrt{\eta}\right),$$
(G13)

where

$$\tilde{r} = S_j(q_1, \bar{p}_1, q_2, p_2, \dots, q_m, p_m), 
\bar{r} = (q_1, \bar{p}_1, q_2, p_2, \dots, q_m, p_m),$$
(G14)

and  $S_j$  is the symplectic matrix associated with  $\mathcal{G}_j$ . Therefore, defining  $\sigma_j = |(S_j)_{q_1,p_1}|$ , we get

$$\|\mathcal{B}_{j}(D(\mathbf{r}))\|_{\mathbb{F},1} = \frac{1}{\sqrt{\eta}} \int_{\mathbb{R}} d\bar{p}_{1} \left| \frac{\exp\left(i\left(-\frac{(p_{1}+\bar{p}_{1})^{2}}{24\gamma_{j-1}q_{1}} + 4\gamma_{j-1}q_{1}^{3} + \pi/4 - \mathbf{d}_{j}^{T}\Omega S_{j}\bar{\mathbf{r}}\right)\right) \exp\left(-(1/2+\bar{n})(1/\eta - 1)(\tilde{q}_{1}^{2} + \tilde{p}_{1}^{2})\right)}{\sqrt{24\pi\gamma_{j}\tilde{q}_{1}}} \right|$$

$$\leq \frac{1}{\sqrt{24\pi|\gamma_{j}|^{1/2}\eta^{1/2}}} \int_{\mathbb{R}} d\bar{p}_{1} \frac{\exp\left(-(1/2+\bar{n})(1/\eta - 1)(\sigma_{j}\bar{p}_{1} + (...))^{2}\right)}{\sqrt{|S_{q_{1},p_{1}}|\bar{p}_{1} + (...)|}}$$

$$\leq \frac{\Gamma(1/4)}{\sqrt{24\pi}\sigma_{j}|\gamma_{j}|^{1/2}\eta^{1/4}} \times ((1/2+\bar{n})(1-\eta))^{-1/4}, \tag{G15}$$

where (...) in the second line consists of terms depending on  $(q_1, p_1, ..., q_m, p_m)$  and where we have used Lemma B.3.  $\Box$ 

We also require an analogous bound to control the evolution across the final noisy layer. The next lemma provides such a bound.

**Lemma G.3.** Given an operator O and the linear map

$$\mathcal{B}_t = \Lambda_{\bar{n},\eta} \circ \mathcal{G}_t \circ \mathcal{C}_{t-1,\mathfrak{C}},\tag{G16}$$

we have that

$$\|\mathcal{B}_t(D(r))\|_{\mathbb{F},1} \leqslant \frac{\sqrt{\pi}}{\sigma_t \sqrt{\eta}} ((1/2 + \bar{n})(1 - \eta))^{-1/2},$$
 (G17)

 $\forall \mathbf{r} \in (q_1, p_1, \dots, q_m, p_m), \text{ where}$ 

$$\sigma_t = |(S_t)_{q_1, p_1}|. \tag{G18}$$

*Proof.* The evolved operator  $\mathcal{B}_j(D(r))$  can be expressed as follows:

$$\mathcal{B}_{t}(D(\boldsymbol{r})) = \frac{1}{\eta} \int_{\mathbb{R}} d\bar{p}_{1} \exp\left(i\left(-\frac{(p_{1} + \bar{p}_{1})^{2}}{24\gamma_{t-1}q_{1}} + 4\gamma_{t-1}q_{1}^{3} + \pi/4 - \boldsymbol{d}_{t}^{T}\Omega S_{t}\boldsymbol{r}\right)\right) \exp\left(-(1/2 + \bar{n})(1/\eta - 1)(\tilde{q}_{1}^{2} + \tilde{p}_{1}^{2})\right) D(\tilde{\boldsymbol{r}}/\sqrt{\eta}), \tag{G19}$$

where

$$\tilde{r} = S_t(q_1, -\bar{p}_1, q_2, p_2, \dots, q_m, p_m) 
\bar{r} = (q_1, -\bar{p}_1, q_2, p_2, \dots, q_m, p_m)$$
(G20)

and  $S_t$  is the symplectic matrix associated with the Gaussian channel  $\mathcal{G}_t$ . Therefore,

$$\|\mathcal{B}_{t}(D(\boldsymbol{r}))\|_{\mathbb{F},1} = \frac{1}{\eta} \int_{\mathbb{R}} d\bar{p}_{1} \left| \exp\left(i\left(-\frac{(p_{1} + \bar{p}_{1})^{2}}{24\gamma_{t-1}q_{1}} + 4\gamma_{t-1}q_{1}^{3} + \pi/4 - \boldsymbol{d}_{t}^{T}\Omega S_{t}\boldsymbol{r}\right)\right) \exp\left(-(1/2 + \bar{n})(1/\eta - 1)(\tilde{q}_{1}^{2} + \tilde{p}_{1}^{2})\right) \right|$$

$$\leq \frac{1}{\eta} \int_{\mathbb{R}} d\bar{p}_{1} \leq \exp\left(-(1/2 + \bar{n})(1/\eta - 1)(\sigma_{t}\bar{p}_{1} + (...))^{2}\right) = \frac{\sqrt{\pi}}{\sigma_{t}\sqrt{\eta}} ((1/2 + \bar{n})(1 - \eta))^{-1/2}$$
(G21)

where (...) in the second line are terms depending on  $(q_1, p_1, ..., q_m, p_m)$ .

Equipped with the above lemmas, we can now combine these ingredients to obtain a global concentration result. In particular, we show that expectation values of global observables decay exponentially with the number of layers, thereby justifying the noise-induced concentration regime described in Theorem 1 in the main text.

**Theorem G.1.** Given the input state  $\rho = |0\rangle \langle 0|^{\otimes m}$ , an output global operator O, we have that

$$|\text{Tr}[\mathcal{U}(\rho)O]| \leq 2^m \times \frac{((1/2 + \bar{n})(1 - \eta))^{-1/2}}{\sqrt{2}\sigma_t\sqrt{\eta}} \left( \frac{\Gamma(1/4)}{\sigma_{\min}\eta^{1/4}\sqrt{24\pi}|\gamma|_{\min}} ((1/2 + \bar{n})(1 - \eta))^{-1/4} \right)^{L-1} \times ||O||_1, \tag{G22}$$

where

$$\sigma_{\min} = \min_{j} \sigma_{k},$$

$$|\gamma|_{\min} = \min_{j} |\gamma_{j}|.$$
(G23)

Therefore, assuming phase-transition and for sufficiently large  $t = \Omega(m)$ , the output expectation value exponentially concentrates to zero.

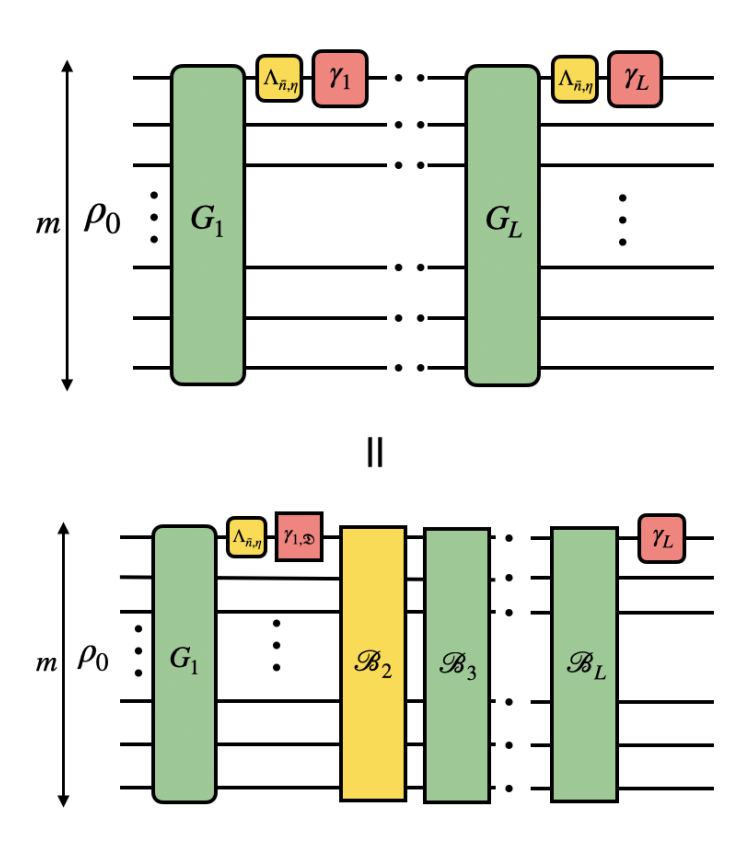


Figure 5. The circuit decomposition of the noisy bosonic circuit  $\mathcal{U}$  (Eq. G1) that helps us in proving Theorem G.1. The expression for  $\mathcal{B}_L$  and  $\mathcal{B}_j, \forall j \in \{2, ..., L-1\}$  are given by Equations G16 and G10 respectively. Conjugating the cubic phase gate with output operator  $\hat{O}$  and upper bounding the Fourier one-norm of  $\mathcal{B}_L \circ ... \circ \mathcal{B}_2 \circ \mathcal{C}_{1,\mathfrak{D}} \circ \Lambda_{\bar{n},\eta} \circ \mathcal{G}_1(\rho)$ , we prove that the expectation value of output operators with at most exponential Schatten 1-norm concentrates exponentially to zero whenever  $\mathfrak{c}_1 < 1$  (Eq. G36) for sufficiently large circuit depth  $L = \Omega(m)$ .

*Proof.* First we decompose the noisy bosonic circuit as

$$\mathcal{U} = \mathcal{C}_L \circ \mathcal{B}_L \circ \mathcal{B}_{L-1} \circ \cdots \circ \mathcal{B}_2 \circ \mathcal{C}_{1,\mathfrak{D}} \circ \Lambda_{\bar{n},\eta} \circ \mathcal{G}_1, \tag{G24}$$

where  $\mathcal{B}_L$  and  $\mathcal{B}_j$ ,  $\forall j \in \{2, ..., L-1\}$  are given by Equations G16 and G10 respectively (Figure 5). Then we have that

$$|\operatorname{Tr}[OU(\rho)]| = |\operatorname{Tr}[\mathcal{C}_L^*(O) \mathcal{B}_L \circ \dots \circ \mathcal{B}_2 \circ \mathcal{C}_{1,\mathfrak{D}} \circ \Lambda_{\bar{n},\eta} \circ \mathcal{G}_1(\rho)]|$$
(G25)

$$\leq \|\mathcal{C}_{L}^{*}(O)\|_{1} \|\mathcal{B}_{L} \circ \dots \circ \mathcal{B}_{2} \circ \mathcal{C}_{1,\mathfrak{D}} \circ \Lambda_{\bar{n},\eta} \circ \mathcal{G}_{1}(\rho)\|_{\infty} \tag{G26}$$

$$\leq \|O\|_1 \|\mathcal{B}_L \circ \dots \circ \mathcal{B}_2 \circ \mathcal{C}_{1,\mathfrak{D}} \circ \Lambda_{\bar{n},\eta} \circ \mathcal{G}_1(\rho)\|_{\mathbb{F},1},$$
 (G27)

where, in the second line, we applied Hölder's inequality (Lemma B.5), and in the last line, we used the unitary invariance of Schatten norms, the unitarity of  $\mathcal{C}_L^*$ , and the fact that the operator norm is upper bounded by the Fourier 1-norm (Lemma C.1). We now expand the operator  $\mathcal{C}_{1,\mathfrak{D}} \circ \Lambda_{\bar{n},\eta} \circ \mathcal{G}_1(\rho)$  int the displacement operator basis.

$$C_{1,\mathfrak{D}} \circ \Lambda_{\bar{n},\eta} \circ C_{1}(\rho) = \frac{1}{\pi^{m}} \int_{\mathbb{C}^{m}} d\boldsymbol{r} \chi_{\rho}(\boldsymbol{r}) \frac{\exp\left(-(1/2 + \bar{n})(1/\eta - 1)(\tilde{q}_{1}^{2} + \tilde{p}_{1}^{2})\right)}{\sqrt{24\pi\gamma_{1}\eta\tilde{q}_{1}}} e^{i\boldsymbol{d}\Omega\boldsymbol{r}} D\left(\frac{\tilde{\boldsymbol{r}}}{\sqrt{\eta}}\right)$$
(G28)

The characteristic function of the operator  $\mathcal{C}_{1,\mathfrak{D}} \circ \Lambda_{\bar{n},\eta} \circ \mathcal{G}_1(\rho)$  is  $L^1$  integrable, and moreover the associated Fourier

1-norm equals

$$\|\mathcal{C}_{1,\mathfrak{D}} \circ \Lambda_{\bar{n},\eta} \circ \mathcal{G}_{1}(\rho)\|_{\mathbb{F},1} = \frac{1}{\pi^{m}} \int_{\mathbb{C}^{m}} d\boldsymbol{r} \chi_{\rho}(\boldsymbol{r}) \frac{\exp\left(-(1/2 + \bar{n})(1/\eta - 1)(\tilde{q}_{1}^{2} + \tilde{p}_{1}^{2})\right)}{\sqrt{6|\gamma_{1}\eta\tilde{q}_{1}|}}$$
(G29)

$$\leq \frac{2^{m}\Gamma(1/4)}{\sqrt{48}\pi|\gamma_{1}|^{1/2}\eta^{1/4}\sigma_{1}} \times ((1/2+\bar{n})(1-\eta))^{-1/4}, \tag{G30}$$

where  $\tilde{r} = S_1(q_1, p_1, \dots, q_m, p_m)$  in the first line, and the second line follows from the fact that for the input vacuum state

$$\chi_{\rho}(\mathbf{r}) = \prod_{i=1}^{m} \exp\left(-\frac{q_i^2 + p_i^2}{2}\right). \tag{G31}$$

We use Lemma B.3 for integral over  $p_1$  and standard Gaussian integral formula for integration over rest of the coordinates. By using the fact that  $\exp(-x^2) \leq 1 \forall x$  and carefully choosing which terms to discard, we obtain the given upper bound on  $\|\mathcal{C}_{1,\mathfrak{D}} \circ \Lambda_{\bar{n},\eta} \circ \mathcal{G}_1(\rho)\|_{\mathbb{F},1}$ .

We will now apply the Fourier-one norm of  $\mathcal{B}_L \circ ... \circ \mathcal{B}_1 \circ \mathcal{C}_{1,\mathfrak{D}} \circ \Lambda_{\bar{n},\eta} \circ \mathcal{G}_1(\rho)$  applying iteratively Lemma B.2. In particular, applying L-2 times Lemma G.2 and Lemma G.3, we can upper bound the Fourier 1-norm of the evolved state as follows:

$$\|\mathcal{B}_{L} \circ \dots \circ \mathcal{B}_{1} \circ \mathcal{C}_{1,\mathfrak{D}} \circ \Lambda_{\bar{n},\eta} \circ \mathcal{G}_{1}(\rho)\|_{\mathbb{F},1}$$
(G32)

$$\leq 2^{m} \times \frac{((1/2 + \bar{n})(1 - \eta))^{-1/2}}{\sqrt{2}\sigma_{t}\sqrt{\eta}} \times \Pi_{i=1}^{L-1} \left( \frac{\Gamma(1/4)}{\sigma_{i}\eta^{1/4}\sqrt{24\pi|\gamma_{i}|}} ((1/2 + \bar{n})(1 - \eta))^{-1/4} \right)$$
 (G33)

$$\leq 2^{m} \times \frac{((1/2 + \bar{n})(1 - \eta))^{-1/2}}{\sqrt{2}\sigma_{t}\sqrt{\eta}} \left(\frac{\Gamma(1/4)}{\sigma_{\min}\eta^{1/4}\sqrt{24\pi|\gamma|_{\min}}}((1/2 + \bar{n})(1 - \eta)^{-1/4})\right)^{L-1},\tag{G34}$$

and therefore

$$|\text{Tr}[O\mathcal{U}(\rho)]| \leqslant 2^m \times \frac{((1/2 + \bar{n})(1 - \eta))^{-1/2}}{\sqrt{2}\sigma_t\sqrt{\eta}} \left( \frac{\Gamma(1/4)}{\sigma_{\min}\eta^{1/4}\sqrt{6|\gamma|_{\min}}} ((1/2 + \bar{n})(1 - \eta)^{-1/4}) \right)^{L-1} \times ||O||_1.$$
 (G35)

Therefore, if we have a sufficiently high depth  $L = \Omega(m)$  the noisy bosonic circuit with circuit parameters such that

$$\mathfrak{c}_1 := \frac{\Gamma(1/4)}{\sigma_{\min} \eta^{1/4} \sqrt{24\pi |\gamma|_{\min}}} ((1/2 + \bar{n})(1 - \eta)^{-1/4}) < 1, \tag{G36}$$

then the overlap of the output state of the circuit with global operators with a finite Schatten 1-norm (a prominent example being global projectors) exponentially concentrates to zero and hence the classical simulation of such overlaps becomes trivial.

In the next two sections, we detail classical simulation algorithms to identify regimes where efficient classical simulation of overlap estimation with coherent state projectors and quadrature moment estimation is possible.

#### 2. Unbiased estimator

In this section, we will describe how to estimate the characteristic function at the output of the noisy bosonic circuit described by Eq. G1 using an unbiased estimator that works under the assumption that the Gaussian unitaries  $G_j$  have

all non-zero symplectic coherence with respect to the first mode, i.e. they mix the position and momentum quadratures of the first mode [27]:

$$\sigma_j^{-1} := \left| \left( S_j^{-1} \right)_{q_1, q_2} \right|, \tag{G37}$$

$$(\sigma^{-1})_{\min} = \min_{j \in [L]} \sigma_j^{-1} > 0.$$
 (G38)

Given the channel  $\mathcal{U}_{\lfloor 1,t \rfloor}$  modeling the first t circuit layers, i.e.

$$\mathcal{U}_{\lfloor 1,t \rfloor} = \mathcal{U}_t \circ \mathcal{U}_{t-1} \circ \dots \circ \mathcal{U}_1, \tag{G39}$$

its adjoint can be rewritten as

$$\mathcal{U}_{|1,t|}^* = \bigcirc_{j=t-1}^0 \mathcal{U}_{t-j}^* \tag{G40}$$

$$= \bigcirc_{j=t-1}^{0} \left( \mathcal{G}_{t-j}^{*} \circ \Lambda_{\bar{n},\eta}^{(\text{shift}),*} \circ \Lambda_{\bar{n},\eta}^{(\text{Im}),*} \circ \mathcal{C}_{t-j,\mathfrak{C}}^{*} \circ \mathcal{C}_{t-j,\mathfrak{D}}^{*} \circ \Lambda_{\bar{n},\eta}^{(\text{Re}),*} \right)$$

$$(G41)$$

$$= \mathcal{G}_{1}^{*} \circ \Lambda_{\bar{n},\eta}^{(\text{shift}),*} \circ \Lambda_{\bar{n},\eta}^{(\text{Im}),*} \circ \mathcal{C}_{1,\mathfrak{C}}^{*}$$

$$(G42)$$

$$\circ \left[ \bigcirc_{j=t-2}^{0} \left( \mathcal{C}_{t-j-1,\mathfrak{D}}^{*} \circ \Lambda_{\bar{n},\eta}^{(\mathrm{Re}),*} \circ \mathcal{G}_{t-j}^{*} \circ \Lambda_{\bar{n},\eta}^{(\mathrm{shift}),*} \circ \Lambda_{\bar{n},\eta}^{(\mathrm{Im}),*} \circ \mathcal{C}_{t-j,\mathfrak{C}}^{*} \right) \right]$$
(G43)

$$\circ C_{t,\mathfrak{D}}^* \circ \Lambda_{\bar{n},\eta}^{(\mathrm{Re}),*} \tag{G44}$$

$$:= \left[ \bigcirc_{j=t-1}^{0} \mathcal{A}_{t-j} \right] \circ \mathcal{C}_{t,\mathfrak{D}}^{*} \circ \Lambda_{\bar{n},\eta}^{(\mathrm{Re}),*}$$
(G45)

Here, the maps  $A_i$  are defined as

$$\mathcal{A}_{j} := \begin{cases} \mathcal{G}_{1}^{*} \circ \Lambda_{\bar{n},\eta}^{(\text{shift}),*} \circ \Lambda_{\bar{n},\eta}^{(\text{Im}),*} \circ \mathcal{C}_{1,\mathfrak{C}}^{*} & \text{if } j = 1\\ \mathcal{C}_{j-1,\mathfrak{D}}^{*} \circ \Lambda_{\bar{n},\eta}^{(\text{Re}),*} \circ \mathcal{G}_{j}^{*} \circ \Lambda_{\bar{n},\eta}^{(\text{shift}),*} \circ \Lambda_{\bar{n},\eta}^{(\text{Im}),*} \circ \mathcal{C}_{j,\mathfrak{C}}^{*} & \text{if } 2 \leqslant j \leqslant t \end{cases}$$

$$(G46)$$

Expressing the noisy circuit layers in terms of the linear maps  $A_j$  is particularly convenient for classical simulation. As shown in Section F1, these maps can be modeled by unbiased Monte Carlo estimators, which form the basis of the following technical result:

**Lemma G.4** (Unbiased estimation of expectation values of displacement operators). Assume that  $\eta, \bar{n}, |\gamma|_{\min} \in \Theta(1)$ . Let  $\mathfrak{c}$  be defined as

$$c_2 := \frac{\Gamma(\frac{1}{4})}{(\sigma^{-1})_{\min}\sqrt{24\pi} \left\{ \eta \, |\gamma|_{\min} (1/2 + \bar{n})(1 - \eta) \right\}^{1/4}}.$$
 (G47)

Let  $r \in \mathbb{R}^{2m}$  such that  $q_1 \neq 0$ . Then there is a randomized classical algorithm that runs in time

$$\mathcal{O}\left(mt\epsilon^{-2}\log(1/\delta)|q_1|^{-1}\mathfrak{c}^{2(t-1)}\right) \tag{G48}$$

and approximates the expectation value  $\operatorname{Tr}[D(r)\mathcal{U}_{\lceil 1,t \rceil}(\rho_0)]$  with additive error  $\epsilon$  and success probability  $1-\delta$ .

*Proof.* We will show that the procedure formalized in Algorithm 1 yields the desired approximation. By Lemmas F.2 and F.3, we can simulate the oracles associated to the linear maps  $A_j$  with zero bias and magnitudes  $A_j$  equal to

$$A_{j} := \begin{cases} \sqrt{\pi} \left( \left( \frac{1}{2} + \bar{n} \right) (1 - \eta) \right)^{-1/2} & \text{if } j = 1, \\ \frac{\Gamma\left( \frac{1}{4} \right) \left( \left( \frac{1}{2} + \bar{n} \right) (1 - \eta) \right)^{-1/4}}{(\sigma^{-1})_{j} \sqrt{24\pi \eta} |\gamma_{j-1}|} & \text{if } 2 \leqslant j \leqslant t. \end{cases}$$
(G49)

By iteratively applying the "Chained Sampling Lemma" (Lemma F.1), we can simulate the oracle  $\mathsf{Sample}(\bigcirc_{j=0}^{t-1}\mathcal{A}_{t-j}(D(r)))$  with zero bias and magnitude A, where

$$A = \prod_{j=1}^{t} A_j = \frac{\sqrt{\pi} \Gamma(\frac{1}{4})^{t-1} \left( (\frac{1}{2} + \bar{n})(1 - \eta) \right)^{-\frac{t-1}{4}}}{(24\pi\eta)^{\frac{t-1}{2}} \prod_{j=2}^{t} (\sigma^{-1})_j \sqrt{|\gamma_{j-1}|}}$$
(G50)

$$\leqslant \frac{\sqrt{\pi} \Gamma(\frac{1}{4})^{t-1} \left( \left( \frac{1}{2} + \bar{n} \right) (1-\eta) \right)^{-\frac{t-1}{4}}}{(24\pi\eta)^{\frac{t-1}{2}} \left( (\sigma^{-1})_{\min} \sqrt{|\gamma|_{\min}} \right)^{t-1} \left( \frac{1}{2} + \bar{n} \right)^{1/2} (1-\eta)^{1/2}}$$
(G51)

Let  $Y \in \mathbb{C}$ ,  $\mathbf{r}' \in \mathbb{R}^{2m}$  such that

$$C_{t,\mathfrak{D}}^* \circ \Lambda_{\bar{n},\eta}^{(\mathrm{Re}),*}(D(\boldsymbol{r})) = \sqrt{\frac{1}{24\pi\gamma_t q_1}} \exp\left(-(1+2\bar{n})(1-\eta)\frac{q_1^2}{2}\right) D(\boldsymbol{r}) := YD(\boldsymbol{r}), \tag{G52}$$

where we set  $Y := \sqrt{\frac{1}{6\gamma_t q_1}} \exp\left(-(1+2\bar{n})(1-\eta)\frac{q_1^2}{2}\right)$ . Then, given (Z, s) drawn from the oracle  $\mathsf{Sample}(\bigcirc_{j=0}^{t-1} \mathcal{A}_{t-j}(D(r')))$ , it holds that

$$\mathbb{E}_{Z,s} YZ \operatorname{Tr}[D(s)\rho_0] = \operatorname{Tr}\left[\left[\bigcirc_{j=0}^{t-1} \mathcal{A}_{t-j}\right] \circ \mathcal{C}_{t,\mathfrak{D}}^* \circ \Lambda_{\bar{n},\eta}^{(\operatorname{Re}),*}(D(r))\rho_0\right] = \operatorname{Tr}\left[D(r)\mathcal{U}_{\lceil 1,t \rceil}(\rho_0)\right]. \tag{G53}$$

Defining

$$\mathfrak{c} := \frac{\Gamma(\frac{1}{4})}{(\sigma^{-1})_{\min} \sqrt{24\pi\eta |\gamma|_{\min}}} \left\{ (1/2 + \bar{n})(1-\eta) \right\}^{1/4}.$$
 (G54)

We observe that

$$|YZ\operatorname{Tr}[D(\boldsymbol{s})\rho_{0}]| \leqslant |YZ| \leqslant A\sqrt{\frac{1}{24\pi|\gamma|_{\min}|q_{1}|}} \leqslant \frac{\sqrt{\pi}}{\sqrt{24\pi}(\sigma^{-1})_{\min}|\gamma|_{\min}^{1/2}|q_{1}|^{1/2}(1/2+\bar{n})^{1/2}(1-\eta)^{1/2}} \mathfrak{c}^{t-1}.$$
 (G55)

By Chernoff-Hoeffding bound (Lemma B.7), we can upper bound the number of draws N from  $\mathsf{Sample}(\bigcirc_{j=0}^{t-1} \mathcal{A}_{t-j}(D(\mathbf{r}')))$  required to estimate the  $\mathsf{Tr}[D(\mathbf{r})\mathcal{U}_{\lceil 1,t\rceil}(\rho_0)]$  with additive error at most  $\epsilon$  and success probability at least  $1-\delta$ , obtaining

$$N \in \mathcal{O}\left(\epsilon^{-2}\log(1/\delta)\frac{\pi}{24\pi|\gamma|_{\min}|q_1|(1/2+\bar{n})(1-\eta)}\mathfrak{c}^{2(t-1)}\right). \tag{G56}$$

In particular, this implies that

$$N \in \mathcal{O}\left(\epsilon^{-2}\log(1/\delta)|q_1|^{-1}\mathfrak{c}^{2(t-1)}\right). \tag{G57}$$

As drawing a single sample from  $\mathsf{Sample}(\bigcirc_{j=0}^{t-1}\mathcal{A}_{t-j}(D(\boldsymbol{r}')))$  takes time  $\mathcal{O}(mt)$ , the total runtime scales as

$$\mathcal{O}\left(mt\epsilon^{-2}\log(1/\delta)|q_1|^{-1}\mathfrak{c}^{2t}\right). \tag{G58}$$

Note that this implies that whereas the unbiased estimator works well for large  $q_1$  or  $q_1 = 0$  (in this case, the first discrete cubic gate simply acts as identity so we do not have the factor  $q_1^{-1}$  in the runtime scaling), for  $q_1$  very small but not equal to zero, the runtime of the estimator blows up and therefore, we need better estimation algorithms that work well for all values of  $q_1$ .

 $\triangleright$  cf. Lemmas F.2 and F.3

## Algorithm 1 Unbiased estimator for expectation values of displacement operators

**Parameters:** number of estimation rounds N

Input: Classical descriptions of noisy circuit  $\mathcal{U}_{[1,t]} = \mathcal{U}_t \circ \mathcal{U}_{t-1} \circ \dots \circ \mathcal{U}_1$  with non-zero symplectic coherence with respect to the first mode, classical description of an initial state  $\rho_0$ , and a vector  $\mathbf{r} \in \mathbb{R}^{2m}$  such that  $q_1 \neq 0$  Output: An estimate of  $\text{Tr}[D(\mathbf{r})\mathcal{U}_{[1,t]}(\rho_0)]$ 

```
1: Initialize:
2: r_t \leftarrow r = (q_1, p_1, \dots, q_m, p_m)
3: B_t \leftarrow (24\pi\gamma_t q_1)^{-1/2} \exp\left(-(\frac{1}{2} + \bar{n})(1 - \eta)q_1^2\right)
4: for j = 1 to N, do
5: for k = t to 1, do
6: (r_{k-1}, Z_{k-1}) \leftarrow \mathsf{Sample}(\mathcal{A}_k(r_k))
7: B_{k-1} \leftarrow B_k Z_{k-1}
8: end for
9: X_j \leftarrow B_0 \operatorname{Tr}(D(r_0)\rho_0)
10: end for
11: Return output X \leftarrow \frac{1}{N} \sum_{j=1}^{N} X_j
```

#### 3. Adaptive algorithms

We now turn to adaptive algorithms, which refine the unbiased estimation procedure introduced in the previous section. While the unbiased estimator already allows for the approximation of displacement operator expectation values, it suffers from two limitations: (i) its computational cost scales inversely with  $|q_1|$ , making it efficient only when  $|q_1|$  is sufficiently large; and (ii) it requires both the Gaussian unitaries to have non-vanishing symplectic coherence and the cubic gates to have non-vanishing cubicity. To overcome these drawbacks, we design two adaptive algorithms based on the biased oracle introduced in Section F 2. Both algorithms achieve a runtime independent of  $|q_1|$ : the first still requires non-vanishing symplectic coherence and cubicity, whereas the second is tailored to regimes the cubicity is sufficiently small compared to other parameters, such as the noise rate and the energy, and presents a runtime independent of the symplectic coherence.

## a. General case

To overcome the limitations of small initial  $q_1$  when estimating characteristic function at the output of the noisy bosonic circuit, instead of using the unbiased sampling oracle in the beginning, we use the biased sampling oracle for the first few layers to take care of the small  $q_1$ . After we implement the biased oracle for a layer, at the end of each such layer, we check the value of r that has been sampled by the biased oracle and if  $q_1$  is sufficiently large, we switch to the unbiased oracle for the rest of the circuit, otherwise we use the biased oracle for the next layer as well, and we repeat the process after each layer. This algorithm allows for simulation of characteristic function with the following time complexity:

**Lemma G.5** (Adaptive estimation of expectation values of displacement operators). Let  $\rho_0$  be an initial state and  $\mathcal{U} := \mathcal{U}_L \circ \mathcal{U}_{L-1} \circ \ldots \circ \mathcal{U}_1$  be a noisy bosonic circuit. For all  $j \in [L]$ , assume that the partially evolved state  $\rho_j := \mathcal{U}_j \circ \mathcal{U}_{j-1} \circ \ldots \circ \mathcal{U}_1(\rho_0)$  satisfies the following curvature bound:

$$\max_{\boldsymbol{r}' \in \mathbb{R}^{2m}} \left| \left\{ \frac{\partial^2}{\partial^2 p_1} \operatorname{Tr}[D(\boldsymbol{r}) \Lambda_{\bar{n}, \eta}(\rho_j)] \right\}_{\boldsymbol{r} = \boldsymbol{r}'} \right| \leqslant M.$$
 (G59)

For all  $r \in \mathbb{R}^{2m}$ , there is a classical randomized algorithm running in time

$$\mathcal{O}(m\mathfrak{c}^a M L^2 \epsilon^{-3} \log(1/\delta)),\tag{G60}$$

where

$$\mathfrak{c}_2 := \frac{\Gamma(\frac{1}{4})}{(\sigma^{-1})_{\min} \sqrt{24\pi\eta |\gamma|_{\min}} \left\{ (1/2 + \bar{n})(1 - \eta) \right\}^{1/4}},\tag{G61}$$

and  $0 \le a \le 2L$  that approximates  $\operatorname{Tr}[D(r)\mathcal{U}(\rho_0)]$  with additive error  $\epsilon$  and success probability  $1 - \delta$ .

*Proof.* We will show that the procedure formalized in Algorithm 2 yields the desired approximation. Consider the expectation value  $\text{Tr}[D(\mathbf{r})\mathcal{U}(\rho)]$ . Let  $\mathbf{r}^{(j)} = (q_1^{(j)}, p_1^{(j)}, \dots, q_m^{(j)}, p_m^{(j)})$  be defined iteratively as follows:

$$\boldsymbol{r}^{(L)} = \boldsymbol{r},\tag{G62}$$

$$\tilde{\boldsymbol{r}}^{(j)} = S^{-1} \boldsymbol{r}^{(j+1)},$$
 (G63)

$$\boldsymbol{r}^{(j)} = \left(\tilde{q}_1^{(j)} \sqrt{\eta}, \tilde{p}_1^{(j)} \sqrt{\eta}, \tilde{q}_2^{(j)}, \tilde{q}_2^{(j)}, \dots, \tilde{q}_L^{(j)}, \tilde{q}_L^{(j)}\right) \tag{G64}$$

We also define the partially evolved state  $\rho_j$  and the partially Heisenberg-evolved observable  $O_j$ 

(G65)

$$\rho_j = \mathcal{U}_j \circ \mathcal{U}_{j-1} \circ \dots \circ \mathcal{U}_1(\rho), \tag{G66}$$

$$O_j = \mathcal{U}_{j+1}^* \circ \dots \circ \mathcal{U}_L^*(O), \tag{G67}$$

where  $O_L = D(\mathbf{r})$ . We also denote by  $\tilde{O}_j$  the observable obtained by approximating the cubic gates

$$\tilde{O}_j = \prod_{i=i+1}^L \exp\left(-i4\gamma \left(q_1^{(i)}\right)^3\right) D(\boldsymbol{r}^{(j)}),\tag{G68}$$

and we set  $\tilde{O}_L = O_L = D(r)$ . Given a threshold  $\tau \ge 0$ , let  $j^*$  be the largest j such that

$$\left| q_1^{(j)} \gamma_j \right| \geqslant \tau. \tag{G69}$$

We assume that all the states  $\rho_j$  with  $j \geqslant j^*$  lies in the set  $\mathcal{S}_M$ , i.e. they satisfy the "curvature bound". We have,

$$\left| \operatorname{Tr} \left[ \left( O_{j^*} - \tilde{O}_{j^*} \right) \rho_{j^*} \right] \right| = \left| \operatorname{Tr} \left[ O_L \rho_L \right] - \operatorname{Tr} \left[ \tilde{O}_{j^*} \rho_{j^*} \right] \right| = \left| \operatorname{Tr} \left[ \tilde{O}_L \rho_L \right] - \operatorname{Tr} \left[ \tilde{O}_{j^*} \rho_{j^*} \right] \right|$$
(G70)

$$= \left| \sum_{j=j^*}^{L-1} \operatorname{Tr} \left[ \tilde{O}_{j+1} \rho_{j+1} \right] - \operatorname{Tr} \left[ \tilde{O}_{j} \rho_{j} \right] \right| \leqslant (L - j^*) 6\tau M \leqslant 6\tau M L, \tag{G71}$$

The first line follows from the identity  $\text{Tr}[O_{j^*}\rho_{j^*}] = \text{Tr}[O_L\mathcal{U}_L \circ \mathcal{U}_{L-1} \circ \dots \circ \mathcal{U}_1(\rho)] = \text{Tr}[O_L\rho_L]$ . The second line follows by definition  $(\tilde{O}_L = O_L = D(r))$ , the third line by telescoping, and the final step from the triangle inequality together with Lemma F.4.

For achieving additive error at most  $\epsilon/2$ , we need to set  $\tau = \epsilon/(12ML)$  We estimate  $\mathrm{Tr}\big[\widetilde{O}_{j^*}\rho_{j^*}\big]$  with the unbiased estimator. By Lemma G.4,  $\mathrm{Tr}\big[\widetilde{O}_{j^*}\rho_{j^*}\big]$  can be estimated with precision  $\epsilon/2$  and success probability  $1-\delta$  in time  $\mathcal{O}(m(L-j^*)\epsilon^{-2}\log(1/\delta)|q_1|^{-1}\mathfrak{c}^{2(L-j^*-1)}) = \mathcal{O}(m(L-j^*)\epsilon^{-2}\log(1/\delta)|\gamma|_{\max}/\tau \times \mathfrak{c}^{2(L-j^*-1)})$ . Inserting  $\tau = \epsilon/12ML$  gives us the required expression.

The circuit decomposition that helps us in devising the simulation algorithm used in Lemma G.5 is given in Figure 6.

## Algorithm 2 Adaptive algorithm for expectation values of displacement operators

**Parameters**: number of estimation rounds N, threshold  $\tau \geqslant 0$ 

Input: Classical descriptions of noisy circuit  $\mathcal{U} = \mathcal{U}_L \circ \mathcal{U}_{L-1} \circ ... \circ \mathcal{U}_1$  with non-zero symplectic coherence with respect to the first mode, classical description of an initial state  $\rho_0$ , and a vector  $\mathbf{r} \in \mathbb{R}^{2m}$  (possibly with  $q_1 = 0$ )

**Output**: An estimate of  $Tr[D(r)\mathcal{U}(\rho_0)]$ 

```
1: Initialize:  \mathbf{r}^{(L)} = \left(q_1^{(L)}, p_1^{(L)}, \dots, q_m^{(L)}, p_m^{(L)}\right) \leftarrow \mathbf{r} 
3: B_L \leftarrow 1
4: v \leftarrow \left|q_1^{(L)}\gamma_L\right|
5: j \leftarrow L
6: while v \leqslant \tau do \qquad \qquad \triangleright Check adaptive condition; if not satisfied, switch from biased to unbiased estimator
7: j \leftarrow j - 1
8: \tilde{\mathbf{r}}^{(j)} \leftarrow S_j^{-1} \mathbf{r}^{(j+1)} = \left(\tilde{q}_1^{(L)}, \tilde{p}_1^{(L)}, \dots, \tilde{q}_m^{(L)}, \tilde{p}_m^{(L)}\right)
9: \mathbf{r}^{(j)} \leftarrow \left(\sqrt{\eta} \tilde{q}_1^{(L)}, \tilde{p}_1^{(L)}, \dots, \tilde{q}_m^{(L)}, \tilde{p}_m^{(L)}\right)
10: B_j \leftarrow B_{j+1} \times \exp\left(-i4\gamma_j \left(q_1^{(j)}\right)^3\right)
11: v \leftarrow \left|q_1^{(j)}\gamma_j\right|
12: end while
```

13: Produce an estimate X of  $\text{Tr}[D(r_j)\mathcal{U}_{1,j}|(\rho_0)]$  using Algorithm 1 with N estimation rounds

The algorithm for estimating  $\text{Tr}\left[\mathcal{U}(\rho_0)\hat{D}(\boldsymbol{r})\right]$  for  $\boldsymbol{r}\in\mathbb{R}^{2m}$  allows us to estimate expectation values of local projectors.

The intution is as follows: given that

$$\operatorname{Tr}\left[\mathcal{U}(\rho_0)\hat{O}\right] = \frac{1}{\pi^m} \int_{\mathbb{R}^{2m}} d^{2m} \boldsymbol{r} \chi_{\hat{O}}(\boldsymbol{r}) \chi_{\mathcal{U}(\rho_0)}^*(\boldsymbol{r}), \tag{G72}$$

sampling a phase space point using the (normalized) magnitude of characteristic function of the output operator  $(\chi_O(\mathbf{r})/(\pi^m\|\hat{O}\|_{\mathbb{F},1}))$  as the probability distribution and estimating the characteristic function at that point using Lemma G.5 allows us to calculate the expectation value of these output operators. This algorithm is formalized in the following Lemma:

**Lemma G.6** (Estimation of expectation value of local projectors). Let  $\rho_0$  be an initial state and  $\mathcal{U} := \mathcal{U}_L \circ \mathcal{U}_{L-1} \circ ... \circ \mathcal{U}_1$  be a noisy bosonic circuit (Eq. G1). For all  $j \in [L]$ , assume that the partially evolved state  $\rho_j := \mathcal{U}_j \circ \mathcal{U}_{j-1} \circ ... \circ \mathcal{U}_1(\rho_0)$  satisfies the following curvature bound:

$$\max_{\boldsymbol{r}' \in \mathbb{R}^{2m}} \left| \left\{ \frac{\partial^2}{\partial^2 p_1} \operatorname{Tr}[D(\boldsymbol{r}) \Lambda_{\bar{n}, \eta}(\rho_j)] \right\}_{\boldsymbol{r} = \boldsymbol{r}'} \right| \leqslant M. \tag{G73}$$

For all  $r \in \mathbb{R}^{2m}$ , there is a classical randomized algorithm running in time

$$4^k m \mathfrak{c}^a M L^2 \epsilon^{-3} \log(1/\delta), \tag{G74}$$

where

14: Return  $B_i \times X$ 

$$c_2 = \frac{\Gamma(\frac{1}{4})}{(\sigma^{-1})_{\min} \sqrt{24\pi\eta |\gamma|_{\min}} \left\{ (1/2 + \bar{n})(1-\eta) \right\}^{1/4}},$$
(G75)

and  $1 \leqslant a \leqslant 2L$ , that approximates  $\operatorname{Tr}\left[\hat{O}\mathcal{U}(\rho_0)\right]$  for  $\hat{O}=\left(\bigotimes_{i=1}^k |\alpha_i\rangle \langle \alpha_i|\right) \otimes \mathbb{I}^{\otimes m-k}$  with additive error  $\epsilon$  and success probability  $1-\delta$ .

*Proof.* From Lemma G.5, we know that, we can sample a  $\tilde{r} \in \mathbb{R}^{2m}$  with the appropriate probability distribution using Monte Carlo Markov chain sampling, such that

$$\left| \operatorname{Tr} \left[ \mathcal{U}(\rho_0) \hat{D}(\boldsymbol{r}) \right] - Z \times \mathbb{E}_{\tilde{\boldsymbol{r}}} \left[ \operatorname{Tr} \left[ \rho_0 \tilde{\boldsymbol{r}} \right] \right] \right| \leqslant 6\tau M L, \tag{G76}$$

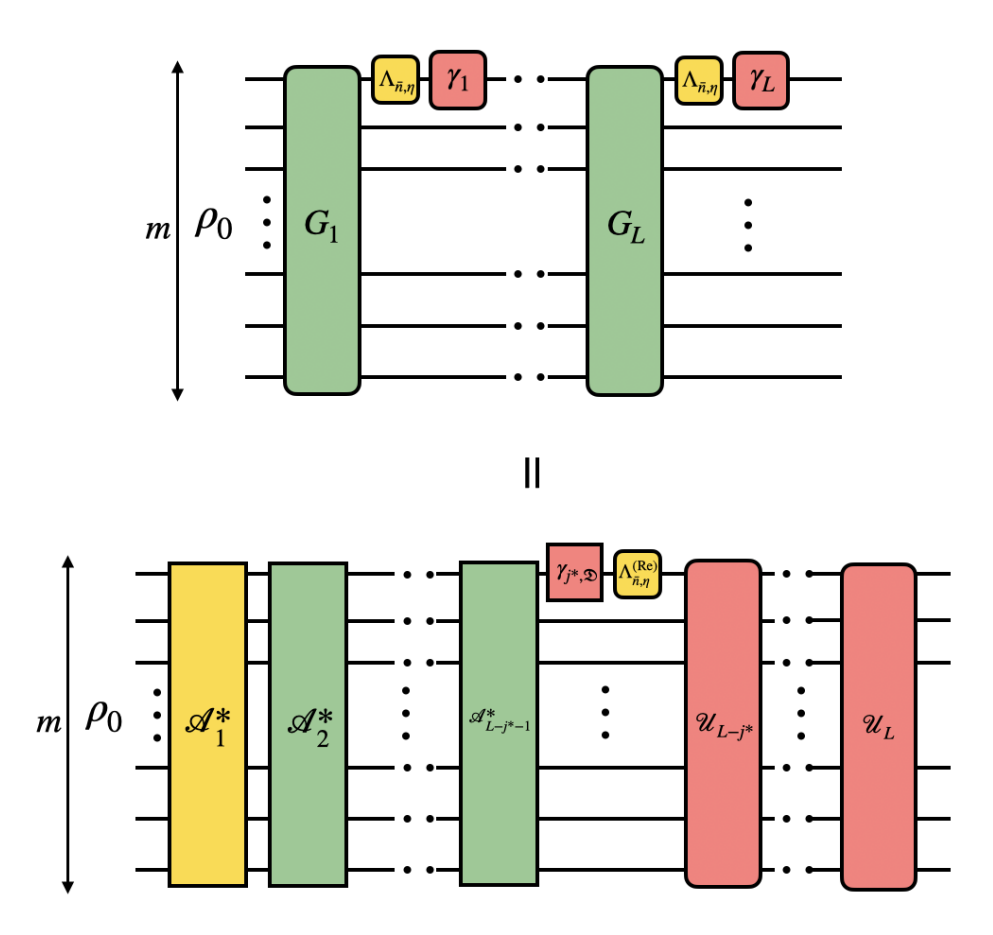


Figure 6. Circuit decomposition of the noisy bosonic circuit  $\mathcal{U}$  (Eq. G1) behind the simulation algorithm that leads to the time complexity of estimation of characteristic function given by Lemma G.5. The expression for  $\mathcal{A}_1$  and  $\mathcal{A}_j$ ,  $\forall j \geq 2$  is given by Eq. G49. Given a phase space point  $\mathbf{r} \in \mathbb{R}^{2m}$  at which we want to estimate the characteristic function, we sample phase space points in the first  $j^*$  layers using the biased oracle (Section F2) until the sampled phase space point has large enough  $q_1$ , after which we use the unbiased oracle (Section F1) to sample the phase space points.

where  $Z = \mathfrak{c}^{a/2}/\sqrt{\tau}$  and  $\tau$  is a freely choosen parameter. Therefore, given

$$\operatorname{Tr}\left[\mathcal{U}(\rho_0)\hat{O}\right] = \|\hat{O}\|_{\mathbb{F},1} \mathbb{E}_{p_{\hat{O}}(\boldsymbol{r})} \left[\operatorname{Tr}\left[\mathcal{U}(\rho_0)\hat{D}(\boldsymbol{r})\operatorname{arg}(\operatorname{Tr}\left[\hat{O}\hat{D}(-\boldsymbol{r})\right])\right]\right]. \tag{G77}$$

We have that,

$$\left| \| \hat{O} \|_{\mathbb{F},1} \mathbb{E}_{p_{\hat{O}}(\boldsymbol{r})} \left[ \operatorname{Tr} \left[ \mathcal{U}(\rho_{0}) \hat{D}(\boldsymbol{r}) \right] \operatorname{arg} \left( \operatorname{Tr} \left[ \hat{O} \hat{D}(-\boldsymbol{r}) \right] \right) \right] - \| \hat{O} \|_{\mathbb{F},1} \mathbb{E}_{p_{\hat{O}}(\boldsymbol{r})} \left[ \operatorname{arg} \left( \operatorname{Tr} \left[ \hat{O} \hat{D}(-\boldsymbol{r}) \right] \right) \times Z \mathbb{E}_{\tilde{\boldsymbol{r}}} \left[ \operatorname{Tr} \left[ \rho_{0} \hat{D}(\tilde{\boldsymbol{r}}) \right] \right] \right] \right] \\
\leqslant \| \hat{O} \|_{\mathbb{F},1} \mathbb{E}_{p_{\hat{O}}(\boldsymbol{r})} \left[ \left| \operatorname{Tr} \left[ \mathcal{U}(\rho_{0}) \hat{D}(\boldsymbol{r}) \right] - Z \mathbb{E}_{\tilde{\boldsymbol{r}}} \left[ \operatorname{Tr} \left[ \rho_{0} \hat{D}(\tilde{\boldsymbol{r}}) \right] \right] \right] \right] = 6\tau M L \| \hat{O} \|_{\mathbb{F},1}, \tag{G78}$$

where we have used the trianle inequality in the second line, Therefore, for the bias error to be  $\epsilon/2$  we choose

$$\tau = \frac{\epsilon}{12\|O\|_{\mathbb{F},1}ML}.\tag{G79}$$

Finally, through the Chernoff–Hoeffding bound, the statistical average of N samples of  $\|\hat{O}\|_{\mathbb{F},1}Z \times \arg(\text{Tr}\left[\hat{O}\hat{D}(-r)\right]) \operatorname{Tr}\left[\rho\hat{D}(\tilde{r})\right]$  over appropriately chosen phase-space points r and  $\tilde{r}$  will be  $\epsilon$  close to the actual ex-

pectation value with probability  $1 - \delta$  as long as number of samples

$$N = \frac{\|\hat{O}\|_{\mathbb{F},1}^2 |Z|^2}{\epsilon^2} \log(1/\delta) \leqslant 4^k \mathfrak{c}^a M L \epsilon^{-3} \log(1/\delta). \tag{G80}$$

The last inequality comes from the expression of Z (specified earlier) and the expression for Fourier 1-norm of  $\hat{O} = \left(\bigotimes_{i=1}^{k} |\alpha_i\rangle \langle \alpha_i|\right) \otimes \mathbb{I}^{\otimes m-k}$  (specified in Eq. (C50)). Combining the sample complexity with the time required to sample once gives the required time complexity.

Note that from Lemma D.1, bounding the first four moments of the position quadrature throughout the circuit is equivalent to bounding M throughout the circuit. Further, reflecting on Lemma G.6, this gives us two regimes of classical simulation of expectation value of local projectors: (i) For  $\mathfrak{c} > 1$ ,  $k = \mathcal{O}(\log(m))$  and  $L = \mathcal{O}(\log(m))$  allows for efficient classical simulation of output local projectors, whereas for (ii)  $\mathfrak{c} < 1$ ,  $k = \mathcal{O}(\log(m))$  and  $L = \mathcal{O}(\operatorname{poly}(m))$  allows for efficient classical simulation of output local projectors. This gives the first two regimes of efficient classical simulation detailed in Theorem 2 of the main text.

Further, combining Lemmas D.2 and G.5 also allows for efficient estimation of expectation value of first two quadrature moments, provided additional guarantees on the magnitude of expectation value of quadrature moments on the output state. This is summarized in the following Lemma:

**Lemma G.7** (Quadrature moment estimation). Let  $\rho_0$  be an initial state and  $\mathcal{U} := \mathcal{U}_L \circ \mathcal{U}_{L-1} \circ ... \circ \mathcal{U}_1$  be a noisy bosonic circuit. For all  $j \in [L]$ , assume that the partially evolved state  $\rho_j := \mathcal{U}_j \circ \mathcal{U}_{j-1} \circ ... \circ \mathcal{U}_1(\rho_0)$  satisfies the curvature bound:

$$\max_{\boldsymbol{r}' \in \mathbb{R}^{2m}} \left| \left\{ \frac{\partial^2}{\partial^2 p_1} \operatorname{Tr}[D(\boldsymbol{r}) \Lambda_{\bar{n}, \eta}(\rho_j)] \right\}_{\boldsymbol{r} = \boldsymbol{r}'} \right| \leqslant M.$$
 (G81)

and up to sixth moment of position and momentum quadratures are upper bounded by E on the output state  $\mathcal{U}(\rho_0)$ , then  $\text{Tr}[\hat{q}_j\mathcal{U}(\rho_0)], \text{Tr}[\hat{p}_j^2\mathcal{U}(\rho_0)], \text{Tr}[\hat{p}_j^2\mathcal{U}(\rho_0)]$  can be estimated with precision  $\epsilon$  and failure probability  $1 - \Delta$  by a classical algorithm running in time

$$\mathcal{O}(mL\mathfrak{c}^a ML(4E+3)^{12}\epsilon^{-12}\log(1/\Delta))m\tag{G82}$$

where

$$c_2 = \frac{\Gamma(\frac{1}{4})}{(\sigma^{-1})_{\min} \sqrt{24\pi\eta |\gamma|_{\min}} \left\{ (1/2 + \bar{n})(1-\eta) \right\}^{1/4}},$$
(G83)

and  $0 \leqslant a \leqslant 2L$ .

*Proof.* We explain the estimation of  $\text{Tr}[\hat{q}_1\mathcal{U}(\rho)]$  and  $\text{Tr}[\hat{q}_1^2\mathcal{U}(\rho)]$ , the estimation of first mode momentum quadrature as well as quadrature moments of other modes follows similar time complexity. From Lemma D.2,

$$\frac{\operatorname{Tr}\left[\mathcal{U}(\rho_0)\hat{D}_1(0,\delta) - 1\right]}{i\delta} \tag{G84}$$

approximates  $\text{Tr}[\mathcal{U}(\rho_0)\hat{q}_1]$  up to precision  $\delta \text{Tr}[\mathcal{U}(\rho_0)\hat{q}_1^4] \leqslant \delta \text{Tr}[\mathcal{U}(\rho_0)\hat{q}_1^4] \leqslant \delta E$ . Further, from Lemma G.5, we can approximate  $\text{Tr}[\mathcal{U}(\rho_0)\hat{q}_1]$  up to precision  $\varepsilon$  with probability  $1-\Delta$  in time

$$mL\mathfrak{c}^a ML\varepsilon^{-3}\log(1/\Delta).$$
 (G85)

Here we require  $\varepsilon = \delta^2$  for the precision on the estimate of  $\text{Tr}[\rho\hat{q}_1]$  to be of the order  $\delta$ . Further we require  $\delta = \epsilon/(E+1)$  for the precision in estimation of the quadrature moment to be  $\epsilon$ . This gives the required time complexity for estimation of  $\text{Tr}[\mathcal{U}(\rho_0)\hat{q}_1]$ . Similarly, from Lemma D.2,  $\text{Tr}[\mathcal{U}(\rho_0)\hat{q}_1^2]$  can be estimated by

$$\frac{2}{\delta^2} \left( (1 - \text{Tr} \left[ \mathcal{U}(\rho_0) \hat{D}_1(0, \delta) \right]) + \frac{1}{\delta} (\text{Tr} \left[ \mathcal{U}(\rho_0) \hat{D}_1(0, \delta^2) \right] - 1) \right). \tag{G86}$$

up to precision  $2/3 \times \delta \operatorname{Tr}\left[\rho \hat{q}_{j}^{6}\right] + 2\delta \operatorname{Tr}\left[\rho \hat{q}_{j}^{4}\right] \leq 8/3 \times E$ . Similar to the previous discussion, we want to estimate  $\operatorname{Tr}\left[\mathcal{U}(\rho_{0})\hat{D}_{1}(0,\delta)\right]$  up to precision  $\delta^{3}$  and  $\operatorname{Tr}\left[\mathcal{U}(\rho_{0})\hat{D}_{1}(0,\delta^{2})\right]$  up to precision  $\delta^{4}$ . And we choose  $\delta = \frac{3}{2} \times \frac{\epsilon}{4E+3}$  for the precision of estimation of quadrature moment to be  $\epsilon$ . This gives the required time complexity. We keep the most significant time complexity in the statement of the Lemma.

Therefore, Lemma G.7, this gives us two regimes of classical simulation of expectation value of first two quadrature moments, provided that first four quadrature moments are bounded throughout the circuit, and up to sixth moment of quadrature are bounded in the output state: (i) For  $\mathfrak{c} > 1$ ,  $k = \mathcal{O}(\log(m))$  and  $L = \mathcal{O}(\log(m))$  allows for efficient classical simulation of first two quadrature moments, whereas for (ii)  $\mathfrak{c} < 1$ ,  $k = \mathcal{O}(\log(m))$  and  $L = \mathcal{O}(\operatorname{poly}(m))$  allows for efficient classical simulation of first two quadrature moments. This gives the first two regimes of efficient classical simulation detailed in Theorem 3 of the main text.

In the final section, we detail simulation algorithm to estimate expectation value of local coherent state projectors and quadrature moments for noisy bosonic circuits where cubicity of all the cubic phase gates is close to zero, i.e. "near-Gaussian" circuits.

### b. Near-gaussian circuits

In this section, we will consider circuits whose cubicity is below a certain threshold, depending on M (Eq. (G81)), the desired bias of the sampling oracle  $\epsilon'$  and the noise parameters  $\bar{n}$  and  $\eta$ .

$$\max_{j \in [L]} |\gamma_j| < \frac{\epsilon'}{6M} \sqrt{\frac{(1+2\bar{n})(1-\eta)}{2\log(2)\log(M/\epsilon')}}.$$
(G87)

We refer to this parameter regime as the *near-Gaussian* regime, reflecting the fact that the strength of non-Gaussian gates in these circuits is small. In this setting, the sampling oracle provided in Lemma F.4 has a magnitude

$$\mathfrak{d}_{\epsilon'} = \frac{1}{2} \sqrt{\frac{M}{\epsilon'}} \exp\left[-\left(\frac{1}{2} + \bar{n}\right) (1 - \eta) \frac{(\epsilon')^2}{36M^2 \gamma^2}\right] < \frac{1}{2}.$$
 (G88)

By chaining L such oracles via Lemma F.1, we obtain an efficient classical algorithm for estimating characteristic functions and hence expectation values. Importantly, the runtime of this algorithm scales linearly both in the number of modes and in the circuit depth. This is summarized in the following Lemma:

**Lemma G.8** (Expectation values of displacement operators in near-Gaussian circuits). Let  $\rho_0$  be an initial state and  $\mathcal{U} := \mathcal{U}_L \circ \mathcal{U}_{L-1} \circ \ldots \circ \mathcal{U}_1$  be a noisy bosonic circuit. For all  $j \in [L]$ , assume that the partially evolved state  $\rho_j := \mathcal{U}_j \circ \mathcal{U}_{j-1} \circ \ldots \circ \mathcal{U}_1(\rho_0)$  satisfies the following curvature bound:

$$\max_{\boldsymbol{r}' \in \mathbb{R}^{2m}} \left| \left\{ \frac{\partial^2}{\partial^2 p_1} \operatorname{Tr}[D(\boldsymbol{r}) \Lambda_{\bar{n}, \eta}(\rho_j)] \right\}_{\boldsymbol{r} = \boldsymbol{r}'} \right| \leqslant M.$$
 (G89)

and the cubicity of the cubic phase gates is such that

$$\max_{j \in [L]} |\gamma_j| < \frac{\epsilon}{6M} \sqrt{\frac{(1+2\bar{n})(1-\eta)}{2\log(2)\log(2M/\epsilon)}},\tag{G90}$$

then for all  $\mathbf{r} \in \mathbb{R}^{2m}$ , there is a classical randomized algorithm running in time

$$mL\epsilon^{-2}\log(1/\delta),$$
 (G91)

that approximates  $\text{Tr}[D(r)\mathcal{U}(\rho_0)]$  with additive error  $\epsilon$ . and success probability  $1-\delta$ .

*Proof.* We will show that the procedure formalized in Algorithm 3 yields the desired approximation. The result follows by iteratively applying the Chained Sampling Lemma (Lemma F.1) and Lemma F.4, which provides a biased oracle for each noisy circuit layer  $U_i$ . From Lemma F.1, after j iteration, we obtain a new oracle for the channel  $U_{L-j+1} \circ ... \circ U_j$  with magnitude  $A^j < 1$  and bias

$$\epsilon' + A\epsilon' + A^2\epsilon' + \dots + A^{j-1}\epsilon' = \epsilon' \sum_{i=0}^{j-1} A^i \leqslant \epsilon' \sum_{i=0}^{\infty} A^i = \frac{\epsilon'}{1-A} \leqslant 2\epsilon', \tag{G92}$$

where we used the fact that A < 1/2. Setting  $\epsilon' = \epsilon/2$ , j = L and using the Chernoff-Hoeffding bound (Lemma B.7) yields the desired result.

# Algorithm 3 Adaptive algorithm for expectation values of displacement operators in the near-Gaussian regime

**Parameters**: number of estimation rounds N, bias  $\epsilon'$ 

Input: Classical descriptions of noisy circuit  $\mathcal{U} = \mathcal{U}_L \circ \mathcal{U}_{L-1} \circ ... \circ \mathcal{U}_1$ , classical description of an initial state  $\rho_0$ , and a vector  $\mathbf{r} \in \mathbb{R}^{2m}$  (possibly with  $q_1 = 0$ )

```
Output: An estimate of \operatorname{Tr}[D(r)\mathcal{U}(\rho_0)]

1: Initialize:

2: r^{(L)} = \left(q_1^{(L)}, p_1^{(L)}, \dots, q_m^{(L)}, p_m^{(L)}\right) \leftarrow r

3: B_L \leftarrow 1

4: for j = 1 to N, do

5: for k = L to 1, do

6: (r^{(k-1)}, Z_{k-1}) \leftarrow \operatorname{Sample}^{(S_M)}(\Lambda_{\bar{n}, \eta}^* \circ \mathcal{C}_k^*(D(r^{(k)}))) with bias \epsilon'

7: B_{k-1} \leftarrow e^{id_{k-1}^T \Omega r^{(k-1)}} B_k Z_{k-1}

8: end for

9: X_j \leftarrow B_0 \operatorname{Tr}(D(r_0)\rho_0)

10: end for

11: Return output X \leftarrow \frac{1}{N} \sum_{j=1}^N X_j
```

Similar to the previous section, the estimation of characteristic function in this regime also allows for expectation value estimation of local projective measurements and quadrature moment estimation. Since the sample complexity argument is essentially the same as Lemmas G.6 and G.7 in the last section, with the only difference being that the sample complexity of estimation of characteristic function is different in this regime, which is detailed in Lemma G.8, we directly state the results here:

**Lemma G.9** (Expectation value of local projectors and quadrature moments in near Gaussian circuits.). Let  $\rho_0$  be an initial state and  $\mathcal{U} := \mathcal{U}_L \circ \mathcal{U}_{L-1} \circ \dots \circ \mathcal{U}_1$  be a noisy bosonic circuit. For all  $j \in [L]$ , assume that the partially evolved state  $\rho_j := \mathcal{U}_j \circ \mathcal{U}_{j-1} \circ \dots \circ \mathcal{U}_1(\rho_0)$  satisfies the following curvature bound:

$$\max_{\boldsymbol{r}' \in \mathbb{R}^{2m}} \left| \left\{ \frac{\partial^2}{\partial^2 p_1} \operatorname{Tr}[D(\boldsymbol{r}) \Lambda_{\bar{n}, \eta}(\rho_j)] \right\}_{\boldsymbol{r} = \boldsymbol{r}'} \right| \leqslant M. \tag{G93}$$

and the cubicity of the cubic phase gates is such that

$$\max_{j \in [L]} |\gamma_j| < \frac{\epsilon}{6M} \sqrt{\frac{(1+2\bar{n})(1-\eta)}{2\log(2)\log(2M/\epsilon)}},\tag{G94}$$

then for all  $r \in \mathbb{R}^{2m}$ , there is a classical randomized algorithm running in time

$$4^k m L \epsilon^{-2} \log(1/\delta), \tag{G95}$$

that approximates  $\operatorname{Tr}\left[\hat{O}\mathcal{U}(\rho_0)\right]$  for  $\hat{O}=\left(\bigotimes_{i=1}^k |\alpha_i\rangle \langle \alpha_i|\right) \otimes \mathbb{I}^{\otimes m-k}$  with additive error  $\epsilon$  and and success probability  $1-\delta$ .

Further, if the expectation value of the sixth moment of quadratures are upper bounded by E on the output state  $\mathcal{U}(\rho_0)$ , then there is a classical algorithm running in time

$$mL(4E+3)^8\epsilon^{-8}\log(1/\delta) \tag{G96}$$

that estimates  $\operatorname{Tr}[\hat{q}_{j}\mathcal{U}(\rho_{0})], \operatorname{Tr}[\hat{q}_{j}^{2}\mathcal{U}(\rho_{0})], \operatorname{Tr}[\hat{p}_{j}\mathcal{U}(\rho_{0})], \operatorname{Tr}[\hat{p}_{j}^{2}\mathcal{U}(\rho_{0})], \forall j \in \{1, \dots, m\} \text{ with additive error } \epsilon \text{ with success probability } 1 - \delta.$ 

Lemma G.9 gives an additional regime of efficient classical simulation of expectation value of local projective measurements and first two moments of quadrature, marked by the coefficient

$$\mathfrak{d}_{\epsilon} = \sqrt{\frac{M}{\epsilon}} \exp\left[-\left(\frac{1}{2} + \bar{n}\right)(1 - \eta)\frac{\epsilon^2}{36M^2\gamma^2}\right] < 1. \tag{G97}$$

In this regime, the efficient classical simulation of local projective measurements requires the additional condition that the number of modes being measured  $k = \mathcal{O}(\log(m))$  and gives point three of Theorem 2 of the main text, whereas the efficient classical simulation of first two quadrature moments requires the additional condition that the first six quadrature moments are bounded on the output state and gives point three of Theorem 3 of the main text.